

**Spatiotemporal variability of water and energy fluxes:
TERENO prealpine hydrometeorological data analysis and
inverse modeling with GEOtop and PEST**

Dissertation im Fachgebiet Klima- und Umweltwissenschaften
vorgelegt der
Fakultät für Angewandte Informatik
der Universität Augsburg

zur Erlangung des akademischen Grades
eines Doktors der Naturwissenschaften (Dr. rer. nat.)

von
Mohsen Soltani

Augsburg, Oktober 2018

Erstgutachter: Prof. Dr. Harald Kunstmann
Zweitgutachter: Prof. Dr. Karl-Friedrich Wetzel
Datum der mündlichen Prüfung: 28.06.2019

Acknowledgements

I would like to express my deepest appreciation to my main advisor Prof. Dr. Harald Kunstmann for the continuous support of my Ph.D research project, for his patience, motivation, and immense knowledge. I would like also to thank the rest of my thesis supervisors, Dr. Patrick Laux and Dr. Matthias Mauder, for their insightful comments and encouragement. I was lucky enough to have knowledgeable and distinguished advisors as hydrologist, climatologist, and micrometeorologist. This enabled me to do an interdisciplinary research project in such a way that without their guidance and persistent help this dissertation would not have been possible.

I also sincerely thank Prof. Dr. Karl-Friedrich Wetzel (University of Augsburg) for his kind agreement to act as secondary referee.

A special gratitude goes to the Helmholtz Research School on “Mechanisms and Interactions of Climate Change in Mountain Regions” (MICMoR), for funding the Ph.D research. In this regard, my sincere thanks goes to the MICMoR Coordination Team & IFU Graduate Office, Dr. Bärbel Elija Bleher and Dipl.-Kulturw. Petra Guppenberger, who were helpful throughout my Ph.D period and provided me a great opportunity to join to the valuable MICMoR courses like Summer School, Professional Skills, etc. What wonderful courses!

Contents

Acknowledgements	i
List of abbreviations	iv
List of figures	vi
List of tables	viii
Abstract	ix
Zusammenfassung	xi
1 Introduction	1
1.1 Motivation and objectives	1
1.1.1 Turbulent flux variability and energy balance closure	4
1.1.2 Forward modeling: coupled water and energy variables	4
1.1.3 Inverse modeling: parameter sensitivity and uncertainty analysis ..	5
1.2 Innovation	6
1.3 Thesis structure	7
2 Turbulent flux variability and energy balance closure in TERENO prealpine observatory: A hydrometeorological data analysis	9
2.1 Introduction	9
2.2 Site characterization and measurement setup	10
2.2.1 Geography and climate	10
2.2.2 Data processing	11
2.2.3 Micrometeorological measurements	14
2.2.4 Data coverage	15
2.3 Results and discussion	17
2.3.1 Soil temperature and soil volumetric water content	17
2.3.2 Energy partitioning	19
2.3.3 Turbulent flux variability on different time scales	20
2.3.4 Energy balance closure	26
2.4 Conclusions	32

3	Spatiotemporal variability and empirical Copula-based dependence structure of modeled and observed coupled water and energy fluxes	34
3.1	Introduction	34
3.2	Study area and hydrometeorological dataset	36
3.2.1	Catchments description	36
3.2.2	Hydrometeorological data	37
3.3	Methodology	38
3.3.1	Hydrological modeling	38
3.3.2	Bivariate density estimation using empirical Copulas	43
3.4	Results and discussion	44
3.4.1	Spatiotemporal variability of water and energy fluxes	44
3.4.2	Joint simulation of water and energy fluxes using GEOtop	46
3.4.3	Copula-based dependence structures of water and energy fluxes	54
3.5	Conclusions	58
4	Inverse distributed modeling of streamflow and turbulent fluxes: A sensitivity and uncertainty analysis coupled with automatic optimization	59
4.1	Introduction	59
4.2	Catchment characterization and available datasets	61
4.3	Methods	63
4.3.1	Hydrological modeling	63
4.3.2	Parameter estimation strategy	64
4.3.3	The GEOtop-PEST interface	66
4.4	Results and discussion	67
4.4.1	Sensitivity analysis	67
4.4.2	Inverse modeling using the developed GEOtop-PEST interface	69
4.4.3	Uncertainty analysis pertaining to the model parameters	74
4.4.4	Correlations and contributions of the model parameters: PCA-based analysis	79
4.5	Conclusions	81
5	Conclusions and outlook	83
5.1	Conclusions	83
5.2	Outlook	86
	Bibliography	88
	Appendix A: PEST control file	105
	Curriculum Vita	108

List of abbreviations

AirT	Air Temperature
AVG	Alpha VanGenuchten
B	Bowen Ratio
COE	Coefficient Of Efficiency
DEM	Digital Elevation Map
DWD	Deutscher Wetterdienst
EC	Eddy Covariance
EBC	Energy Balance Closure
EBR	Energy Balance Ratio
ET	Evapotranspiration
G	Soil Heat Flux
GEOtop	Hydrological Model
GIS	Geographic Information System
GENLINPRED	Uncertainty Analysis Program – PEST utility
GMLA	Gauss-Marquardt-Levenberg Algorithm
H	Sensible Heat Flux
HHC	Horizontal Hydraulic Conductivity
ISR	Incoming Shortwave Radiation
IOA	Index Of Agreement
LES	Large-Eddy Simulations
LE	Latent Heat Flux
MB	Mean Bias
NSC	Normalized Sensitivity Coefficient
OSR	Outgoing Shortwave Radiation
PCA	Principle Component Analysis

List of abbreviations

Prec	Precipitation
PPFD	Photosynthetic Photon Flux Density
PEST	Parameter ESTimation (tool)
PREDVAR	PREDictive error VARiance – PEST utility
PREDUNC	PREDictive UNCertainty – PEST utility
PWTADJ1	Automate Weights-Adjustment – PEST utility
QC	Quality Control
R ²	Coefficients Of Determination
Res	Energy Balance Residual
RH	Relative Humidity
RMSE	Root Mean Square Error
Rn	Net Radiation
SD	Standard Deviation
SENSAN	Sensitivity Analysis Program – PEST utility
SoilM	Soil Moisture
SoilT	Soil Temperature
SurfaceT	Infrared Surface Temperature
SRTM	Shuttle Radar Topographic Mission
TERENO	TERrestrial ENvironmental Observatories
T _s	Soil Temperature
VHC	Vertical Hydraulic Conductivity
WindD	Wind Direction
WindS	Wind Speed

List of figures

1.1	The PhD dissertation flowchart	8
2.1	Satellite images of the EC sites in TERENO prealpine region	11
2.2	Missing value percentage of the turbulent fluxes at the EC sites	17
2.3	Daily variations of T_s , R_n , θ_v and Prec at Fendt site	18
2.4	Daily variations of OSR and albedo values in the TERENO region	21
2.5	Turbulent flux deriviers via a PCA analysis	23
2.6	Monthly mean diurnal variation of H and LE at the TERENO EC sites	24
2.7	Diurnal cycle of seasonal variations of the energy fluxes at Fendt site	25
2.8	Intercomparison of turbulent fluxes <i>vs.</i> available energy in TERENO sites ..	27
2.9	Seasonal 24-h cycle of the residual energy at the TERENO EC sites	28
2.10	Turbulent fluxes <i>vs.</i> available energy at the EC sites	29
2.11	Diurnal variations of surface heat fluxes and EBR in TERENO region	30
2.12	Footprint climatology of the Fendt EC site	31
2.13	Footprint climatology of the Rottenbuch EC site	31
2.14	Footprint climatology of the Graswang EC site	32
3.1	Rott and Upper-Ammer catchments in the TERENO prealpine region	36
3.2	Landuse, soil type/texture and terrain slope maps of TERENO catchments ..	37
3.3	Calendar plots for daily concentrations of turbulent fluxes at the EC sites	45
3.4	Distributions of ET and surface temperature in TERENO catchments	46
3.5	Simulated <i>vs.</i> measured discharges in Rott and Upper-Ammer catchments ..	47
3.6	Simulated <i>vs.</i> measured soil moisture values at the EC sites	49
3.7	Distributed soil moisture maps for the TERENO catchments	50
3.8	Simulated <i>vs.</i> measured diurnal cycle of EB components at the EC sites	51
3.9	Intercomparison of EB components at the TERENO EC sites	52

List of figures

3.10	Distributed maps of surface energy fluxes at the TERENO catchments	53
3.11	Copula densities of discharge and soil moisture in TERENO region	56
3.12	Copula densities of H and LE in TERENO region	57
4.1	Maps of elevation, soil type and landuse for the Rott catchment	62
4.2	Inverse modeling flowchart for the developed GEOtop-PEST interface	67
4.3	Parameter sensitivity results for the variables of discharge, H and LE	69
4.4	Development of Φ and λ during PEST optimization iteration process	70
4.5	Measured vs. simulated: hourly discharge and monthly diurnal H/LE	73
4.6	Parameter group's contribution analysis	76
4.7	Worth of observation groups on landuse parameter confidence ellipses	77
4.8	Same as in Fig. 4.7, but for soil parameters	78
4.9	Same as in Fig. 4.7, but for landuse and soil/water flow parameters	79
4.10	PCA-based analysis of the model parameters	80

List of tables

2.1	EC sites description at the TERENO prealpine region	12
2.2	Measurement devices and meteorological parameters at the Fendt site	14
2.3	Overall flag system for the EC data	15
2.4	Percentage of missing values for turbulent fluxes in TERENO EC sites	16
2.5	Energy partitioning for individual seasons at the EC sites	20
2.6	Seasonal EBR for the TERENO region	27
3.1	Calibrated model parameters	42
3.2	Statistical metrics used for model performance evaluation	43
3.3	Statistical metrics for discharge and soil moisture at TERENO region	48
3.4	Statistical metrics for EB components at Fendt and Rottenbuch sites	51
4.1	GEOtop model input parameters selected for the sensitivity analysis	68
4.2	Summary of the calibrated parameters	71
4.3	Summary of the residuals calculated for the observation groups	72
4.4	Summary of the statistical metrics	73
4.5	Summary of the model parameter's uncertainty analysis	74

Abstract

In the TERrestrial ENvironmental Observatories (TERENO) prealpine region, the temporal and spatial variability of water and energy fluxes is highly influenced by the heterogeneity of land-surface characteristics. In this region, ecohydrometeorological variables and processes like soil moisture, evapotranspiration (ET), vegetation type and dynamics, and surface heat fluxes exhibit rapid changes within short distances. This is mainly due to the heterogeneity in topography, soil-landuse properties, and land-surface interactions. The energy –and water budgets in such environments are thus highly controlled by the domain characteristics. Therefore, accurate spatial variability of the hydrometeorological variables can be only achieved with a distributed physically-based high resolution hydrologic modelling approach. Such models take into account all domain characteristics by simultaneously solving the water and energy balance over complex mountain terrain.

This PhD thesis investigates: i) the turbulent flux variability and energy balance closure, ii) the spatiotemporal variability and dependence structure of the coupled water –and energy fluxes (via forward modeling), iii) and the sensitivity and uncertainty pertaining to hydrological model parameters (via inverse modeling) in the TERENO prealpine region, southern Germany. This is achieved by i) using the Eddy Covariance technique (EC), ii) application of the distributed hydrological model GEOtop and empirical Copulas, iii) and a combination of GEOtop and the Parameter ESTimation tool (PEST) for this complex region. To obtain the above research objectives as best as possible, this thesis is structured and organized into three main-result parts as follows:

In the first part, the turbulent flux variability and energy balance closure (EBC) is characterized for the TERENO EC sites during 2013-2014. The main goals are to characterize the multiscale variations and drivers of the turbulent fluxes, as well as to quantify the EBC. The results show significant differences in the mean diurnal

variations of the turbulent fluxes. The radiation (29.5%) and temperature (41.3%) components are found as the main drivers of turbulent fluxes. A general lack of EBC is observed. On average, 80% of the flux footprint is emitted from a radius of 250 m around the EC stations.

In the second part, the spatiotemporal variability and dependence structure patterns of the coupled water and energy fluxes are quantified using the GEOtop model and empirical Copulas for the Rott (~55 km²) and Upper-Ammer (~300 km²) catchments in the TERENO prealpine region over two summer episodes in 2013 and 2015. GEOtop is capable of quantifying the temporal and spatial variability of the water and energy budgets with consideration for elevation-gradient effect of this heterogeneous landscape, which is confirmed by the linear statistical metrics applied for the model performance evaluation. Furthermore, the empirical Copula-based dependence structures of the measured and simulated hydrometeorological variables indicate that the highest densities are found in the lower and upper ranks. This suggests a reasonable performance of the model for the low and high values, which, the model has poorer performance in the middle ranks of the data.

In the third part, an inverse modeling of the streamflow and turbulent fluxes together with the associated parameter sensitivity and uncertainty analysis is performed using the developed GEOtop-PEST interface in the Rott catchment over two summer episodes in 2013 and 2015. Using this interface, the value added by including turbulent flux data in the parameter estimation process is particularly investigated, and the impact of the additional flux data on the uncertainty bounds is analyzed. A set of model parameters that allowed reproducing both observed streamflow and turbulent heat fluxes were identified. The majority of the estimated parameters were highly sensitive to the considered variables. It was found that the confidence bounds of estimated parameters are narrowed significantly when considering not only streamflow observations, but additionally turbulent flux measurements in the calibration process. Also, correlations between estimated parameters could be reduced.

The results presented in this thesis contribute to further improve our understanding of the hydrometeorological impacts, land-atmosphere interactions and the hydrological cycle in time and space over the TERENO prealpine region.

Zusammenfassung

Die Region Bayerische Voralpen ist eine der Zielregionen der Observatorien des interdisziplinären und langfristigen Forschungsprogramms TERENO (TERrestrial ENVironmental Observatories). In dieser Region sind die zeitliche und räumliche Variabilität von Wasser- und Energieflüssen stark von der Heterogenität der Landoberflächenparameter abhängig. Ökohydrometeorologische Variablen und Prozesse, wie etwa Bodenfeuchte, Evapotranspiration (ET), Vegetationstyp und –dynamik oder turbulente Wärmeflüsse, weisen starke Änderungen innerhalb geringer Distanzen auf, hauptsächlich aufgrund der Heterogenität von Topographie, Boden und Landnutzungseigenschaften und Land-Oberflächen-Interaktionen. Der Energie- und Wasserhaushalt in solchen Regionen wird folglich in besonderem Maße von den Gebietseigenschaften kontrolliert. Daher kann eine akkurate räumliche Vorhersage von hydrometeorologischen Variablen nur mit einem räumlich distributiven und hochaufgelösten Modellansatz erfolgen. Solche Modelle berücksichtigen alle Gebietseigenschaften und lösen gleichzeitig die Wasser- und die Energiebilanz.

Diese Dissertation untersucht: i) die Variabilität der turbulenten Flüsse sowie die Schließung der Energiebilanz, ii) die raumzeitliche Variabilität und Abhängigkeitsstruktur der gekoppelten Wasser- und Energieflüsse (mittels Vorwärtsmodellierung), und iii) die Sensitivität und Unsicherheit in Bezug auf die hydrologischen Modellparameter (mittels inverser Modellierung) in der TERENO-Region Voralpenland. Erzielt wird dies durch i) Benutzung der Eddy-Kovarianz Methode (EC), ii) Anwendung des distributiven hydrologischen Modell GEOTop und empirischen Copulas, und iii) einer Kombination von GEOTop und dem Parameter ESTimation tool (PEST). Diese Dissertation ist wie folgt in drei Hauptkapitel unterteilt:

Im ersten Teil werden die Variabilität der turbulenten Flüsse sowie die Schließung der Energiebilanz (*energy balance closure*, EBC) für die TERENO EC Standorte charakterisiert (2013-2014). Die Hauptziele sind die Charakterisierung der mehrskaligen Variationen und Einflussfaktoren der turbulenten Flüsse, sowie die

Quantifizierung der EBC. Die Ergebnisse zeigen signifikante Unterschiede in den durchschnittlichen täglichen Variationen der turbulenten Flüsse. Als Haupteinflussfaktoren der turbulenten Flüsse konnten die Komponenten Strahlung (29,5%) und Temperatur (41,3%) festgestellt werden. Insgesamt konnte die Energiebilanz nur mäßig bis schlecht geschlossen werden. Durchschnittlich stammen 80% der Flussgrundfläche (*footprint*) aus einem Radius von 250 m um die EC-Stationen.

Im zweiten Teil werden die raumzeitliche Variabilität und Muster der Abhängigkeitsstruktur der gekoppelten Wasser- und Energieflüsse unter Benutzung des GEOTop Modells und empirischen Copulas für die Einzugsgebiete Rott (~ 55km²) und Obere Ammer (~ 300 km²) in der TERENO Voralpenlandregion über die zwei Sommerepisoden 2013 und 2015 quantifiziert. GEOTop ist in der Lage, die temporäre und räumliche Variabilität von Wasser- und Energiehaushalten unter Berücksichtigung von verschiedenen Höhengradienten in dieser heterogenen Landschaft zu quantifizieren. Dies wird durch die zur Evaluierung der Modellperformanz angewandten linearen statistischen Kriterien bestätigt. Darüber hinaus indizieren die empirischen Copula-basierten Abhängigkeitsstrukturen der gemessenen und simulierten hydrometeorologischen Variablen, dass die höchsten Copula-Abhängigkeiten in den unteren und oberen Rängen gefunden werden. Das spricht für eine sinnvolle Performanz des Modells für die niedrigen und hohen Werte. Die Modellperformanz ist für die mittleren Ränge der Daten geringer.

Im dritten Teil wird eine inverse Modellierung des Abflusses und der turbulenten Flüsse zusammen mit den assoziierten Parametersensitivitäten und Unsicherheitsanalysen unter Anwendung des entwickelten GEOTop-PEST Interface für das Rott-Einzugsgebiet und für die Sommerepisoden 2013 und 2015 ausgeführt. Unter Benutzung dieses Interface wird der durch die Integration von turbulenten Flüssen in den Prozess der Parameterschätzung hinzugefügte Wert ermittelt und der Einfluss der zusätzlichen Fluss-Daten auf die Unsicherheitsgrenzen analysiert. Eine Auswahl von Modellparametern, welche das Reproduzieren des Abflusses und der turbulenten Wärme Flüsse erlaubt, wurde identifiziert. Der Großteil der geschätzten Parameter war sehr sensitiv für die betrachteten Variablen. Es konnte festgestellt werden, dass sich die Konfidenzintervalle der geschätzten Parameter reduzieren, wenn man nicht nur Abflussmessungen, sondern zusätzlich Messungen turbulenter Flüsse in den Kalibrierprozess miteinbezieht. Weiterhin konnten Interkorrelationen zwischen den geschätzten Parametern reduziert werden.

Die in dieser Dissertation präsentierten Resultate tragen zu einem besseren Verständnis von hydrometeorologischen Einflüssen, Land-Atmosphären Interaktionen sowie dem hydrologischen Kreislauf in der TERENO Voralpenregion bei.

Chapter 1

Introduction

1.1 Motivation and objectives

Mountain areas are characterized by steep topographically induced-climate gradients, enabling the study of climatic-zones in short distances. An amplified climate change and high variability has been notably observed in such regions. Global change has induced alterations in climate and environment, water resources and land productivity as well as hydrometeorological variables including water- and energy cycles. However, these changes are diverse, interlinked, exhibit complex feedback mechanisms, and happen in different times and spaces. In general, mountains and the prealpine areas take up some considerable parts of the lands in our planet *Earth*, and are recognized as water-towers. Thus, the spatiotemporal variability of the water cycle over mountain areas and in prealpine areas needs to be better understood. In this context, the importance of prealpine regions could be even more highlighted than highlands; as in many cases, unlike the high-mountain areas, the prealpine areas are typically densely populated regions. Therefore, finding solutions to the impacts of global change i.e., climate and land-cover change, on prealpine environments remains an important environmental research.

To address these challenges specifically for prealpine areas, improved process understanding of water-, energy- and matter exchanges and the development of mitigation and adaptation strategies are required. Hence, an integrated, multi-compartment of atmosphere-pedosphere-hydrosphere measuring infrastructure for environmental monitoring and research has been established in the TERrestrial ENvironmental Observatories (TERENO) region in southern Germany. TERENO prealpine aims at interdisciplinary-research studies in the region. This includes the analysis of the spatiotemporal variability and interaction of water-, energy- and

nutrient cycles and the associated exchange processes with the atmosphere and the hydrosphere.

The region of the TERENO-prealpine observatory has been exposed to more intense warming compared to the global average trend. Also, more frequencies of extreme-hydrological-related events like droughts and intensive rainfall have been observed in the region (Böhm et al., 2001, Calanca, 2007). For instance, the temperature time-series analysis for the Mount Hohenpeissenberg station has been revealed a mean temperature increase of 1.5°C for the years 1880-2012. This corresponds to around twice the globally averaged combined land and ocean surface temperature increase of 0.78 °C, and also clearly exceeds the average global land temperature increase of 1.17 °C for the same period (<https://www.ncdc.noaa.gov/>), as described in Kiese et al. (2018).

Previous studies in the TERENO-prealpine observatory and the surrounding areas like e.g. Bavarian Alpine foothills and low mountain-range, have mainly focused on how climate change impacts runoff generation (Kunstmann et al., 2004), runoff production processes and discharge-related analysis (Wetzel et al., 2003, 2004a, 2005a), surface and sub-surface water balances (Kunstmann et al., 2006; Ott et al., 2013; Wolf et al., 2016), biosphere-atmosphere exchange and greenhouse gases (Unteregelsbacher et al., 2013; Wang et al., 2014; Wolf et al., 2016; Zeeman et al., 2017), energy balance closure parameterization (Eder et al., 2014), and calibrations of different hydrological models against runoff measurements (Kunstmann et al., 2006) and water and energy fluxes (Kunstmann et al., 2013; Hingerl et al., 2016).

An important question has not been yet fully addressed in the TERENO-prealpine observatory, that is: *what is the hydrometeorological variability and the hydrological processes in time and space for this region?* To appropriately consider this issue, very comprehensive measurements are needed. With no doubt, these measurements are costly, and thus limited as they are only available for some selected points within a large area. In other words, obviously the available in-situ measurements do not cover the entire region. This lack of data could be even more challenging for the southern portion of the TERENO-prealpine region, which is mostly described by a steep-gradient and heterogeneous landscape. A solution to this crucial problem of course is to employ a distributed process-based hydrological model.

In brief, in the TERENO-prealpine region, rainfall, temperature, soil moisture, as well as the radiative and turbulent heat fluxes etc., exhibit rapid changes within short distances due to the complex orography and heterogeneity in topography, soil hydraulic properties, landuse, landscape, climate as well as surface-subsurface and atmospheric boundary layer interactions. The energy- and water budgets in such environments are thus highly controlled by soil type properties (Pielke et al., 1998), landcover characteristics (Dirmeyer et al., 2010), and vegetation structure (Pielke et al., 2011). Therefore, the full spatial prediction of hydrometeorological variables can

only be achieved with a distributed high-resolution hydrologic modeling approach. Such models explicitly take into account all of the domain characteristics by simultaneously solving the water- and energy balance over complex mountain terrain (Beven, 2001; Bronstert et al., 2002). To validate the performance of hydrological models, the outputs are compared against observation-based runoff data and, more recently, micrometeorological measurements derived from Eddy Covariance (EC) techniques (e.g. Hingerl et al., 2016). Traditionally, linear statistical metrics such as correlation coefficient (r) are used for model evaluation. However, using simple linear r -values between simulated and observed hydrometeorological variables, which typically exhibit nonlinear characteristics, may not be appropriate to determine these complex relationships (Bárdossy and Pegram, 2009). Instead, Copula-based functions can appropriately obtain underlying dependence structures of these variables (Genest et al., 2007; Laux et al., 2011).

Furthermore, the estimation of parameters is crucial for the successful application of distributed hydrological models, as heterogeneity needs to be accounted for and large uncertainties exist in the parameter values, which usually cannot be measured directly at fields. Even in physically based hydrological models, some parameters may remain that must be calibrated to obtain a satisfactory output (Liu et al., 2005). Fully distributed and physically based hydrological models are usually much more CPU-time demanding than pure lumped models. Typically, the “trial and error” method is applied for model calibration, which is simple and accordingly has been widely used for hydrological models (e.g. Kunstmann et al., 2006; Hingerl et al., 2016). As this approach is time consuming, automatic optimization algorithms like the Gauss-Marquardt-Levenberg (GML) algorithm, as realized in the Parameter ESTimation tool (PEST), are applied allowing to facilitate this effort (Kunstmann et al., 2006; Lin, 2011). GML algorithm estimates the parameters using fewer model runs than any other optimization technique for nonlinear models (e.g. Monte-Carlo-based algorithms) (Doherty, 2002; Bahremand and Smedt, 2006). Thus, automatic calibration approach can be fast and the results are expected to be more robust than those obtained by the manually based calibration approach (Bahremand and Smedt, 2008).

In this dissertation, accordingly, to fully describe and analyze the hydrometeorological variability and the hydrological processes in the TERENO-prealpine observatory, the following three major parts are conducted:

- *In the first part*, the observed radiative and turbulent fluxes variabilities at monthly- and seasonally-based scales, the energy balance closure problem (EBC), together with the flux footprint climatology are quantified. More details are given at *Sect. 1.1.1*.
- *In the second part*, a forward modeling with a focus on *model’s variables* is conducted using the hydrological model GEOTop and Copula-based functions, where the spatiotemporal variability and dependence structure of the coupled

water and energy variables is in turn modeled and analyzed. More details are given at *Sect. 1.1.2*.

- *In the third part*, an inverse modeling with a focus on *model's parameters* is performed using the developed GEOTop-PEST interface, where the model parameter's sensitivity and uncertainty analysis is considered. More details are given at *Sect. 1.1.3*.

1.1.1 Turbulent flux variability and energy balance closure

The energy exchange processes between the land surface and the atmosphere is one of the central research questions in the TERENO-prealpine observatory. The surface turbulent fluxes, for example, are highly influenced both by the characteristics of the airflow and the structures of the underlying surface. Also, the Energy Balance Ratio (EBR) or the relative Energy Balance Closure (EBC) (Aubinet et al., 2000) remains unclosed at most Eddy Covariance (EC) sites (e.g. Hendricks Franssen et al., 2010; Stoy et al., 2013; Imukova et al., 2016). In the literature, there are not adequate research studies on the surface energy and water flux variations for the TERENO prealpine region.

Therefore, the objectives of the first part of the thesis are to quantify: i) the surface energy and water fluxes variability, i.e. the spatiotemporal variations of the sensible and latent heat fluxes, soil moisture contents, and the energy partitioning conditions, ii) the main drivers of the turbulent heat fluxes, iii) the EBC and residual energy, as well as the possible reasons for the lack of EBC at the TERENO-prealpine EC sites.

1.1.2 Forward modeling: coupled water and energy variables

In the TERENO-prealpine observatory the hydrometeorological variables and the hydrological processes exhibit rapid changes within short distances. This is mainly due to the complex orography and small-scale heterogeneity in the land-surface characteristics (Kunstmann et al., 2006; Hingerl et al., 2016). For this environment, therefore, the distributed hydrological model GEOTop is applied to accurately quantify the variability of the water and energy budgets in time and space. For model performance evaluation, unlike the traditional ways, Copula-based functions are employed to obtain underlying dependence structures between simulated and observed hydrometeorological datasets. In the literature, the hydrological models were only calibrated against discharge (i.e. Kunstmann et al., 2006; Hingerl et al., 2016), and no soil moisture profile variation or turbulent flux variability have been accounted for in the simulation. Moreover, previous studies only attempted to evaluate the models' performances using the traditional linear statistical metrics (e.g. R^2 , RMSE).

Therefore, in the second part of the thesis the focus is on the *model's variables* in time and space, and the following specific objectives are addressed: i) quantifying the spatiotemporal variability of the hydrometeorological variables of the turbulent fluxes as well as the surface temperature and ET with respect to the elevation-gradient effect using EC-based measurements and hydrological simulations, ii) simulating the coupled water and energy balances at a very high spatial resolution using GEOtop, and iii) estimating the underlying dependence structures of the observed and modeled water and energy fluxes using the nonlinear-based approach bivariate empirical Copula in the TERENO-prealpine region.

1.1.3 Inverse modeling: parameter sensitivity and uncertainty analysis

The fully distributed and physically-based hydrological model GEOtop is quite complex, and thus its parameters need to be estimated. For model calibration, unlike the typical method i.e. “trial and error”, the GML automatic optimization algorithm as realized in PEST is used. Traditionally, only discharge data have been available for model calibration. However, the TERENO region is rather rich in terms of data availability e.g. hydrometeorological datasets of surface heat fluxes and streamflow. This data availability, together with the use of PEST, makes it possible to characterize how the additional values of observations involved in the calibration process may influence the uncertainty range and confidence ellipses pertaining to the model parameters. Thus, the hydrological model GEOtop is coupled to PEST, for an inverse modeling to estimate the model's parameters and their uncertainties in the Rott catchment located in the northern portion of the TERENO-prealpine observatory.

Therefore, in the third part of the thesis the focus is on the *model's parameters*. Using the developed GEOtop-PEST interface, the main objectives are to quantify: i) the uncertainties pertaining to the estimated model parameters, for which it is particularly examined the benefit of additional heat flux observations on the parameter confidence bounds, and ii) the intercorrelations between the model estimable parameters and their contributions in the calibration process.

In the literature, there is no attempt yet to describe and analyze the model's parameters-related uncertainty and their intercorrelations for this region.

1.2 Innovation

The principle innovations of this dissertation include:

- The first analysis on the multiscale turbulent flux variability, as well as further investigation on the EBC problem and the possible reasons for the energy imbalance in the TERENO prealpine region;
- Identification of the main drivers of turbulent fluxes via a Principal Component Analysis (PCA) technique in the TERENO-prealpine EC sites for the first time;
- The first analysis of flux footprint climatology for the study EC sites;
- Distributed modeling of the complete terrestrial water and energy cycle including most relevant physical processes using a high-resolution model in the TERENO-prealpine catchments;
- Employing new approach for the evaluation of the model's performance based on empirical Copula-based functions;
- Inverse modeling via developing the GEOtop-PEST interface, *not only* for automatic optimization, *but also* for the model's parameter sensitivity and uncertainty analyses; particularly to examine the added value of the additional hydrometeorological variables on top of runoff for the parameter estimation in the TERENO-prealpine observatory.

The scientific findings of this dissertation, *either* as first-author *or* co-author, have been successfully resulted in four peer-reviewed-ISI publications as listed below:

- **Soltani, M.**, Mauder, M., Laux, P., Kunstmann, H. (2017) Turbulent flux variability and energy balance closure in the TERENO prealpine observatory: A hydrometeorological data analysis. *Theor Appl Climatol*. DOI: 10.1007/s00704-017-2235-1.
- **Soltani, M.**, Laux, P., Mauder, M., Kunstmann, H. (2018) Spatiotemporal variability and empirical Copula-based dependence structure of modeled and observed coupled water and energy fluxes. *Hydrology Research*. DOI: 10.2166/nh.2018.163.
- Mauder M. S. Genzel, J. Fu, R. Kiese, **M. Soltani**, R. Steinbrecher, M. Zeeman, H. Kunstmann (2017). Evaluation of two energy balance closure adjustment methods by independent evapotranspiration estimates from lysimeters and hydrological simulations. *Hydrological Processes*. 2018;32:39-50. <https://doi.org/10.1002/hyp.11397>.
- Kiese, R., B. Fersch, C. Baeßler, C. Brosy, K. Butterbach-Bahl, C. Chwala, M. Dannenmann, J. Fu, R. Gasche, R. Grote, C. Jahn, J. Klatt, H. Kunstmann, M. Mauder, T. Rödiger, G. Smiatek, **M. Soltani**, R. Steinbrecher, I. Völksch, J. Werhahn, B. Wolf, M. Zeeman, H.P. Schmid (2018). The TERENO-preAlpine

Observatory integrating meteorological, hydrological and biogeochemical measurements. *Accepted in Vadose Zone Journal*.

Also, one additional article has been submitted for publication as follows:

- **Soltani, M.**, Laux, P., Mauder, M., Kunstmann, H. (2018) Inverse distributed modeling of streamflow and turbulent fluxes: A sensitivity and uncertainty analysis coupled with automatic optimization. *Under Review*.

1.3 Thesis structure

This dissertation consists of three main-result parts. Each part could be independent and requires specific techniques and strategies. Each of these parts thus starts with an introduction on the particular background followed by a description of the methods applied and ends with a main summary. In total, this PhD dissertation has five chapters, as described below.

Chapter 1 is describing the motivation and objectives of three main parts of the thesis and highlights the innovations. Chapter 2 characterizes the turbulent flux variability and EBC in the TERENO prealpine EC sites. It follows closely of the findings of Soltani et al. (2017). Chapter 3 quantifies the spatiotemporal variability and empirical Copula-based dependence structure of the coupled water and energy fluxes. This chapter is based on Soltani et al. (2018). Chapter 4 describes the combination of GEOTop with PEST for inverse modeling, and the model's parameter sensitivity and uncertainty analysis. This chapter is related to Soltani et al. (2018) (submitted). Chapter 5 draws the synthesized-final conclusions along with the corresponding outlook. Figure 1.1 illustrates how the five chapters of this dissertation are interconnected.

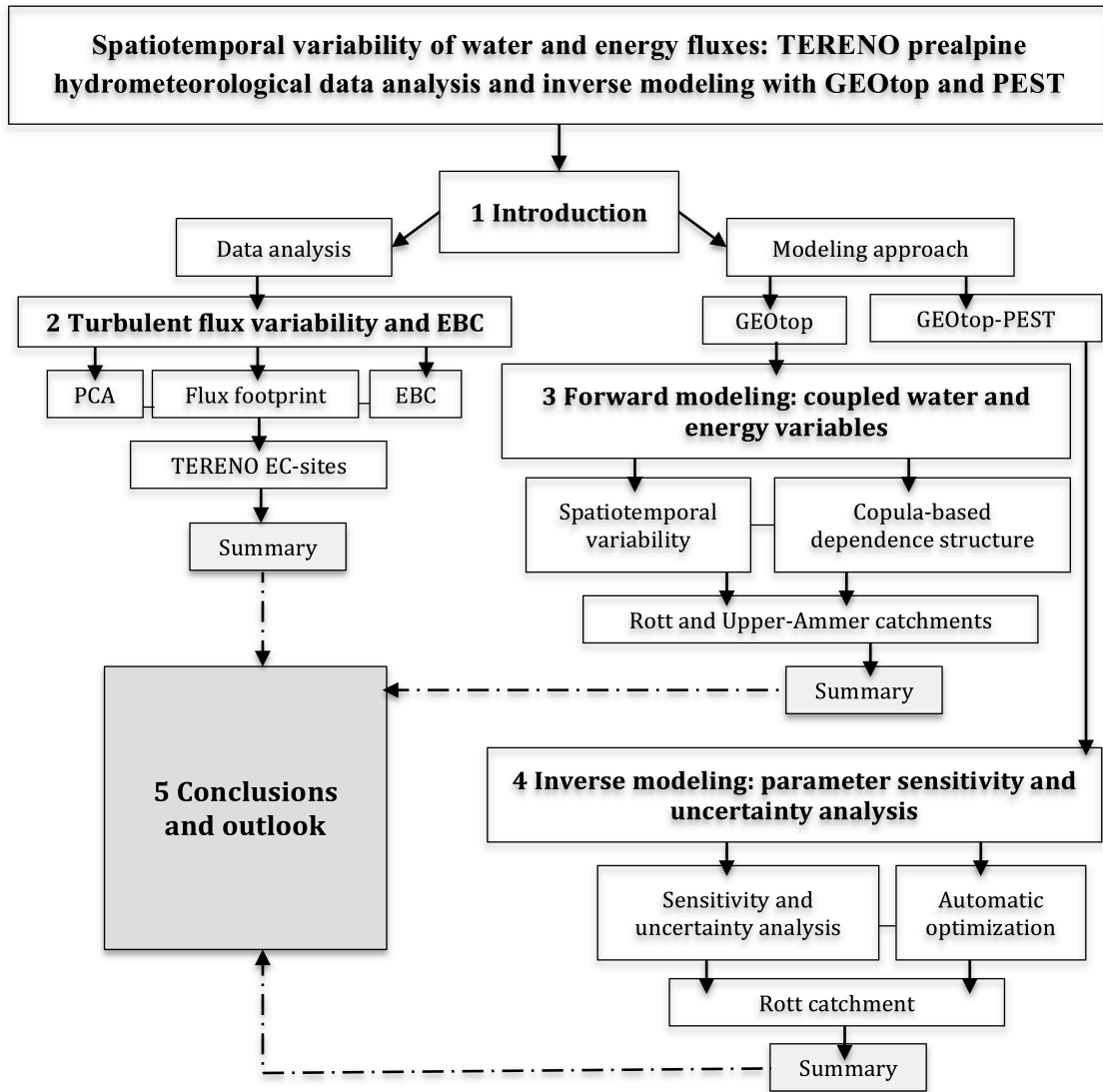


Figure 1.1: The PhD dissertation flowchart.

Chapter 2

Turbulent flux variability and energy balance closure in the TERENO prealpine observatory: A hydrometeorological data analysis*

2.1 Introduction

The energy exchange between the land surface and the atmosphere is one of the crucial processes in any ecosystem (Berry and Dennison 1993). The surface turbulent fluxes are influenced both by the characteristics of the airflow and the structures of the underlying surface (Wyngaard 1990). The Eddy Covariance (EC) technique is the most direct way to estimate turbulent fluxes within the atmospheric boundary layer in any ecosystem (Swinbank 1951; Baldocchi et al., 1988; Verma 1990; Mauder and Foken, 2006; Mauder et al., 2006). Its main challenges include system design, implementation, and processing of a large volume of data (Stull 1988; Foken 2009; Foken et al., 2010; Burba 2013). Via the EC technique, flux footprint information can be assessed (Schmid 1994) and quasi continuous flux measurements can be aggregated across different time scales, i.e. at hourly, daily, seasonal and annual time scales (Wofsy et al., 1993; Baldocchi et al., 2001; Cava et al., 2008; Nakai et al., 2006). Moreover, the general characteristics of hydrometeorological variability and canopy exchange processes can be identified (Foken et al., 2011).

A multitude of experimental research has been conducted on the measurements of the daily, monthly and seasonal variations of heat, water vapor and CO₂ exchanges over heterogeneous lands in different ecosystems using the EC technique, such as cropland sites (e.g. Xu et al., 2011; Schmidt et al., 2011; Wizenmann et al., 2014), forest environments (e.g. Launiainen et al., 2005; Sanchez et

* This chapter follows closely Soltani *et al.*, (2017)

al., 2010), grasslands and paddy fields (e.g. Wang et al., 2010; Wohlfahrt et al., 2010; Li et al., 2013), and tropical and savanna areas (e.g. Steven et al., 2005; Mauder et al., 2007).

Currently, there are not many research studies on the surface energy and water flux variations for the prealpine region in the literature. Here, an analysis of a two-year dataset of the EC measurements (2013-2014) over three experimental sites, situated in prealpine and mountainous areas in southern Germany, is presented. Previous work in this region has focused on the impact of climate change on the runoff generation and hydrological aspects of the Ammer river catchment (Kunstmann et al., 2004; Ott et al., 2013), greenhouse gas fluxes (Unteregelsbacher et al., 2013), water –and energy flux observation and modeling (Kunstmann et al., 2013; Hingerl et al., 2016), soil-atmosphere exchange of N₂O and CH₄ (Wang et al., 2014), biosphere-atmosphere exchange of greenhouse gases (Wolf et al., 2017; Zeeman et al., 2017), and the evaluation purposes of semi-empirical energy balance closure (EBC) parameterizations (Eder et al., 2014). Since the diurnal –and daily flux variability is represented by the data, the focus is set on the characterization of the monthly and seasonal variability of the water and energy fluxes, as well as the energy balance closure between the study sites. Therefore, the objectives are to quantify: i) the surface energy and water fluxes variability, i.e. the spatiotemporal variations of the sensible and latent heat fluxes, soil moisture contents and the energy partitioning conditions, the main drivers of the turbulent heat fluxes; and ii) the EBC and residual energy, as well as the possible reasons for the lack of EBC at the TERENO prealpine EC sites.

2.2 Site characterization and measurement setup

2.2.1 Geography and climate

The TERrestrial ENvironmental Observatories (TERENO) prealpine region is located in southern Germany, where three EC stations are established in the areas of Fendt, Rottenbuch, and Graswang. Geographically, the Fendt site is within the northern part of the region and it is recognized as the TERENO prealpine super site, while the Rottenbuch and Graswang sites are located in the middle and southern parts of the region, respectively (see Figure 2.1). The elevation ranges between 543 m in the north and 2129 m a.s.l. in the southern regions. The climate of the region is cool-temperate and humid. The mean annual air temperature is approximately 7-8 °C in the alpine foreland and approximately 4-5 °C in the southern mountainous region. The northern area of the region receives an annual mean precipitation of approximately 1100 mm, while the summits of the Ammer Alps in the southern regions receive approximately 2000 mm. Maximum precipitation is in June and July (Kunstmann et al., 2006). Summer rains are characterized by convective events, causing a high variability in the location and intensity of rainfall. The main prevailing wind flow at individual stations

is shown in Figure 2.1. More details about the characteristics of the TERENO prealpine EC sites are provided in Table 2.1.

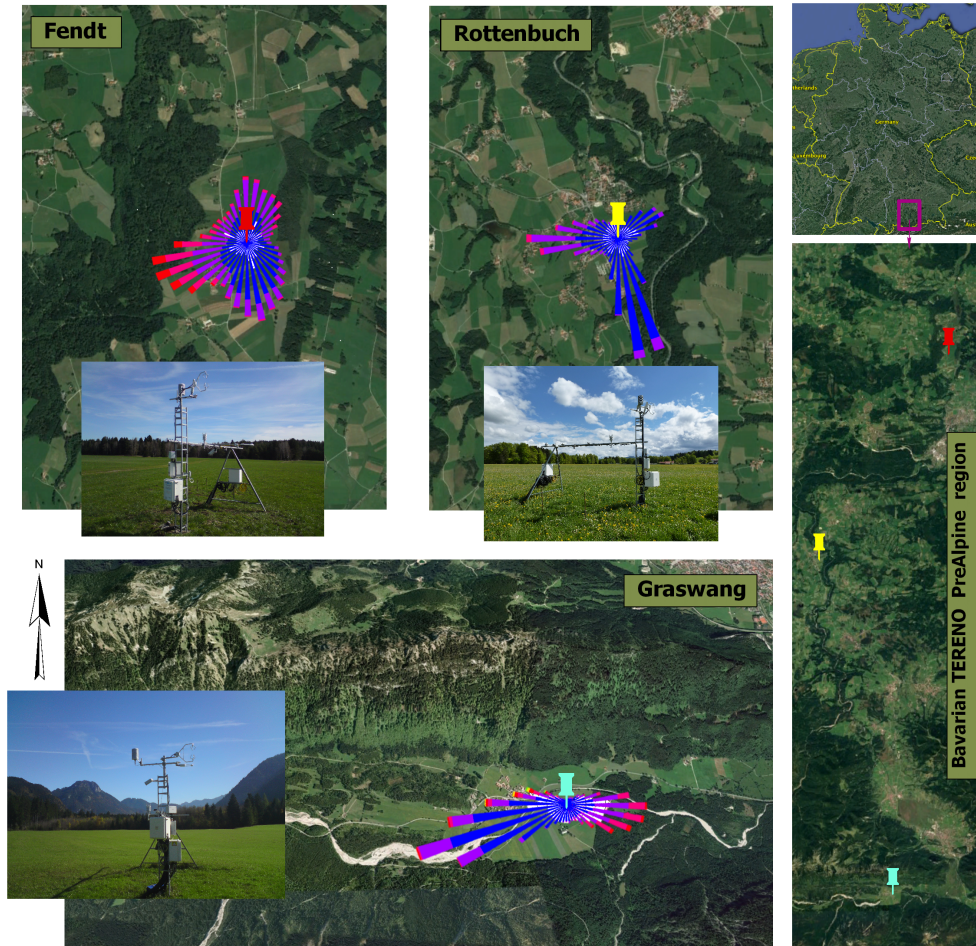


Figure 2.1: Satellite images of the EC sites in the TERENO prealpine region (the approximate landscape area is $10 \text{ km} \times 40 \text{ km}$) in southern Germany are shown at the maps on the right; the pins in the maps on the left indicate the approximate location of each EC site (the approximate flux footprint area is $2.5 \text{ km} \times 5 \text{ km}$). The wind-rose diagrams are also overlaid (with the wind speed ranging from 1 to 11 m s^{-1} identified by the colors from blue to red, respectively). The prevailing background vegetation type is grassland for the three sites.

2.2.2 Data processing

Calculation of turbulent fluxes

The calculation of turbulent fluxes was done using the TK3 eddy covariance software. TK3 is able to perform all of the post-processing of turbulence measurements to produce the turbulent fluxes (Mauder and Foken, 2015). It includes necessary

2 Turbulent flux variability and EBC

corrections and tests (Lee et al., 2004, Aubinet et al., 2012). The basic principle of the EC measurements is that the vertical flux is calculated as a covariance between the concentration of a scalar (e.g. air temperature, water vapor, etc.) and the vertical wind velocity measured at the same point in space and time (Mauder and Foken, 2015).

Table 2.1: EC sites description at the TERENO prealpine region. Soil type characteristics and analysis of soil texture is according to Pütz et al. (2016).

Site name	Fendt	Rottenbuch	Graswang
Location	47.831 °N, 11.061 °E	47.730 °N, 10.061 °E	47.571 °N, 11.032 °E
Elevation	598 m	770 m	860 m
Slope	< 5 °	< 5 °	< 5 °
Climate	Cool-temperate and humid	Cool-temperate and humid	Cool-temperate and humid
Mean annual air temperature	9.3 °C	8.6 °C	7.0 °C
Mean annual precipitation	962 mm	1047 mm	1464 mm
Vegetation type	Grassland	Grassland	Grassland
Soil type (Texture: sand/silt/clay [%])	Cambic Stagnosol (27/43/30)	Cambic Stagnosol (26/45/29)	Fluvisol Calcic (9/39/52)
Canopy height range	5-30 cm	5-45 cm	5-35 cm

The turbulent fluxes of sensible heat (H) and latent heat (LE) can be calculated as (Kaimal and Finnigan, 1994):

$$H = \bar{\rho} C_p \overline{w' T'} \quad (2.1)$$

$$L_E = \bar{\rho} L_v \overline{w' q'} \quad (2.2)$$

where ρ , C_p and L_v denote the density of air (kg/m^3), the specific heat of air (J/kg K), and latent heat of evaporation (J/kg), respectively. w' , T' and q' are the fluctuations in the vertical wind component (m/s), air temperature ($^{\circ}\text{C}$) and specific humidity, respectively. For more information regarding the calculation of turbulent fluxes and quality control (QC) using the TK3 software, it is referred to Mauder et al. (2013) and Mauder and Foken (2015).

The energy balance ratio (EBR) or the relative energy balance closure is defined as (Aubinet et al., 1999):

$$\text{EBR} = \frac{\sum(\text{LE} + \text{H})}{\sum(\text{Rn} - \text{G})} \quad (2.3)$$

with LE denoting the latent heat flux (W/m^2), H the sensible heat flux (W/m^2), Rn the net radiation (W/m^2), and G the soil heat flux (W/m^2) at the surface (Harazono et al., 1998; Burba et al., 1999). EBR remains unclosed at most EC sites (e.g. Panin et al., 1998; Lamaud et al., 2001; Turnipseed et al., 2002; Wilson et al., 2002; Meyers and Hollinger, 2004; Oncley et al., 2007; Hendricks Franssen et al., 2010; Stoy et al., 2013; Imukova et al., 2016). The energy storage change in the upper layer of the soil

can be as high as 40 W/m^2 , which can amount up to $\sim 20\%$ of the net radiation (Culf et al., 2004). In the study EC sites, the soil heat flux (G) plates were buried at 8 cm depth to avoid disturbances, e.g. by losing contact with underlying soil and/or water accumulation below the plates (Sanchez et al., 2010). Thus, the soil heat storage in the above 8cm depth was added to G to calculate EBR properly. The soil heat storage and the heat capacity were calculated according to the PlateCal approach of Liebethal et al. (2006) and DeVries (1963), respectively. The volumetric fraction of organic matter at the Fendt EC site is approximately 30%. In this thesis, a rain-free half-hourly dataset was collected in order to calculate the EBR. This is because open-path systems perform poorly during rainfall. Therefore, such periods must be excluded from the dataset to calculate the energy balance closure (Culf et al., 2004). The measurements by the enclosed-path systems may also be compromised, in general, when water is sucked into the sampling tube or when condensation occurs leading to severe damping of the humidity fluctuations (Kabat et al., 2004). However, at the Rottenbuch EC site, a rain-cap is used at the inlet of the enclosed-path gas analyzer in order to prevent this sucking of water during rain events and a heating at a rate of 5 W/m is applied to prevent condensation. Generally, the EC measurement are less reliable during rainy periods, turbulence cannot develop properly under these conditions. Therefore, no matter what instruments are used, data recorded during rainfall periods do not fulfill one of the basic requirements of the EC technique.

Principal component analysis

To determine the turbulent flux drivers at the study sites, a Principal Component Analysis (PCA) is applied. PCA is a technique that is used to summarize the information (i.e. the total variation it contains) in a dataset described by multiple variables and can be applied to produce linear combinations of the variables that are mutually uncorrelated. In other words, PCA reduces the dimensionality of a multivariate dataset. This is achieved by transforming the initial variables into a new small set of variables without losing the most important information in the original dataset. These new variables correspond to a linear combination of the originals and are called principal components (PCs). The PCs are ranked in that way that PC1 explains the largest fraction of the variance in a dataset, PC2 the second largest, etc. (Abdi and Williams, 2010). The main goals of the PCA include to: identify hidden patterns in the hydrometeorological dataset, reduce the dimensionality of the data by removing the noise and redundancy in the data, rank the importance of single variables within this multivariate dataset, and finally to identify and group correlated variables. In this study, the *prcomp* and *fviz_pca* functions from the built-in R *stats* and *factoextra* packages were used to perform and visualize the PCA, respectively (R Core Team, 2017). The procedure of the PCA includes the following steps:

- Preprocessing of the dataset: first, the data were centered by subtracting the mean from each variable. Second, the data were scaled in order to have a unit variance.

2 Turbulent flux variability and EBC

- Calculation of the covariance matrix of the preprocessed data.
- Calculation of the eigenvectors and eigenvalues of the covariance matrix: the numbers on the diagonal of the diagonalized covariance matrix are the eigenvalues of the covariance matrix (large eigenvalues correspond to large variances). The directions of the new rotated axes are called the eigenvectors of the covariance matrix.
- Dimension reduction and selection of principal components: eigenvectors were ordered by eigenvalues from the highest to the lowest. The number of chosen eigenvectors is then the number of dimensions of the new dataset.
- Computation of the new dataset: the transpose of the selected eigenvectors (PCs) were multiplied by the transpose of the original dataset.

The PCA technique followed closely the mathematical formulation as given in Jolliffe (2002), Dray (2008), Abdi and Williams (2010), and Lay (2012).

2.2.3 Micrometeorological measurements

The instruments for measuring the radiation components and also the turbulent fluxes at the surface layer were installed on three towers in the TERENO prealpine region. The EC instruments were installed on a station 3.5 m above the surface at all three sites. The turbulent fluxes were measured with a 3-D sonic anemometer (CSAT3, Campbell Scientific Inc, Logan, UT), oriented towards the prevailing wind direction along with an open-path gas analyzer.

Table 2.2: Measurement devices and meteorological parameters at the Fendt site

Variable/Parameter name	Unit	Measurement height	Instrument model
Net radiation	W/m ²	2 m	CNR4, Kipp & Zonen
Relative humidity	%	2.2 m	WXT520, Vaisala
Air temperature	°C	2.2 m	WXT520, Vaisala
Barometric pressure	hPa	1.3 m	CS100, Setra
Wind speed	m/s	2.2 m	WXT520, Vaisala
Wind direction	deg	2.2 m	WXT520, Vaisala
Precipitation	mm	2.2 m	Pluvio, Ott
Soil volumetric water content	m ³ /m ³	2, 6, 12, 25, 35, 50 cm depth	CS616, Campbell
Soil temperature profile	°C	2, 6, 12, 25, 35, 50 cm depth	T107, Campbell
Soil heat flux plate	W/m ²	8, 9 cm depth	HFP01, Hukseflux
3-D sonic anemometer	-	3.5 m	CSAT3, Campbell
Open path CO ₂ and H ₂ O gas analyzer	-	3.5 m	LI7500, Li-Cor

All signals for the sensors were logged to a data logger (CR3000, Campbell Scientific Inc, Logan, UT) at a rate of 20 Hz and were averaged for a half-hourly period. All the required procedures for the corrections and quality control of the turbulent fluxes were applied (Mauder et al., 2013), such as coordinate rotation by the double rotation

method (Wilczak et al., 2001), sonic temperature Schotanus correction (Schotanus et al., 1983), frequency response corrections (Moore 1986), WPL correction (Webb et al., 1980), and quality control following Foken et al. (2004). Simultaneous to the flux measurements, environmental and hydrometeorological data were measured at a 1-minute resolution and averaged for 10-minute intervals. The instrumentation between all three sites is almost identical, except for an enclosed-path infrared CO₂ and H₂O analyzer (LI7200, Licor Biosciences Inc, Licoln, NE) in Rottenbuch instead of the open-path instruments (LI7500, Licor Biosciences Inc, Licoln, NE) at Graswang and Fendt. All the measurement variables used in this study are given in Table 2.2.

2.2.4 Data coverage

Missing data in the measurements inevitably occurred. The gaps in the observed data make it difficult to estimate the annual latent heat (LE) and the sensible heat (H) fluxes and result in reduced quality of the data to validate model outputs (Hui et al., 2004). Some data were removed during the quality control (QC) process by the TK3 software. This was done through two tests i.e. Steady State Test (Gurjanov et al., 1984; Foken and Wichura 1996), and the Integral Turbulence Characteristics Test (Foken et al., 2004). According to Table 2.3, the overall quality flags are:

- Flag 0: high quality data, which is used in fundamental research
- Flag 1: moderate quality data, which have no restrictions to be used in the long-term observation programs, and
- Flag 2: low data quality, which was removed.

For more details see Mauder et al. (2013).

Table 2.3: Overall flag system after the Spoleto agreement (2004) for CarboEurope-IP (Mauder and Foken, 2015)

Steady state (deviation in %)	Integral turbulence characteristics (deviation in %)	Final flags
< 30	< 30	0
< 100	< 100	1
> 100	>100	2

Based on Table 2.4, the highest annual fraction of missing values for H (38%) and LE (44%) were observed at the Graswang site, whereas the lowest ones (H: 13% and LE: 20%) were found at the Rottenbuch site. Meanwhile, 27% of H and 33% of LE annual missing values were observed at the Fendt site. The main reason for this discrepancy could be explained, apart from the different landscape/environmental conditions at the sites, by the dissimilarity in the measurement instruments. In fact, enclosed-path and open-path systems are used in the Rottenbuch and Graswang sites, respectively.

2 Turbulent flux variability and EBC

Enclosed-path gas analyzers, however, have a number of advantages, such as minimal data losses due to precipitation events, no surface heating problems and the possibility of climate control, etc. Therefore, with an enclosed-path gas analyzer installed at the Rottenbuch site, the highest (valid) data availability was observed during the examined period. Despite using the same gas analyzer (open-path system) at the Fendt and Graswang sites, a higher number of missing values were observed at the Graswang site. This could be explained by the weather/climate conditions. Compared to the other sites, Graswang is located in the southern part of the TERENO prealpine region and has more rainfall/snow days throughout the year. As a result, more measured data are invalid and should be removed. Correspondingly, the maximum number of seasonal missing values of the turbulent fluxes was found at Graswang (H-max: 51% and LE-max: 55%) in autumn 2013 and the minimum number for Rottenbuch (H-min: 6% and LE-min: 7%) in summer 2014. More detailed information regarding the missing values of the turbulent fluxes is given in Table 2.4.

Table 2.4: Percentage of the seasonal and annual missing values of the turbulent fluxes at the TERENO EC sites during 2013-2014.

Sites		Percentage of data gaps (%)								
		Winter		Spring		Summer		Autumn		Annual
		2013	2014	2013	2014	2013	2014	2013	2014	2013/2014
Fendt	H	27	20	22	34	26	25	34	31	27
	LE	40	22	28	40	37	30	38	35	33
Graswang	H	46	32	26	41	27	40	51	46	38
	LE	54	34	37	46	41	44	55	50	44
Rottenbuch	H	14	9	10	18	10	6	15	27	13
	LE	25	13	18	39	15	7	20	27	20

Figure 2.2 shows the percentage of the diurnal and nocturnal missing values of the turbulent fluxes for each EC site. Obviously, the nighttime missing values were approximately more than twice the daytime values for all the sites. In addition, slightly more LE values were missing than those of H. This is because the LE measurement requires two fully functional instruments; a sonic anemometer plus gas analyzer, while H can be measured by the sonic anemometer alone, at least if the Schotanus correction is applied.

Furthermore, the Fendt and Graswang sites showed a similar pattern, i.e. distribution of missing values (due to using the same gas analyzer), meaning that the lowest diurnal and highest nocturnal missing values were found. The difference between diurnal and nocturnal missing values was much lower at the Rottenbuch than Fendt and Graswang. Moreover, this site had the lowest turbulent flux missing values (approximately 3-times less) compared to the other EC sites, due to an enclosed-path gas analyzer.

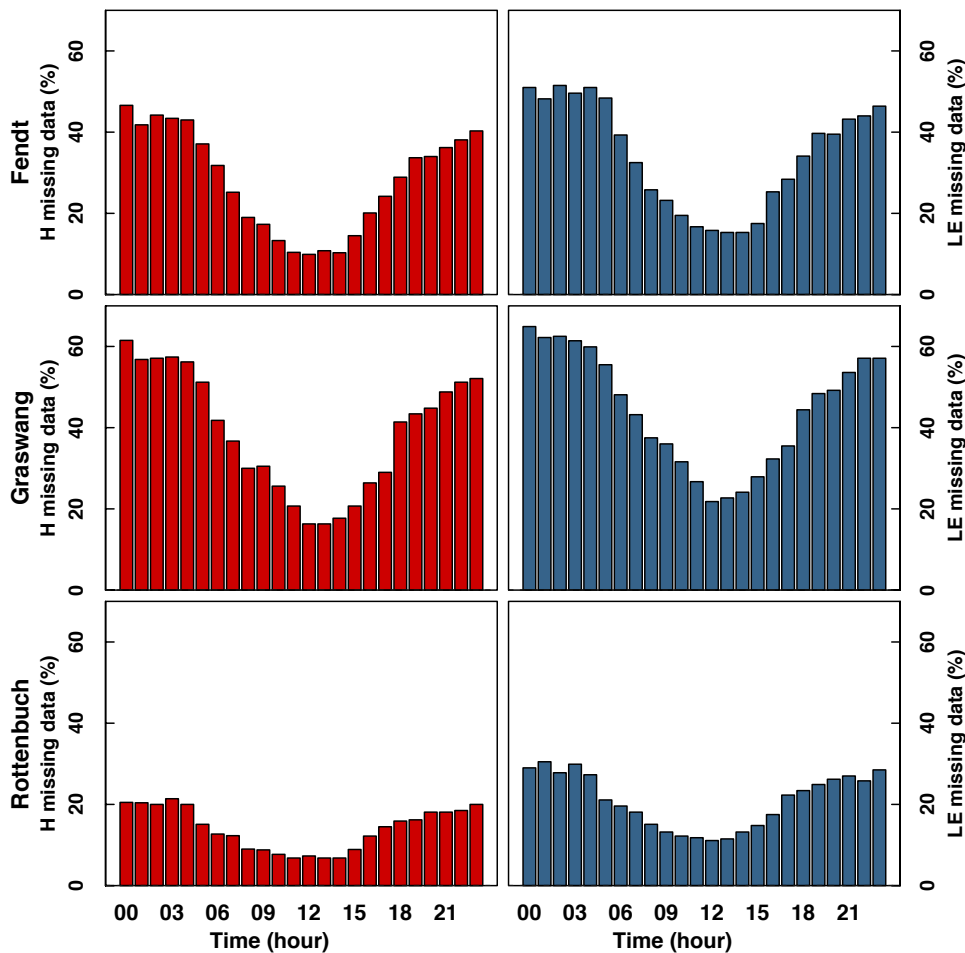


Figure 2.2: The percentage of the diurnal and nocturnal missing values of the turbulent fluxes (H and LE) at the TERENO prealpine EC sites for the period of January 2013 to December 2014.

2.3 Results and discussion

2.3.1 Soil temperature and soil volumetric water content

The near-surface soil temperature and soil moisture are the key variables that control the exchange of water and heat energy between the land surface and the atmosphere (Wei 1995; Wang et al., 2010). The seasonal variations of daily mean of the net radiation (R_n), soil temperature (T_s) and soil volumetric water content (θ_v) at depths of 2, 6, 12, 25, 35 and 50 cm, and 24-hour accumulated precipitation (Prec) at the Fendt EC site during 2013-2014 are shown in Figure 2.3. The monthly mean 24-h R_n showed an obvious daily variation mainly because of the clouds. T_s in shallow layers of 2, 6, 12 cm showed little difference in each season. It is not surprising that mean daily T_s at topsoil does not drop below the zero-degree due to the snow cover during the wintertime. The differences in seasonal T_s between the deep layers at 25, 35, 50 cm were larger than those of measured in the layers close to surface at 2, 6, 12 cm.

This otherwise unusual finding can be explained by a change in soil texture from 35 to 50 cm towards much higher clay content. The maximum T_s was measured in July 2013 (Figs. 2.3a and 2.3b).

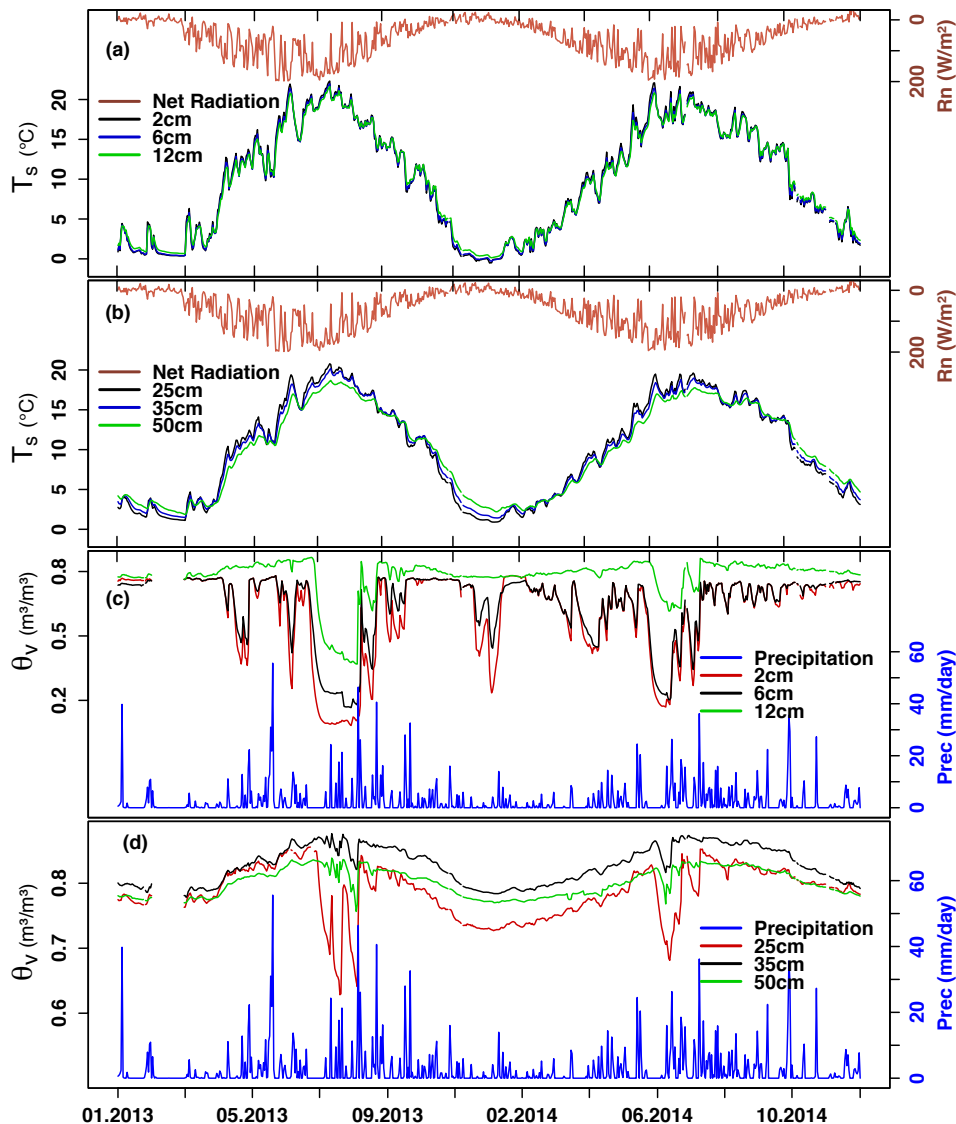


Figure 2.3: Daily mean variations: (a-b) soil temperature (T_s) at depths of 2, 6, 12, 25, 35 and 50 cm; and net radiation (Rn). (c-d) soil moisture (θ_v) at depths of 2, 6, 12, 25, 35 and 50 cm; and precipitation (Prec) at the Fendt EC site for the period of January 2013 to December 2014. The data are averages of 24-h values.

As indicated in Figures 2.3c and 2.3d, the topsoil was highly saturated ($> 0.7 \text{ m}^3/\text{m}^3$) with the water content during the winter and autumn seasons, and only reduced to approximately $0.3 \text{ m}^3/\text{m}^3$ during the winter 2014. Whereas in the deep layers, the maximum and minimum values of θ_v can be found during the summer and winter seasons, respectively. In the summertime, despite the fact that there was a considerable amount of rainfall, the θ_v periodically decreased dramatically, mainly at the layers near to the surface. This can be explained by the following: Fendt as a

grassland site, located at the bottom of a shallow valley with a low gradient, and the groundwater and surface-water interactions can be an important mechanism in the region. Thus, the most probable reason for the sudden θ_v changes might be related to changes in the groundwater level for that site.

Although no groundwater-level measurements were available for this study period 2013-2014, the findings obtained by Wolf et al. (2017) for the ScaleX-2015 campaign at the Fendt site confirmed that interactions between the groundwater level and surface-water exist. After strong rainfall events, the infiltration or drainage of excess water is the dominant runoff, and during the recession of stream flow, the contribution of groundwater to runoff is increased. They also conclude that the full mechanisms for the interactions of runoff generation and storage system for that area have not been fully investigated. In addition to the high influence of the groundwater level on the soil moisture in the region, other factors might be considered, such as unequally distributed summertime rainfall events, high evapotranspiration rate due to the high temperature and runoff generation. Therefore, for the above reasons, the amount of θ_v in some short periods was quite low, especially during the summertime.

2.3.2 Energy partitioning

The average contribution of the turbulent fluxes to the surface energy budget was calculated for each season (Table 2.5). The average seasonal values of H/Rn in spring, summer, autumn and winter was calculated as 0.12, 0.11, 0.34 and 0.64; while LE/Rn values were 0.53, 0.58, 0.50 and -0.20, respectively at the Fendt EC site. Meanwhile at the Rottenbuch site, the corresponding H/Rn values were calculated as 0.14, 0.11, 0.37 and -0.30, and also LE/Rn values measured as 0.37, 0.51, 0.18 and 0.11, respectively. The seasonal value of H/Rn in the autumn and spring seasons at the Graswang EC site was measured as -0.09 and -0.006, respectively, which were quite low and close to zero. This was because of the snow cover, which caused the land surface to be cold and as a result, a negative sensible heat flux (downwards) occurred during that period.

Furthermore, the seasonal noontime variations of the Bowen ratio indicated high seasonal variations throughout the year at the EC sites. In winter, 86.0%, 90.4%, 65.7% and in autumn 89.3%, 92.4%, 78.5% of heat was transferred (either positive/upwards or negative/downwards) as LE flux at the Fendt, Rottenbuch and Graswang EC sites, respectively. Meanwhile, the corresponding values during the spring and summer were 98.5%, 99.6%, 83.4% and 99.8%, 99.3%, 96.7%, respectively at the aforementioned EC sites. The Bowen ratio values in warm periods (spring and summer) were mostly positive with low magnitudes due to the high contribution of LE, while during the cold seasons (winter and autumn) the ratio was negative because of negative H values over those periods (figures not shown).

2 Turbulent flux variability and EBC

Table 2.5: Energy partitioning for individual seasons at the TERENO EC sites during 2013-2014. H/Rn and LE/Rn are the ratios of the turbulent fluxes to Rn and B is the Bowen ratio ($B=H/LE$).

Sites		Spring	Summer	Autumn	Winter
Fendt	H/Rn	0.12	0.11	0.34	0.64
	LE/Rn	0.53	0.58	0.50	-0.20
	B	0.23	0.20	-0.29	-0.30
Rottenbuch	H/Rn	0.14	0.11	0.37	0.37
	LE/Rn	0.37	0.51	0.18	0.11
	B	0.43	0.23	-1.42	2.26
Graswang	H/Rn	0.15	0.13	-0.09	-0.006
	LE/Rn	0.62	0.60	0.34	0.24
	B	0.27	0.21	-0.57	-6.02

2.3.3 Turbulent flux variability on different time scales

Management of grassland at the EC sites

The management of grassland is quite different between the southern and northern parts of the TERENO prealpine region (Fig. 2.4), which indicates an elevation-trend for that area. At the highest elevation site i.e. Graswang (860 m) one or two grass cuts are done per year usually starting from the early June to mid August, which indicates that the grass cutting is exclusively limited to months with the highest temperatures. Meanwhile, at the middle and low elevation sites i.e. Rottenbuch (770 m) and Fendt (598 m), respectively, the farmers begin to cut the grass from mid May to late October, leading to four to five cut times. The last grass cuts of the year are done almost simultaneously at these sites. Furthermore, a coincidence between the grass cutting events and a sudden decrease of albedo after the grass cutting was sometimes observed. A sudden drop of the albedo at the beginning of August 2014 at the Fendt EC site can demonstrate this effect.

The mean daily-based variation of surface albedo, which is highly influenced by the snow cover, soil color and moisture, vegetation cover etc., at the study sites is shown in Figure 2.4, as well. Overall, the highest albedo values were measured during the winter and autumn seasons, whereas the lowest ones observed during the summer and spring periods mainly due to the snow cover in cold periods and rather high soil moisture, as well as high vegetation fraction in the warm periods throughout the year. The maximum surface albedo was measured during January and April 2013 due to the high snow cover at the EC sites. The higher albedo values at the Graswang site (in the southern part) suggest an increase of snow cover in both height and duration for that area, which is also confirmed by the higher values of the outgoing shortwave radiation (OSR) at the higher-elevated sites for the same times. Therefore, the radiative fluxes of OSR and albedo are highly affected by the grass cut events, which

consequently influence the turbulent flux variability at the grassland EC sites in the region.

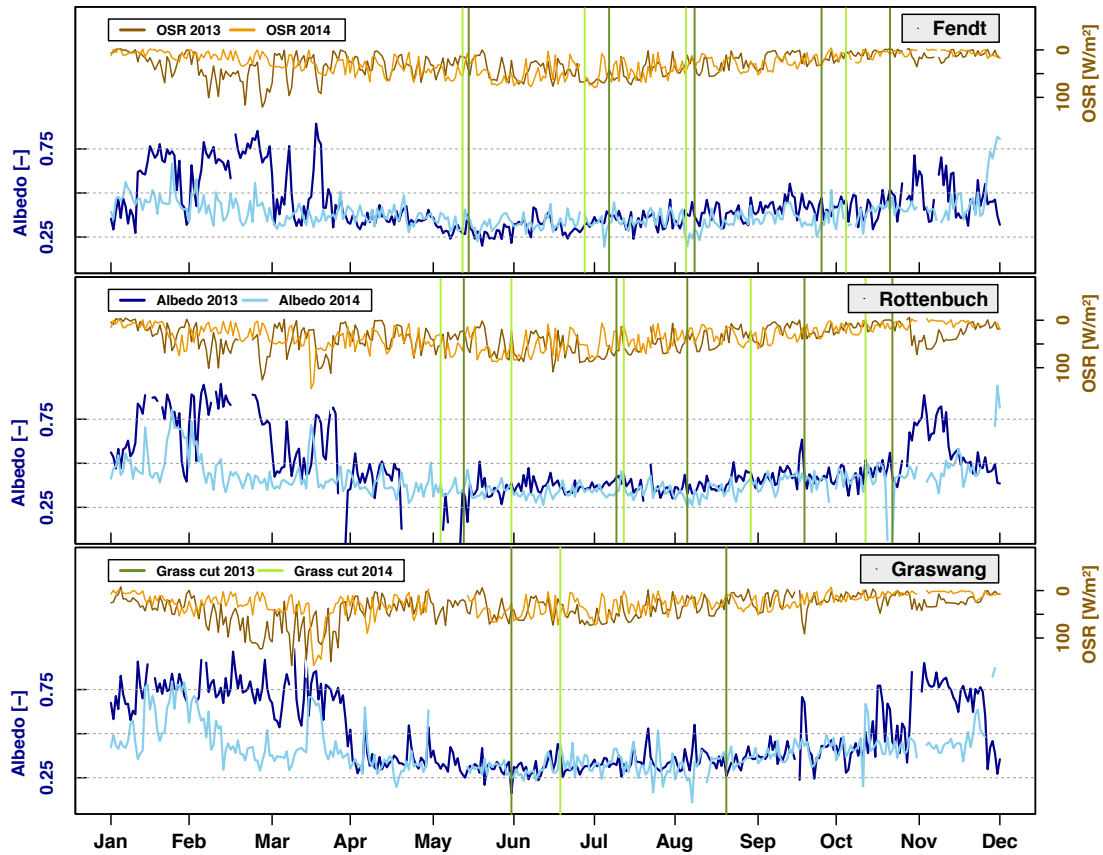


Figure 2.4: Daily mean variations of the outgoing shortwave radiation (OSR) and albedo values, as well as the number of grass cuts at the TERENO prealpine EC sites for the period of January 2013 to December 2014.

Drivers of the turbulent fluxes: PCA based analysis

To determine the most relevant driving variables that influence the turbulent fluxes at the study sites, a PCA was applied. To enable comparability of the impact of the different variables, the data are centered and scaled before application of the PCA. For the sake of visualization, the focus is on the first two PCs (PC1 and PC2), which explain $> 60\%$ of the total variance of the original datasets (Fig. 2.5). The figure illustrates the cross correlation and the contribution of each variable to the PCs at different TERENO prealpine sites. The length (angle) of the arrows represents the magnitude (direction) of the correlation coefficient between the variable and the PCs, which the color of arrows indicates the contributions (importance) of the variables to the turbulent fluxes (12 variables ranked from blue (low importance) to red (high importance)). For Fendt, PC1 shows high positive correlations with the radiation

components of net radiation: Rn ($r = 0.93$) and photosynthetic photon flux density: PPFd ($r = 0.91$) with a total contribution of approx. 28.5% (not shown), as well as with the temperature variables of infrared surface temperature: SurfaceT ($r = 0.92$), air temperature: AirT ($r = 0.91$) and soil temperature at 2cm depth: SoilT ($r = 0.89$) accounting for approximately 42.2% of the total contribution (not shown). The variables of albedo ($r = -0.63$), soil moisture at 2cm depth: SoilM ($r = -0.57$) and relative humidity: RH ($r = -0.56$) are negatively correlated with PC1. Furthermore, PC1 shows the highest correlation with Rn, which identifies net radiation as a key variable for the turbulent flux measurement at the Fendt EC site.

The aforementioned variables also represent approximately the same contributions and correlations to PC1 at the Rottenbuch EC site, except for the wind components of wind direction: WindD ($r = -0.47$) and wind speed: WindS ($r = -0.41$), which show no correlation with PC1 at the Fendt site. Their influence at the Graswang site, however, is lower, representing a rather different pattern compared to the other EC sites, except for the SoilT close to the surface ($r = 0.93$) with the highest contribution of 16% (not shown) and albedo ($r = -0.72$). Thus, the albedo rather follows an elevation-trend in the TERENO region. This finding is in agreement with Zeeman et al. (2017) and might be explained by the lack of irradiation due to a mountain shadowing effect. The Graswang site possesses a mountain climate with high amounts of precipitation and snow events frequently occurring between October and April.

PC2 is highly correlated only with the WindS ($r = 0.81$ at Fendt, $r = 0.79$ at Rottenbuch and $r = 0.60$ at Graswang) with a mean total contribution of 50% (not shown) and WindD (in order of aforesaid sites: $r = 0.78$, $r = 0.77$ and $r = 0.18$), accounting for approximately 35% (not shown) of the mean total contribution. PC2 lacks correlation with radiation and temperature components ($< 5\%$, not shown). Meanwhile, the contribution of WindS (20%, not shown) was much more than WindD (2.5%, not shown) at Graswang. This is because the site is located in a valley, surrounded by high mountains and in such a way that the prevailing wind directions are easterly and westerly (see Fig. 2.1). This component represents the importance of the wind variables to the turbulent flux measurements in the region. Increased wind speed, for instance, also leads to an increase of the turbulence intensity and mixing, thereby increasing the fluxes. With respect to the precipitation: Prec and RH variables, they are ranked as the second and third most important variables that are negatively correlated with PC2. Therefore, Prec holds the highest correlation ($r = -0.60$) at the Graswang site.

Overall, the PCA results found at the TERENO prealpine EC sites were consistent with findings of other studies over different ecosystems (e.g. Schmidt et al., 2011).

2 Turbulent flux variability and EBC

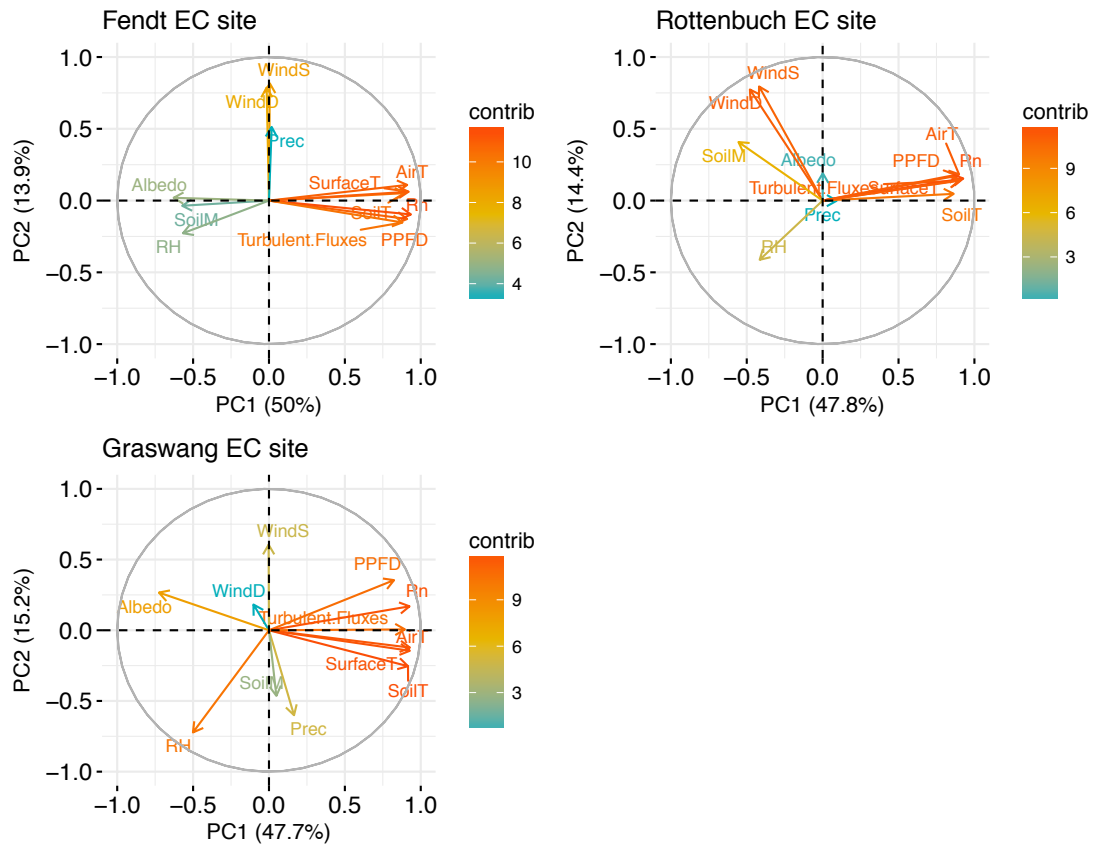


Figure 2.5: Contribution of the meteorological variables to the turbulent fluxes (sum of H and LE) using a multivariate PCA analysis at the TERENO prealpine EC sites for the period from January 2013 to December 2014. Daily mean meteorological data include: wind direction (WindD [°]), wind speed (WindS [m/s]), air temperature (AirT [°C]), relative humidity (RH [%]), precipitation (Prec [mm]), soil temperature at 2cm depth (SoilT [°C]), soil moisture at 2cm depth (SoilM [m³/m³]), photosynthetic photon flux density (PPFD [μmol/(m² s)]), albedo [-], net radiation (Rn [W/m²]) and infrared surface temperature (SurfaceT [°C]). The length (angle) of the arrows represents the magnitude (direction) of the correlation coefficient between the variable and the PCs. The lowest and highest contributions of the variables to the turbulent fluxes are ranked with colors ranging from blue to red, respectively.

Monthly and seasonal variations of the turbulent fluxes

To understand the monthly mean diurnal turbulent fluxes at the study sites, their hourly variations together with the standard deviations (σ) are shown in Figure 2.6. As expected, the variations of H and LE fluxes were low during the winter and autumn periods, whereas they were quite large during the spring and summer seasons in the region. During the cold periods, in winter for example, the peak values were 55.6 W/m² and 92.7 W/m² for H and LE fluxes observed at the Fendt site, respectively. The mean diurnal values of H at the Graswang site were quite different from the other two sites as a result of different landscapes and topography.

meaning that the sun sets rather early as the site is surrounded by high mountains. The highest LE fluxes occurred in July as the highest amount of precipitation takes place during the summertime. The magnitude of variations increased from winter to summer and accordingly, showed a decrease from summer to winter corresponding to the variation of radiation, precipitation patterns, soil moisture/types and different landscapes across the TERENO prealpine region.

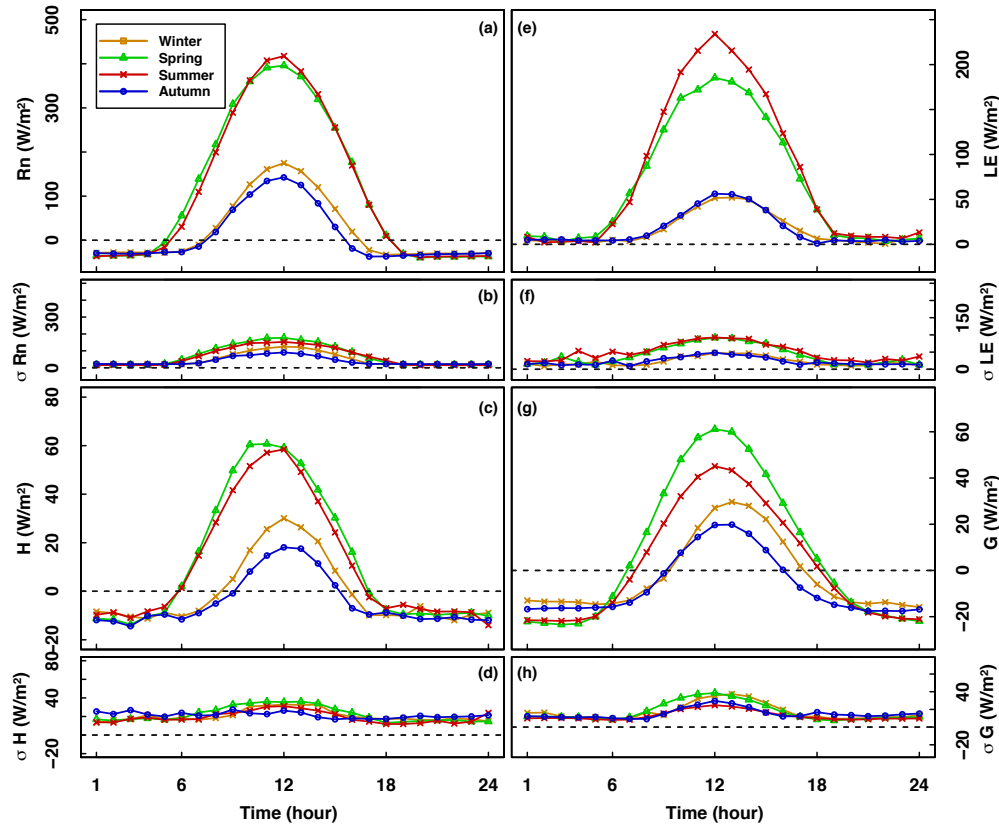


Figure 2.7: Diurnal cycle of seasonal mean variations and standard deviation (σ) of the surface energy fluxes at the Fendt EC site for the period of January 2013 to December 2014. The data represent hourly averages.

Seasonally, all the energy fluxes of Rn, H, LE and G at the Fendt EC site showed distinct diurnal cycles over the experimental time (Fig. 2.7). Rn was highly variable between cold and warm seasons and also the range of the daytime cycle of Rn increased from autumn to summer and decreased vice versa. Thus, the variation of the diurnal cycle of Rn was strong during summer, but weak during autumn (Fig. 2.7a). The range of H values increased from autumn to spring. The nocturnal H value was significantly negative, meaning that the heat was transferred from the atmosphere to the land surface due to the cold surface. The seasonal variation of H was rather small compared to Rn, which was quite large between the cold and warm periods. LE flux had an obvious seasonal diurnal variation during summer with the value of 245.1 W/m^2 , which became rather small in spring (179.1 W/m^2) and then remarkably

decreased during the autumn (58.3 W/m^2) and winter (50.6 W/m^2) seasons (Fig. 2.7e). Finally, the G flux had a rather similar and less seasonal variation throughout the year. The nocturnal G value was significantly negative (upwards) compared to other energy fluxes. Interestingly, the maximum diurnal G flux (25.1 W/m^2) in winter occurred at 13:00 pm, which indicated a shift of around one-hour. This might be explained by the snow cover in the region causing a short delay for the heat to be diffused in the soil (Fig. 2.7g). Overall, the highest seasonal diurnal variations were observed in R_n , followed by LE and H and G.

2.3.4 Energy balance closure

Overall and seasonal energy balance closure

The linear regressions between the turbulent fluxes and the available energy at the TERENO prealpine EC sites of Fendt, Rottenbuch and Graswang are shown in Figure 2.8. The energy balance closure (EBC) is defined as the slope of a regression analysis of turbulent energy transport against available energy. The EBC were 0.65, 0.56 and 0.65 and the coefficients of determination (R^2) values were 0.82, 0.85 and 0.77 at the Fendt, Rottenbuch and Graswang sites, respectively. The lowest R^2 between measured and available energy was found at the Graswang site. This can be explained by the climatic and environmental conditions. This site is surrounded by high mountains (see Fig. 2.1) and the wind speed is relatively low so that the mechanically driven turbulence is reduced in the valley. As a result, many of the calculated H and LE values were removed as unreliable data during the post processing (i.e. quality control) by the TK3 software. Thus, the Graswang site had the lowest number of data ($n=7969$) compared to other EC sites (Fig. 2.8c). In terms of energy balance ratio (EBR), as defined in Eq. 2.3, the highest overall value of EBR (0.73) was calculated at the Graswang site indicating that the minimum heat and water vapor fluxes are lost for that area, which is due to the geographical location of the site.

Furthermore, the lowest slope (0.56) and EBR (0.56) values were found at the Rottenbuch site. A spectral analysis (not shown) indicated that this underestimation of the turbulent fluxes calculated at the Rottenbuch site was not due to the frequency response corrections e.g. through tube attenuation. Therefore, this finding is partially explained by the heterogeneity of the land-surface type around this site, meaning that the site itself is located closely to a town, which has a much higher temperature than the meadow and there is a deep canyon of the Ammer river nearby, which has a lower temperature. Thus, it is likely that the advection of heat and vapor had occurred in that area (Fig. 2.8b). Furthermore, the research done by Eder et al. (2014) show that there is a relationship between landscape-scale heterogeneity and energy balance closure for the TERENO prealpine sites. The mean EBR was 0.65 for the TERENO prealpine region.

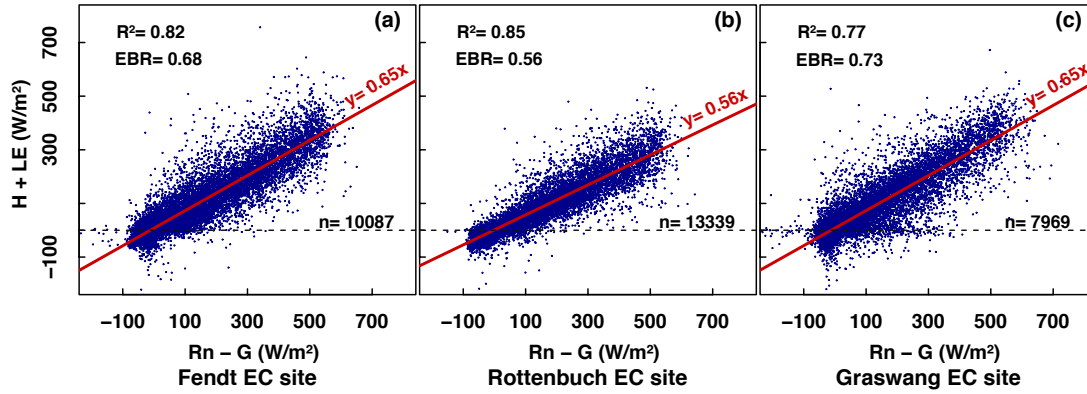


Figure 2.8: Intercomparison of the turbulent fluxes ($H + LE$) against the available energy ($Rn - G$) at the TERENO prealpine EC sites for the period of January 2013 to December 2014. The gray horizontal dashed-line indicates the zero value. The data represent half-hourly averages.

The seasonal differences between the values of EBR at the TERENO EC sites are given in Table 2.6. The highest seasonal EBR were 0.70 in summer and 0.81 in autumn, while the lowest corresponding values were 0.42 and 0.61 in winter at the Fendt and Graswang sites, respectively. The lowest seasonal EBR values were calculated as 0.51, 0.65, 0.47 and 0.33 in spring, summer, autumn and winter, respectively at the Rottenbuch site. Overall, warm seasons showed a higher EBR value compared to the cold ones at the study sites, except for the Rottenbuch site in which a considerable seasonal difference could not be found.

Table 2.6: Seasonal EBR at the TERENO EC sites during 2013-2014.

	Site	Season			
		Spring	Summer	Autumn	Winter
$EBR = \frac{\sum(L E + H)}{\sum(R n - G)}$	Fendt	0.68	0.70	0.69	0.42
	Rottenbuch	0.51	0.65	0.47	0.33
	Graswang	0.76	0.73	0.81	0.61

Seasonal energy balance residual

The seasonal mean of diurnal variation of the energy balance residual (Res) is shown in Figure 2.9. The largest maxima of the Res were 140.8 W/m^2 in spring, 90.1 W/m^2 in summer and 141.9 W/m^2 in summer at Fendt, Graswang and Rottenbuch sites, respectively. The Rottenbuch site had the highest Res in warm periods owing to the heterogeneity of the landscape in that area. The autumn diurnal Res sharply decreased from 40.5 to -30.9 W/m^2 in the afternoon at the Graswang site. This might be explained by the lack of sunshine in the afternoon, as this tower is surrounded by high

mountains (see Fig. 2.1 for the location) and the sun accordingly sets earlier due to the elevated horizon.

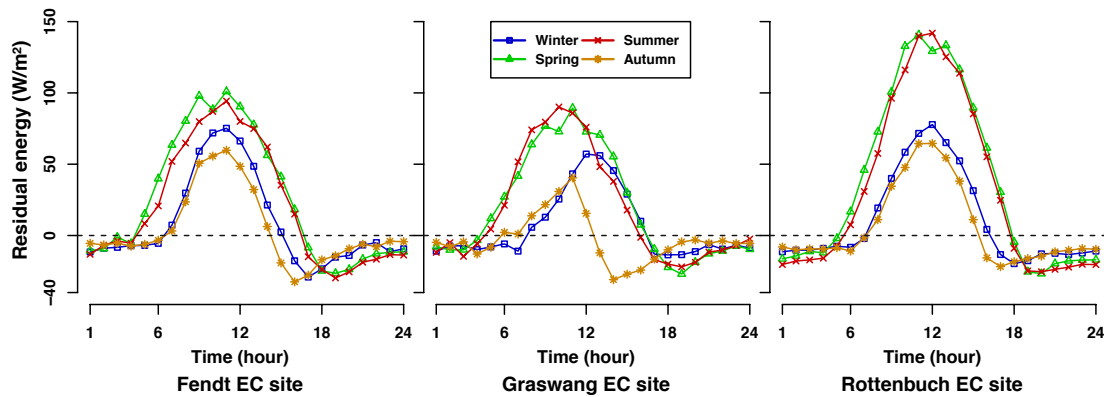


Figure 2.9: Seasonal 24-h cycle of the residual energy ($\text{Res} = R_n - (H + LE + G)$) at the TERENO prealpine EC sites for the period of January 2013 to December 2014. The data represent half-hourly averages.

Overall, the reasons for obtaining poor energy balance closure may result from either measurement -or method limitations. Some of these effects include: a) net radiation sensors, which might perform poorly in the field; b) wind speed and temperature measurements e.g. vertical wind speed underestimation; c) water vapor fluctuation measurements, e.g. inappropriate performance of sonic anemometer during and after rainfall events; and d) the soil heat flux and heat storage measurements (Culf et al., 2004). In all parts of the world, researchers have encountered energy residuals of magnitudes similar to our data sets (e.g. Foken and Oncley, 1995; Panin et al., 1996; Wicke and Bernhofer, 1996; Foken et al., 1999; Kahan et al., 2006; Oncley et al., 2007; Su et al., 2008; Wang et al., 2010). The study of Eder et al. (2014) on the energy balance closure suggests that part of the imbalances might be explained by the mesoscale transport in relation to the heterogeneity of the landscape, which has been hypothesized for other sites by Mauder et al. (2007) and Panin and Bernhofer (2008), as well. Therefore, to quantify the possible reasons for the lack of energy balance at the TERENO EC sites, the diurnal and nocturnal variations of the heat fluxes, influence of the time of day, as well as the effect of flux measurement footprint and the dependence of the energy balance closure on the wind direction are analyzed in the following sub-sections.

Influence of the diurnal and nocturnal conditions

Figure 2.10 shows the daytime and nighttime correlations of the turbulent fluxes vs. the available energy. The daytime and nighttime R^2 were 0.73 and 0.093, respectively

at the Fendt site. The highest/lowest daytime and nighttime R^2 were calculated as 0.79, 0.70 and 0.22, 0.026 at the Rottenbuch and Graswang sites, respectively. Furthermore, the Graswang site had the lowest diurnal and nocturnal data availability (i.e. N:6511 and N:2013, respectively), while the highest corresponding valid values were N:8046 and N:5785 that were observed at the Rottenbuch site. Other researchers have reported a better diurnal energy balance closure (e.g. Wilson et al., 2002). The large nighttime energy imbalances could be explained by weak turbulence at night. Aubinet et al. (1999) and Blanken et al. (1997) also came to the conclusion that when the friction velocity is small, the energy imbalance is usually high during the nocturnal periods. Lee and Hu (2002) found that a low energy balance during nighttime periods was due to mean vertical advection, as well.

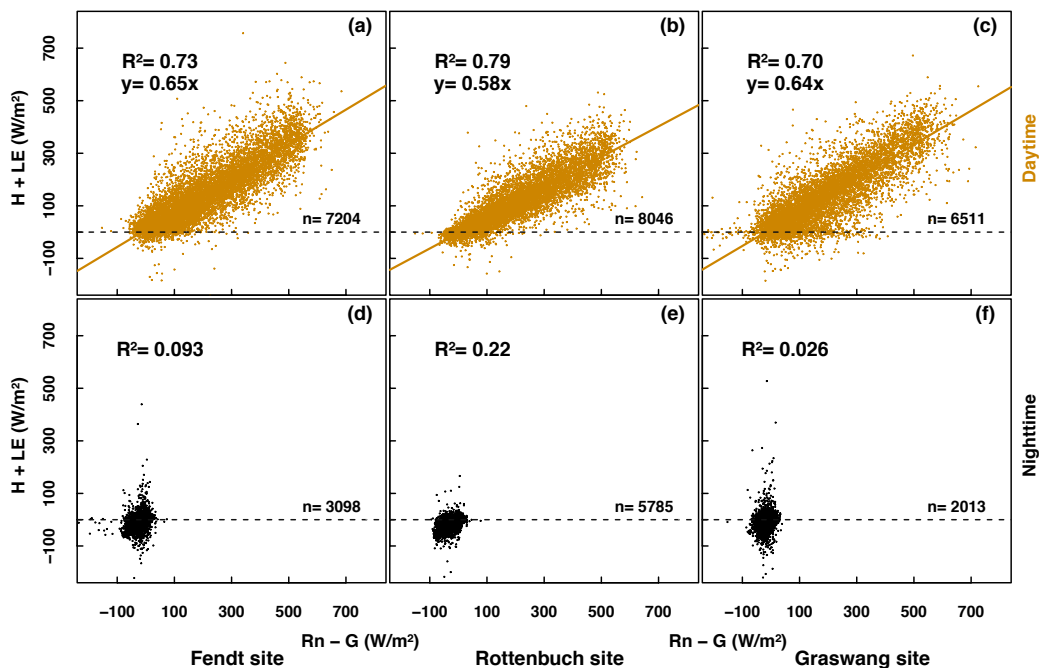


Figure 2.10: Turbulent fluxes ($H + LE$) vs. available energy ($Rn - G$) for daytime and nighttime at the TERENO prealpine EC sites for the period from January 2013 to December 2014. The data represent half-hourly averages. The daytime-hours was defined as the Incoming Shortwave Radiation ($ISR > 25 \text{ W/m}^2$).

Dependence on the time of day

The diurnal courses of the EBR and the energy balance residual, as well as with the mean magnitudes of the measured and available energy are shown in Figure 2.11. It was found that for all sites the EBR is not meaningful from 1:00 UTC to 6:00 UTC and after 17:00 UTC, when the available energy was close to zero. Between these two periods, however, a linear increase in the EBR (with a different pattern and intensity) was observed at the EC sites. At all three EC sites, a sharp increase in the EBR was observed after 15:00 UTC, indicating a better energy balance closure or even over-

closure in the afternoon. Such an observation normally points to an unaccounted storage term, which is filled in the morning and depleted in the afternoon. Since it was included the soil heat storage in G , only the heat stored in the biomass can explain the finding. Thus, the best closure occurred in the afternoon, peaking shortly before the sunset (at approximately 18:00) at all the EC sites. Besides, the residual energy exhibited an almost similar diurnal pattern, but different in magnitude from the study sites, which is characterized by positive values from approximately 4:00 to 15:00, and by negative values outside this time period ranging from 100 W/m^2 at the Rottenbuch site to -24 W/m^2 at the Fendt site, where the energy balance closure peak occurred.

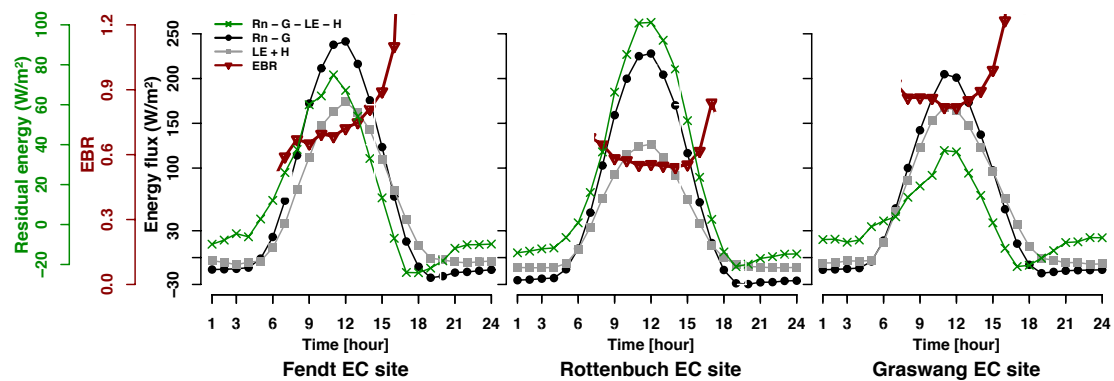


Figure 2.11: The mean diurnal variation of: the available energy ($R_n - G$), the turbulent fluxes ($LE + H$), the energy balance ratio (EBR) and the residual energy ($R_n - G - LE - H$) at the TERENO prealpine EC sites for the period of January 2013 to December 2014.

Effect of the flux footprint

The turbulent vertical flux of a passive scalar measured upwind of the surface area represents the exchange between the atmosphere and the surface over a larger area is known as the atmospheric flux footprint or footprint (Horst 1999; Sanchez et al., 2010). An increase in the measurement height and decrease in the surface roughness, as well as changing the atmospheric stability from unstable to stable would lead to an increase in size of the footprint and move the peak contribution away from the EC site. These are the main factors affecting the size and shape of the flux footprint. The overall flux footprint climatologies at the TERENO prealpine EC sites are shown in Figures. 2.12, 2.13 and 2.14. The aerial Google-Earth images in the region clearly show the heterogeneous surface at the EC sites in which a stronger directional surface inhomogeneity is observed at the Rottenbuch site (Fig. 2.13) as the site is situated close to a town, as well as a deep-canyon (i.e. Ammer river). Figure 2.12 shows that approximately 80% of the turbulent flux contribution is received by the Fendt EC site instruments from the grassland targets 1 (~60%) and 2 (~20%) located in a radius of approximately 220 m from the station and less than 10% of the flux contribution is emitted by target 3, which is farther away from the instruments. In addition, the

2 Turbulent flux variability and EBC

overall shape of the flux footprint strongly matches the direction of the prevailing wind for that area (see Fig. 2.1 for the details).

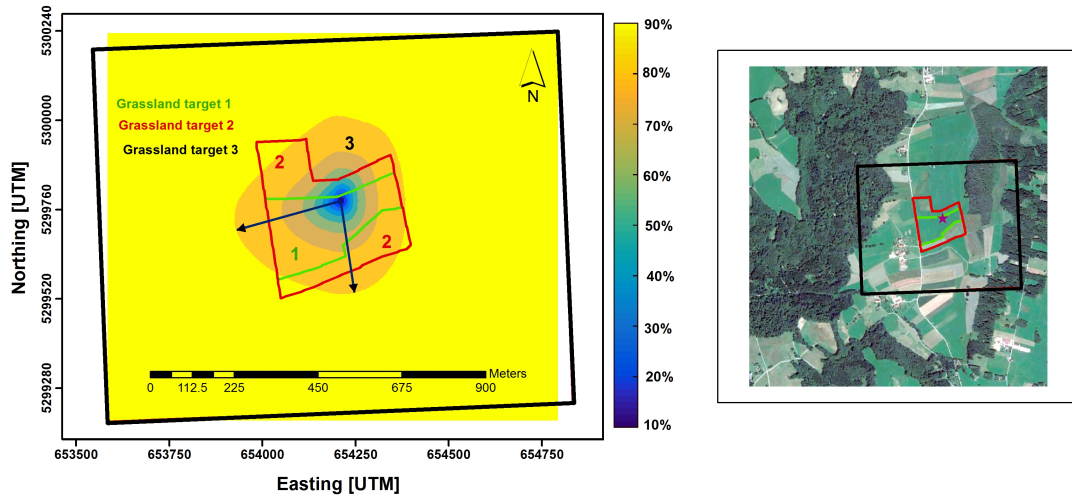


Figure 2.12: Footprint climatology of the Fendt EC site. The left-side map: background filled-contours indicate the cumulative percentages of the annual mean half-hourly flux footprint during 2013-2014, and the overlaid colorful domains represent the different grassland targets, where the canopy height differs at the targets. The dark-blue arrows show the most dominant footprint directions. The right-side map: the domains overlaid on the Google earth image indicate the approximate position of the grassland targets surrounding the site. See Fig. 2.1 for further map details.

As shown in Figure 2.13, instruments of the Rottenbuch EC site receive more than 65% of the annual flux footprint contribution from the grassland target 1 and approximately 25% from the grassland target 2. Thus, the fetch is larger compared to other EC sites.

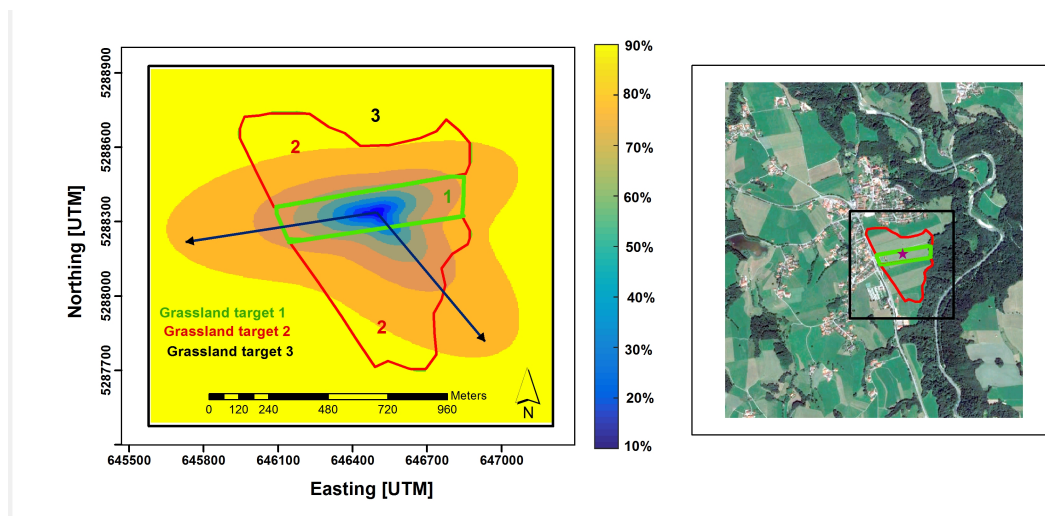


Figure 2.13: Same as in Fig. 2.12, but for the Rottenbuch EC site.

As mentioned earlier, the lowest EBR at the Rottenbuch site could be explained by the combined effects of the presence of the Ammer river located about 600 m east-southeast of the station and the nearby town situated west-north of the EC site. Both these factors are a source of small-scale heterogeneity (Schmid 1997; Eder et al., 2014). The size of the flux footprint also confirms this mismatch, where some percentage of the footprint is emitted from those inhomogeneous areas. The grassland targets 1 and 2 emitted approximately 90% of the flux footprint concentration at the Graswang EC site (Fig. 2.14). The shape of the mean half-hourly flux footprint is highly similar to that of the wind-rose diagram for that area (see Fig. 2.1 for the map). It is worth mentioning that the mean flux footprint did not vary significantly between the four seasons, neither in size nor shape. Thus, the figures were excluded for further interpretations.

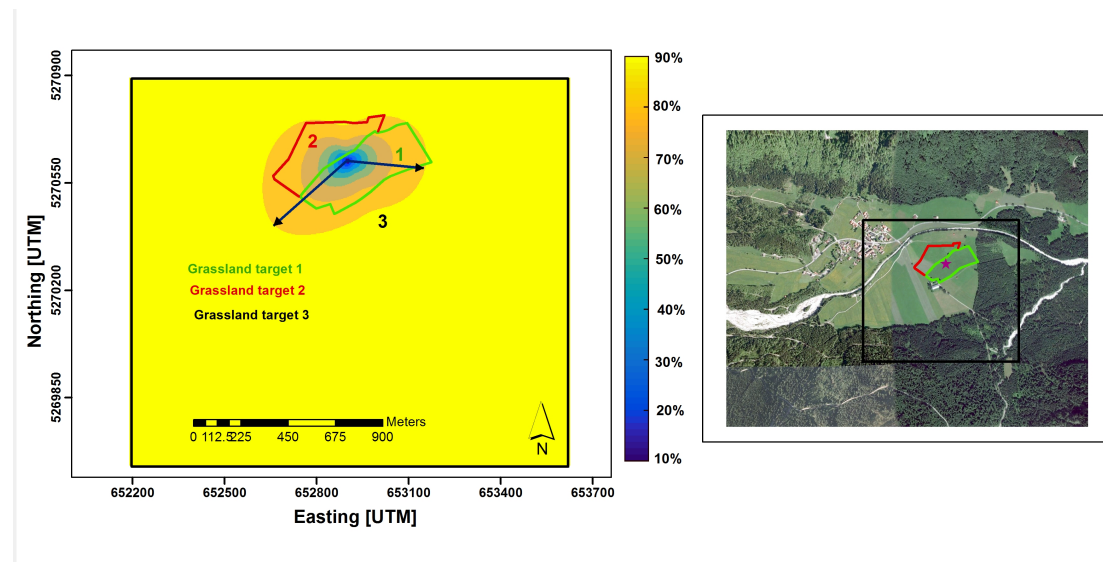


Figure 2.14: Same as in Fig. 2.12, but for the Graswang EC site.

2.4 Conclusions

The temporal multiscale variability of the surface heat fluxes was assessed by the analysis of the turbulent heat and moisture fluxes using the eddy-covariance (EC) technique at the TERrestrial ENvironmental Observatories (TERENO) prealpine region for the period of 2013 to 2014.

The PCA results revealed that, based on PC1, the turbulent flux variability is strongly driven by the radiation components of R_n (with an average contribution of approximately (15%) and PFD (14.5%) followed by the temperature variables of SurfaceT (14.3%), AirT (14%) and SoilT (13%) at the study sites. For PC2, however, the dominant contributing variables were WindS (50%) and WindD (35%). Furthermore, the monthly diurnal turbulent fluxes of H and LE indicated significant intra-annual variability across the different environments due to the variations of the

2 Turbulent flux variability and EBC

radiation components, precipitation events, soil moisture and texture, as well as different landscapes in the region. Besides, the highest seasonal diurnal variation observed was for R_n , followed by LE and H , while the lowest one was found for G .

The surface energy balance closure remained unclosed at the study EC sites. The EBR values were 0.68, 0.56 and 0.73 at the Fendt, Rottenbuch and Graswang sites, respectively. The mean imbalance was approximately 35%. The lowest EBR at the Rottenbuch site was partially due to the advection of heat and vapor caused by the heterogeneity of the land surface in that area leading to an underestimation of turbulent fluxes, which somehow substantiated by the flux footprint analysis. The EBC was poor during nighttime periods mainly due to the weak turbulence mixing at night. Overall, the EBC was better in the early afternoon than in the morning (due to the neglected storage terms) with the highest and the lowest EBC at the Graswang and Rottenbuch EC sites, respectively.

On average, the annual mean energy balance residual and EBR were 60 W/m^2 and 65%, respectively, in the region. In addition, the size and shape of the flux footprint climatology was calculated. Approximately 80%, 75% and 90% of the annual mean half-hourly turbulent flux footprints received by the instruments from the grassland targets 1 and 2 located at a radius of approximately 250 m around the Fendt, Rottenbuch and Graswang stations, respectively. The overall shape of the flux footprints significantly matched the direction of the prevailing winds at the study EC sites.

Chapter 3

Spatiotemporal variability and empirical Copula-based dependence structure of modeled and observed coupled water and energy fluxes^{*}

3.1 Introduction

In alpine and prealpine regions, eco-hydrometeorological variables and processes such as soil moisture, evapotranspiration (ET), vegetation type and dynamics, and surface heat fluxes exhibit rapid changes within short distances. This is mainly due to the heterogeneity in topography, soil hydraulic properties, landuse, and climate, as well as interactions between the earth surface and the atmospheric boundary layer (Kunstmann et al., 2004, 2006; Hingerl et al., 2016; Soltani et al., 2017). The energy and water budgets in such environments are, therefore, highly controlled by the soil type properties (Pielke et al., 1998), landcover characteristics (Dirmeyer et al., 2010), and vegetation structure (Pielke et al., 2011). The accurate spatial prediction of hydrometeorological variables can statistically be achieved with a distributed high-resolution hydrologic modeling approach. Such models explicitly take into account all of the domain characteristics by simultaneously solving the water and energy balance over complex mountain terrain (Bronstert et al., 2002).

In recent years, sophisticated process-based hydrological models have been developed, i.e. ALPINE3D (Lehning et al., 2006), Distributed Hydrology-Soil-Vegetation Model (Cuo et al., 2008) and JGRASS-NewAGE (Formetta et al., 2011). In these models the full system of interactions between different environments is usually taken into account; however, the equations are simplified and parameterized for the process interactions. In models like GEOtop (Rigon et al., 2006; Endrizzi et al., 2014), modeling the interactions between various hydrological, ecological and

^{*} This chapter follows closely Soltani *et al.*, (2018)

atmospheric boundary-layer processes in an interdisciplinary research area is possible, as the model covers a wide spectrum of factors in the terrestrial hydrological cycle (Endrizzi et al., 2014).

To validate the performance of hydrological models, the simulation outputs of these models are compared against observation-based runoff data and, more recently, micrometeorological measurements derived from Eddy Covariance (EC) techniques (e.g. Rigon et al., 2006; Hingerl et al., 2016). EC-based information is now considered as a valid source for model's calibration and validation (e.g. Rosero et al., 2010; Decker et al., 2012). Traditionally, linear statistical measures (e.g. correlation coefficient r) are used for model performance evaluation. However, using simple linear r -values between simulated and observed hydrometeorological datasets, which typically exhibit nonlinear characteristics, may not be an appropriate way to determine these complex relationships (Bárdossy and Pegram, 2009). Copula functions can appropriately obtain underlying dependence structures of hydrometeorological variables (Dupuis, 2007), including their complexities in time and space (Laux et al., 2011). Copula-based models have been used in a variety of experimental studies for different purposes worldwide. In the field of hydrology, Bárdossy (2006) described the spatial variability of the groundwater quality parameters using bivariate empirical copula. Using Copula functions, Sugimoto et al. (2016) made an attempt to detect the temporal changes of catchments independent from climate change by investigating the long-term discharge records. Li et al. (2016) estimated the bivariate flood quantiles by combinations of peak discharge and flood volume using Copulas in China. In a similar study, with regard to urban catchment applications, flood frequency curves were derived using bivariate rainfall distribution based on copula functions by Balistrocchi and Bacchi (2017). The following studies are examples for applying Copulas to hydrometeorological field: modelling the daily precipitation features in West Africa (Laux et al., 2009), spatial recorrelation of regional climate model (RCM) precipitation to generate unbiased climate change scenarios over Rhine basin (Bárdossy and Pegram, 2012), spatiotemporal patterns of precipitation extremes in China (Zhang et al., 2013), and bias correction of dynamically downscaled precipitation fields in Germany (Mao et al., 2015). However, no study has been used Copula-based models so far for evaluating the performance of hydrological simulations, as described and presented in this research.

This study is performed for two heterogeneous (ranging from small to mesoscale) catchments within the TERrestrial ENvironmental Observatories (TERENO) prealpine region located in southern Germany using GEOtop 2.0 to jointly simulate the water and energy budgets over two summer episodes in 2013 and 2015. Previous studies in the region have focused on how climate change impacts runoff generation, surface and sub-surface water balances, biosphere-atmosphere exchange (greenhouse gases), and energy balance closure parameterization (Ott et al., 2013; Kunstmann et al., 2004; Unteregelsbacher et al., 2013; Wang et al., 2014; Eder et al., 2014; Wolf et al., 2016; Zeeman et al., 2017; Soltani et al., 2017). Inverse distributed hydrological modelling has been studied by Kunstmann et al. (2006) for

the alpine/prealpine Ammer River catchment through coupling the Parameter ESTimation tool (PEST) in the WaSiM hydrological model. Hingerl et al. (2016) modeled the spatiotemporal variability of the water and energy flux components using GEOtop 1.45 for a prealpine catchment in the TERENO region. In both cases, however, the hydrological models were calibrated against the runoff measurements only, and no soil moisture profile variation and/or radiative-turbulent flux variabilities have been accounted for in the simulation. Moreover, previous studies only attempted to evaluate the models' performances using the traditional linear statistical metrics (e.g. R^2 , RMSE).

Given the above described gaps, in chapter 3 the following objectives are addressed: i) quantifying the spatiotemporal variability of the hydrometeorological variables of the turbulent fluxes as well as the surface temperature and ET with respect to the elevation-gradient effect using high-resolution EC-based measurements and spatial hydrological simulations, ii) simulating the coupled water and energy balances at a very high spatial resolution using the physically-based hydrological model GEOtop, and iii) estimating the underlying dependence structures of the observed and modeled water and energy fluxes using the nonlinear-based approach bivariate empirical Copula in the TERENO prealpine region.

3.2 Study area and hydrometeorological dataset

3.2.1 Catchments description

The Rott catchment ($\sim 55 \text{ km}^2$) and the Upper-Ammer catchment ($\sim 300 \text{ km}^2$) are located in the TERrestrial ENVIRONMENTAL Observatories (TERENO) prealpine region in southern Germany (Figure 3.1).

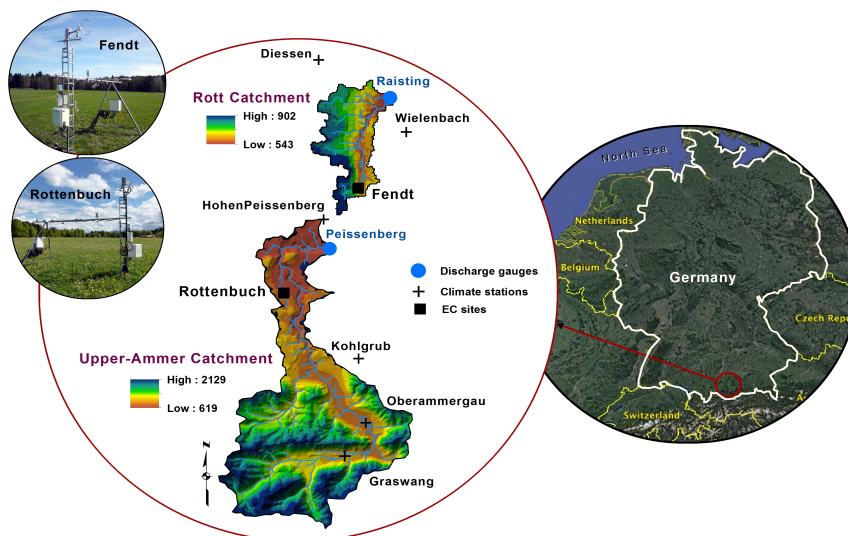


Figure 3.1: The geographical location of the TERENO prealpine observatory in southern Germany, and overview on elevations, river networks and observation stations in the Rott and Upper-Ammer catchments.

3 Forward modeling: coupled water and energy variables

The highest and lowest points in the Rott catchment are ranging from 902 m to 543 m, where the Raisting discharge gauge is located at the outlet of the basin. The corresponding values for the Upper-Ammer catchment are ranging from 2129 m to 619 m, where the Peissenberg discharge gauge is located at the outlet. The micrometeorological measurements from the Fendt EC site (47.831 °N, 11.061 °E) and the Rottenbuch EC site (47.730 °N, 10.061 °E) are used for model validation. The Fendt site is placed in area characterized as a pasture landuse (Figure 3.2a) with a Histosol soil type (Figure 3.2b). The Rottenbuch site is similarly located in pasture (Fig. 3.2a); however, has a soil profile with sandy loam soil (Figure 3.2b) at the surface, and a gravel layer at ~50 cm depth (Soltani et al., 2017). Additionally, the southern portion of each catchment, especially the Upper-Ammer, has the highest elevations and slopes greater than 50° in the southern TERENO region (Figure 3.2c).

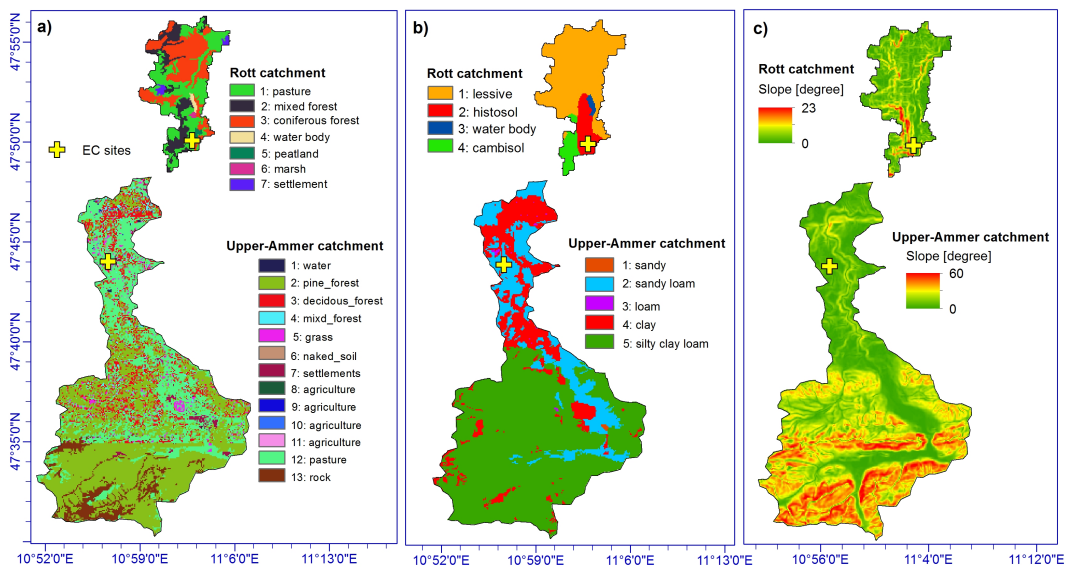


Figure 3.2: Spatial properties of the TERENO prealpine catchments: **a)** landuse, **b)** soil-type [in the Rott catchment] and soil texture [in the Upper-Ammer catchment], and **c)** terrain slope [in degrees]. The original vector data of landuse and soil properties taken from Hingerl et al. (2016) for the Rott catchment, and Kunstmann et al. (2006) for the Upper-Ammer catchment. They then reproduced using ArcMap GIS (ESRI, 2011) for this publication.

3.2.2 Hydrometeorological data

The meteorological dataset was obtained from three major sources for the calibration and validation periods in 01 May to 31 July 2013 and 2015, respectively. First, the EC-based turbulent fluxes and the micrometeorological measurements were obtained from the TERENO EC sites (Mauder et al., 2013). Second, the hourly forcing data for Wielenbach and Hohenpeissenberg, Kohlgrub, and Oberammergau stations were obtained from the Deutscher Wetterdienst (DWD) (<https://werdis.dwd.de>). Third, the hourly data of precipitation for the Diessen rain gauge and runoff for the Raisting and

Peissenberg discharge gauges were compiled from Bayerisches Landesamt für Umwelt (<http://www.hnd.bayern.de>).

The experimental period was selected for the simulation due to the fact that there usually remain uncertainties in the measured wintertime water and energy fluxes over the region (e.g. Hingerl et al., 2016). Additionally, the peak runoff volume and the highest energy balance closure were observed during summer periods (e.g. Soltani et al., 2017).

3.3 Methodology

3.3.1 Hydrological modeling

The model GEOTop V. 2.0 (Endrizzi et al., 2014) was used for the catchment-scale hydrologic simulation. It is a fully distributed physically-based hydrological model of the water and energy balance at and below the soil surface, designed for simulations in continuum in small and mesoscale mountain catchments over complex terrain (Bertoldi et al., 2004; Rigon et al., 2006). The core components of the GEOTop model are fully described in Endrizzi et al. (2014). However, here only a brief overview of the model's capabilities is presented.

The model solves the heat and water flow equations for temperature and moisture in the soil with a coupled three-dimensional numerical scheme (Bertoldi et al., 2014). Furthermore, the model considers radiation correction for complex topography. This includes the following: i) accounting for the solar incidence angle and the shadowing of direct solar radiation by surrounding mountains; ii) partitioning of radiation in direct and diffuse components according to Erbs et al. (1982); and iii) the effects of topography on diffuse radiation coming on the surrounding terrain (Iqbal, 1983), as described in Bertoldi et al. (2014). Therefore, GEOTop covers a variety of aspects of hydrological fluxes, from the energy balance to snow cover and snowmelt (Zanotti et al., 2004), the cryosphere (Endrizzi et al., 2014), the effects of vegetation (Endrizzi and Marsh, 2010), and ecohydrological processes (Bertoldi et al., 2010; Della Chiesa et al., 2014; Hingerl et al., 2016). This makes it a suitable choice for modelling the interacting water and energy fluxes at and beneath the land surface in the TERENO prealpine observatory (Endrizzi et al., 2014).

The model solves the water balance in the soil using the system of equations represented below (Endrizzi et al., 2014):

$$\begin{cases} \frac{\partial \theta_w^{ph}}{\partial t} + \frac{\rho_i}{\rho_w} \frac{\partial \theta_i}{\partial t} = 0 \\ \frac{\partial \theta_w^{fl}}{\partial t} + \nabla \cdot \mathbf{J}_w + S_w = 0 \end{cases} \quad (3.1)$$

where $\partial \theta_w^{ph}$ [-] is the fraction of liquid water content in soil subject to phase change, $\partial \theta_w^{fl}$ [-] the fraction of liquid water content transferred by water flux, ρ_i [kg m^{-3}] the

density of ice, ρ_w [kg m^{-3}] the density of liquid water in the soil, $\partial\theta_i$ [-] the fraction of ice in soil, t [s] time, $\nabla \cdot$ [-] divergence operator, J_w [m s^{-1}] the flux of liquid water, and also S_w [s^{-1}] as the mass sink term. The above equation describes the water flow occurring below the soil surface and is referred to as the variably saturated Richards equation. According to Darcy's law, J_w can be written as:

$$J_w = -K\nabla(\psi + z_f) \quad (3.2)$$

where, K [m s^{-1}] is the hydraulic conductivity, ψ [m] the liquid water gauge pressure head and z_f [m] the elevation head above a reference level. Defining H [m] as the sum of the pressure and potential heads: $H = \psi + z_f$, the second part of Eq. (3.1), combined with Eq. (3.2) becomes:

$$\frac{\partial\theta_w^{\text{fl}}}{\partial t} + \nabla \cdot (-K\nabla H) + S_w = 0 \quad (3.3)$$

Equation (3.3) is solved in a fully three-dimensional way in order to describe the two gradients of H in the direction parallel and normal to the surface. When the soil is saturated (either because of precipitation or melting snow), normal gradients become very small compared to those in the parallel direction, which consequently are responsible for the routing of water through the soil (Endrizzi et al., 2014).

Additionally, to fully describe the water balance in the soil and the runoff mechanisms, the surface (or overland) water flow needs to be taken into account. This process is described with the approximation proposed by Gottardi and Venutelli (1993), who extended to the surface flow the validity of Darcy's law, which would not be valid with the flow being turbulent. Using the water conservation and Darcy's law for the overland flow, the surface water balance is expressed as (Endrizzi et al., 2014):

$$\frac{\partial\psi|_{z=0}}{\partial t} - \nabla \cdot [\psi|_{z=0} K_{\text{sur}}\nabla(\psi|_{z=0} + z_f|_{z=0})] - P_e = 0 \quad (3.4)$$

where $\psi|_{z=0}$ (m) and $z_f|_{z=0}$ (m) are the liquid water pressure head and the elevation head at the soil surface, K_{sur} (m s^{-1}) the conductance, and P_e (m s^{-1}) the effective precipitation per unit horizontal surface that reaches the soil surface, including snowmelt flow and deducting evaporation from the soil. The variable $\psi|_{z=0}$ cannot be negative in Eq. (3.4), and is written in place of water depth above the surface. Following Gottardi and Venutelli (1993) the conductance is:

$$K_{\text{sur}} = c_s \psi|_z^\gamma = 0 \left(\frac{\partial\psi|_{z=0}}{\partial s} \right)^{-0.5} \quad (3.5)$$

where, s [m] is the length along the direction of maximum local slope, c_s [$\text{m}^{1-\gamma} \text{s}^{-1}$] the surface roughness coefficient, and γ an exponent between 0 and 1 varying according to the formulation of c_s .

It is noted that, GEOTop only describes water flow within a certain soil depth i.e. normally a few meters or tens of meters. Deep groundwater and water in the fractured rocks are not considered in the model, as it would require large amounts of data that typically are either not available or difficult to access. Thus, the model considers only a part of the soil water that is close to the surface and hydrologically active. Also, GEOTop uses Darcy's law to describe water flow in a porous medium

(water in the saturated zone close to the surface or aquifers), normally not for water in the deep fractured rocks and gravels.

The turbulent fluxes of sensible heat (H) and latent heat (LE) play a significant role in the surface energy balance closure (EBC). The H (LE) flux, which is associated with convection, driven by difference in temperature (vapour pressure) between land surface and the atmosphere. However, they are both largely driven by wind speed. Thus, it is important to consider in the model a topographically dependent wind field to describe the effect of topography on the surface EBC. According to Endrizzi et al. (2014), a full resolution of the fluid dynamic equations is too computationally heavy for GEOtop. The wind field is therefore parameterised using topography (Liston and Elder, 2006). The model calculates the turbulent fluxes H and LE with the flux-gradient relationship (e.g. Garratt, 1992):

$$H = \rho_a c_p w_s \frac{T_a - T_{sur}}{r_a} \quad (3.6)$$

$$LE = \beta_{YP} L_e \rho_a c_p w_s \frac{Q_a - \alpha_{YP} Q_s^*}{r_a} \quad (3.7)$$

where ρ_a is the air density (kg m^{-3}), c_p the specific heat at constant pressure ($\text{J kg}^{-1} \text{K}^{-1}$), w_s the wind speed (m s^{-1}), L_e the specific heat of vaporisation (J kg^{-1}), Q_s^* the saturated specific humidity (kg kg^{-1}) at the surface, Q_a the specific humidity of the air, and r_a the aerodynamic resistance (-). The α_{YP} and β_{YP} coefficients take into account the soil resistance to evaporation, and only depend on the liquid water pressure close to the soil surface. They are calculated according to the parameterisation of Ye and Pielke (1993), which considers evaporation as the sum of the proper evaporation from the surface and diffusion of water vapour in soil pores at greater depths. The aerodynamical resistance is obtained applying the Monin–Obukhov similarity theory (Monin and Obukhov, 1954), which requires that values of wind speed, air temperature and specific humidity are available at least at two different heights above the surface. In addition, the LE flux also depends on the soil moisture at the surface, which is a further coupling term to the water flow equations, as described above.

Model setup and input data

The following static datasets were used for simulation by the GEOtop model. The DEM $90 \times 90 \text{ m}^2$ ($100 \times 100 \text{ m}^2$) was obtained from the Shuttle Radar Topographic Mission – SRTM (<http://srtm.csi.cgiar.org>) for the Rott (Upper-Ammer) catchment. The river network, as well as, terrain aspect, slope, and sky view were calculated using ArcMap GIS based on techniques described by Ghesla and Rigon (2006).

The land cover, with a resolution of $250 \times 250 \text{ m}^2$ (Rott) and $150 \times 150 \text{ m}^2$ (Upper-Ammer), as well as, the soil type of $2 \times 2 \text{ km}^2$ for both catchments taken from Hingerl et al. (2016) and Kunstmann et al. (2006), respectively. Then, they were separately interpolated to the same resolution of the DEMs following Bertoldi et al. (2004). The soil is discretized in 13 layers, with thicknesses increasing from the surface to the deep layers. The top 8 layers starting from the surface have thicknesses

ranging from 0.1 to 0.5 m, with respect to the vertical gradients of water pressure and temperature (Endrizzi et al., 2014), while the lowest 5 layers have thicknesses ranging from 1.0 to 5.0 m.

The hourly meteorological data of precipitation, temperature, wind speed, wind direction, and radiation components were provided as input forcings for the model simulations. In the GEOtop code, air temperature and precipitation are spatially distributed according to Liston and Elder (2006). The integration of the model run is one-hour interval. Detailed information about the interpolation of the meteorological data in GEOtop is described in Endrizzi et al. (2014).

Model sensitivity and calibration

The GEOtop model was first applied to a summer episode starting from 01 May to 31 July 2013. A two-week spin-up period starting from 15 April to 30 April 2013 was conducted, as it was found experimentally that this is sufficient for the experimental period. The simulation is then used for determining the parameters' sensitivities and model calibration. In the simulation experiments, the key model parameters acting on the water and energy budgets (Table 3.1) are iteratively estimated based on the most sensitive parameters identified by the previous hydrological models run in the study area.

A “trial-and-error” procedure was used for the model calibration within an accepted range of values (Table 3.1). The effect of selected parameters on the model outputs were individually tested and optimized until the best fit was obtained between the simulated and measured data. The calibration results are given in Table 3.1. It was found that changes in the parameter values from the northern (Fendt) to the middle parts (Rottenbuch) of the TERENO prealpine region are realistic and explainable based on changes in e.g. climatic-environmental conditions and land-surface properties for those regions. For example, the difference in the calibrated values of α_w can be explained by differences in the soil properties for those two areas. In Fendt, the dominant soil-type is Histosol, whereas Rottenbuch is covered by a sandy-loam soil-texture.

The soil parameter K_v determines the highest capacity of infiltration and highly affects both the surface runoff generation and the magnitude of peak discharge. The parameter of K_h impacts the flood tail as it determines the subsurface runoff quantity (Rigon et al., 2006). These parameters also were reasonably calibrated (see Table 3.1).

Further, the initial condition on water table depth was set as: *InitWaterTableHeightOverTopoSurface/InitWaterTableDepth* = - 5,000/1,000 mm (Rott catchment) and = -10,000/1,500 mm (Upper-Ammer catchment). The initial condition for the soil pressure i.e. *InitSoilPressure* and *InitSoilPressureBedrock* were kept constant by default for both catchments.

3 Forward modeling: coupled water and energy variables

Table 3.1 Calibrated model parameters. The estimated values of soil parameters (i.e. K_v and K_h and α) represent the topsoil layer. For the remaining 12-layers, the calibrated values of K_v range from 0.12 to 0.26 mm s⁻¹ in Rott and 0.10 to 0.85 mm s⁻¹ in Upper-Ammer, and K_h estimates vary from 1.00E-04 to 3.00E-2 mm s⁻¹ for the Rott catchment and 1.00E-04 to 9.000E-1 mm s⁻¹ for the Upper-Ammer catchment. Also, the values for deeper layers of α were ~ 1.00E-5 to 3.0E-4 mm⁻¹ for both catchments.

Parameter	Description	Unit	Range	Calibrated values	
				Fendt/Rott	Rottenbuch/ Upper-Ammer
C_f	Canopy fraction [0: no canopy in the pixel, 1: pixel fully covered by canopy]	-	0, 1	0.45	0.55
C_h	Canopy height	mm	0, 20000	350	450
α_w	Ground surface albedo without snow in the visible - saturated	-	0, 1	0.15	0.25
V_{ref}	Vegetation reflectivity in the visible	-	0, 1	0.15	0.15
ε	Ground surface emissivity	-	0, 1	0.96	0.99
K_v	Vertical hydraulic conductivity	mm s ⁻¹		1.0	1.0
K_h	Horizontal hydraulic conductivity	mm s ⁻¹		1.0	1.0
α	Van Genuchten parameter α	mm ⁻¹		8.00E-04	5.00E-04
n	Van Genuchten parameter n	-		1.81	1.55
λ_s	Thermal conductivity of the bedrock	W m ⁻¹ K ⁻¹		0.01	0.01
C_m	Coefficient of the law of uniform motion on the surface	m ⁻¹ s ⁻¹	0.01, 5.0	2.0	3.0
γ	Exponent of the law of uniform motion on the surface	-		0.24	0.15
C_w	Fraction of channel width in the pixel width	-		0.5	0.5

Model performance evaluation and validation

Model evaluation statistics are commonly utilized for comparing model outputs against measurements. There is a large variety of evaluation metrics, but no single metric which encapsulates all aspects of interest exists. For this reason, six statistical metrics were used to evaluate the performance of GEOtop in this study. They are described in Table 3.2.

In addition, according to the fact that the relationships between hydrometeorological variables may be highly nonlinear, we employ the concept of the empirical Copula (described in the following section). Unlike the linear statistical measures, the nonparametric empirical Copula-based approach is able to describe the underlying joint behavior of water and energy fluxes (Genest and Favre 2007; Serinaldi, 2009; Laux *et al.*, 2011).

The calibrated GEOtop model simulated an independent period of 01 May to 31 July 2015 for validation.

Table 3.2: The statistical metrics used for the model performance evaluation.

Metrics	Description	References
R ²	<p>Coefficient of Determination: It measures the strength of linear relationship between two variables. It specifies how much of the variation in the dependent variable y is characterized by a variation in the independent variable x</p>	Carslaw (2015)
MB	<p>Mean Bias: It provides a good indication of the mean over –or underestimate of simulations. The optimal value of MB is 0, with low-magnitude values indicating accurate model simulation. Positive values indicate model underestimation bias, and negative values indicate model overestimation bias</p>	Gupta et al. (1999); Moriassi et al. (2007)
RMSE	<p>Root Mean Square Error: It provides a good overall measure of how close modelled values are to observed values. Lower RMSE indicates a better model performance (or less residual)</p>	Singh et al. (2004); Moriassi et al. (2007); Carslaw (2015)
NSE	<p>Nash-Sutcliffe Efficiency: It determines the relative magnitude of residual variance compared to the measured data variance. NSE ranges between $-\infty$ and 1, with NSE = 1 being the optimal value. Values between 0 and 1 are viewed as acceptable levels of performance, whereas values <0 indicates that the mean observed value is a better predictor than the simulated value, which indicates unacceptable performance</p>	Nash and Sutcliffe (1970); Moriassi et al. (2007)
COE	<p>Coefficient of Efficiency: It is used for measuring model performance. A perfect model has a COE = 1. Although COE has no lower bound, a value of COE = 0 implies that the model is no more able to predict the observed values than does the observed mean. Thus, such a model can have no predictive advantage</p>	Legates and McCabe (2012); Legates and McCabe Jr (1999); Carslaw (2015)
IOA	<p>Index of Agreement: It is used in model evaluation. It ranges between -1 and +1 with values approaching +1 representing better model performance. IOA = 0 signifies that sum of the magnitudes of the errors and the sum of the observed-deviation magnitudes are equivalent. Values of IOA near -1 indicate that the model-estimated deviations are poor estimates of the observed deviations</p>	Willmott et al. (2011); Carslaw (2015)

3.3.2 Bivariate density estimation using empirical Copulas

Hydrometeorological variables usually show nonlinear behaviours and hence their relationships are very complex. Traditionally, the pairwise dependence between these variables has been described using classical families of bivariate distributions such as normal, log-normal, gamma, and extreme-value distributions. The main limitation of this approach is that the individual behaviour of the two variables or transformations thereof must then be characterized by the same parametric family of univariate distributions. Copula models, however, avoid this restriction (Genest and Favre, 2007).

The Copula approach is based on the theorem of Sklar (Sklar, 1959). It states that any multivariate distribution function can be decomposed into the marginal distributions and a Copula, which captures the dependence between variables. In this study, the dependence structures of hourly measured and simulated water and energy variables of discharge, soil moisture, sensible heat flux and latent heat flux were estimated for the Fendt and Rottenbuch EC sites located in the Rott and Upper-Ammer catchments, respectively (see Fig. 3.1 for further details).

To calculate the Copula density C , first \hat{F}_x, \hat{F}_y of the marginal distributions was obtained using the empirical distribution function and then the pseudo-observations $(\hat{u}, \hat{v}) = (\hat{F}_x(x), \hat{F}_y(Y))$ were defined. The Copula density was finally estimated as the joint density of (\hat{u}, \hat{v}) . To analyze the real underlying dependence structure, the empirical Copula is estimated. It is purely based on the data (Deheuvels, 1979). When $\{r_1(1), \dots, r_1(n)\}$ and $\{r_2(1), \dots, r_2(n)\}$ denoting the rank space values that are derived from the marginal distributions, the empirical Copula is then as follows (Deheuvels, 1979):

$$C_n(u, v) = 1/n \sum_{t=1}^n \mathbf{1} \left(\frac{r_1(t)}{n} \leq u, \frac{r_2(t)}{n} \leq v \right) \quad (3.8)$$

with $u = F_X(x)$, $v = F_Y(y)$ and $\mathbf{1}(\dots)$ denoting the indicator function and n being the sample size. For more information regarding Copulas, refer to e.g. Nelson (1999) and Salvadori et al. (2007).

3.4 Results and discussion

3.4.1 Spatiotemporal variability of water and energy fluxes

Figure 3.3 shows the temporal variations of surface turbulent fluxes on daily resolution as a calendar plot, where the wind angle scaled to the wind speed to highlight both the direction and the strength of the wind of a particular day for the Fendt and Rottenbuch EC sites. At Fendt, the highest turbulent flux with a magnitude of more than 250 W/m^2 on the 7th of July was associated with northeasterly winds during the experimental period. The corresponding value for the Rottenbuch ($> 140 \text{ W/m}^2$) was connected to northwesterly flows that occurred on the 15th of July.

The results indicate a clear increase in the turbulent flux concentration from May to July at both sites due to the increase in solar radiation; however, the temporal variation patterns are different at the individual sites.

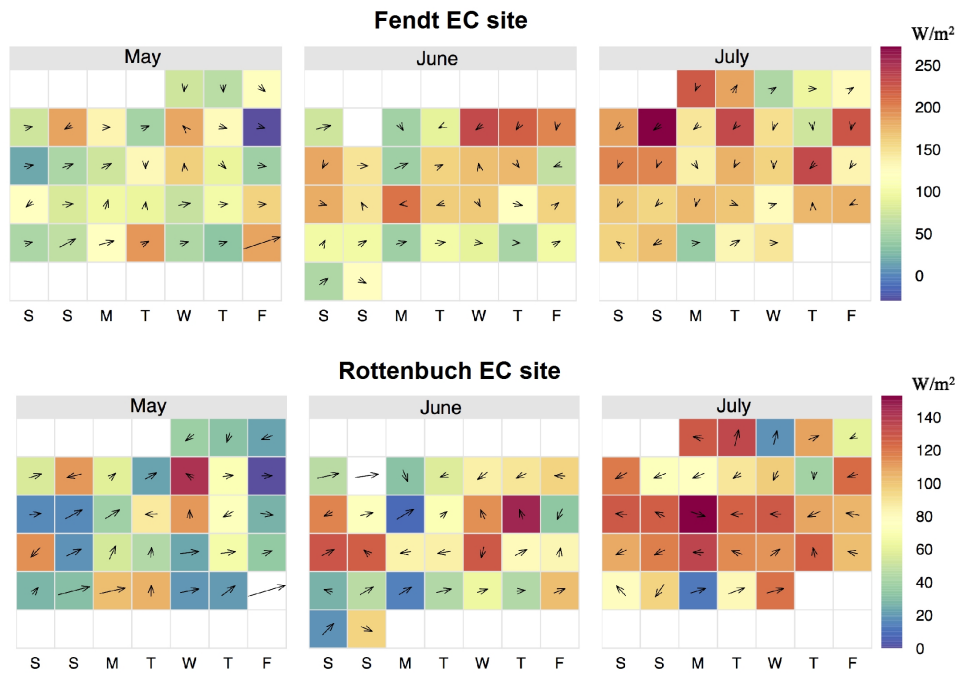


Figure 3.3: Calendar plots for the half-hourly-based mean daily concentrations of the turbulent fluxes (sum of H and LE) in 2013 at the TERENO prealpine EC sites with annotations showing wind angle scaled to wind speed i.e. the longer the arrow, the higher the wind speed. The wind speed ranging from 0.01 (0.04) m s^{-1} to 8.08 (7.44) m s^{-1} at Fendt (Rottenbuch) EC site.

The spatial variability of heat and water fluxes in the TERENO prealpine region is significantly affected by diversity in topography, radiation and wind components, soil moisture properties as well as land cover and vegetation types. The surface temperature and ET values (Figure 3.4) range from 9 to 21 °C and 17 to 160 mm, respectively, in the Upper-Ammer catchment. The corresponding values for the Rott catchment are 15 to 20 °C and 42 to 153 mm, respectively. The maximum values are simulated at parts of the basin with i) the lowest elevation, slope (controls the net radiation e.g. Dubayah et al., 1990), and wind speed (Chow et al., 2006) ii) Histosol or sandy-loam texture soil, and iii) in pasture or peatland vegetation cover (determines storage capacity (e.g. Bertoldi et al., 2010). The different forest types tend to have the lowest ET values across the region. The mean surface temperature reflected the diverse surface topography of the TERENO prealpine region by exhibiting an elevation-dependent temperature variation of 10C in the Upper-Ammer area and 4 °C in Rott. The spatial patterns obtained herein should be interpreted with care, as a soil-type map of $2 \times 2 \text{ km}^2$ used for model input is rather coarse with respect to other model's input layers and computational resolution.

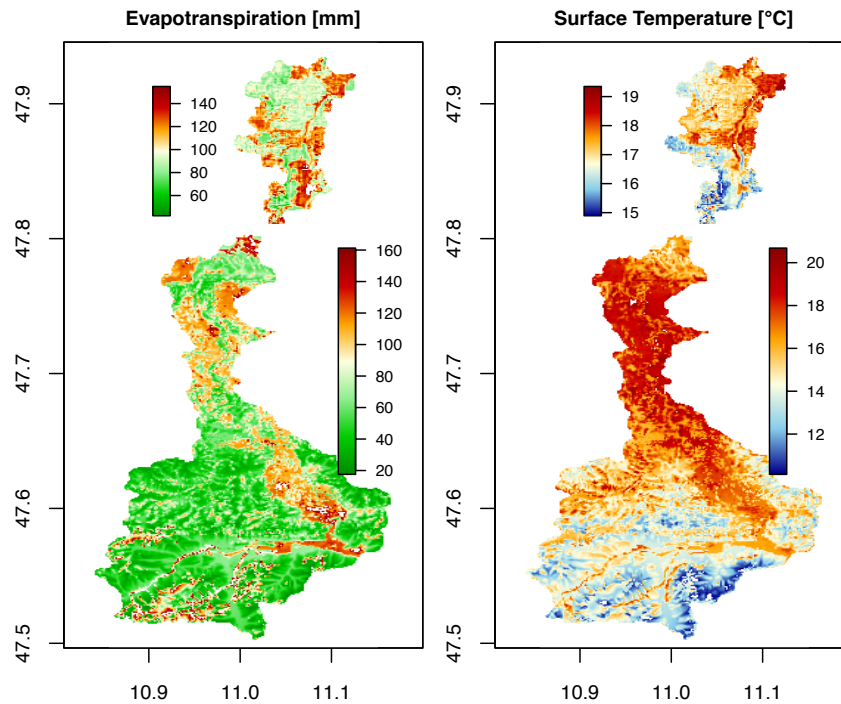


Figure 3.4: Simulated spatial distributions of ET (mm/month) and surface temperature (°C/month) averaged for the period of May to July 2013 at the TERENO prealpine catchments.

3.4.2 Joint simulation of water and energy fluxes using GEOTop

Water balance

The comparison of measured and simulated discharge in the TERENO prealpine catchments are shown in Figure 3.5. Overall, GEOTop was capable of replicating appropriately the river discharge dynamics with a high efficiency (see Table 3.3). The NSE indicates a high performance of the model to represent the temporal variability of discharge (NSE = 0.86 for Rott and NSE = 0.81 for Upper-Ammer) in which the volumes of discharges are reasonably reproduced at both catchments. That is, total simulated discharge volume for the 3-month period was 3886 m³ in Rott and 53884 m³ in Upper-Ammer. This, indicates an underestimation of about 25% and 15%, respectively, compared to the measured discharge volumes of 5168 m³ and 62509 m³. This was also represented by MB values of -0.34 m³ for Rott and -2.01 m³ for Upper-Ammer.

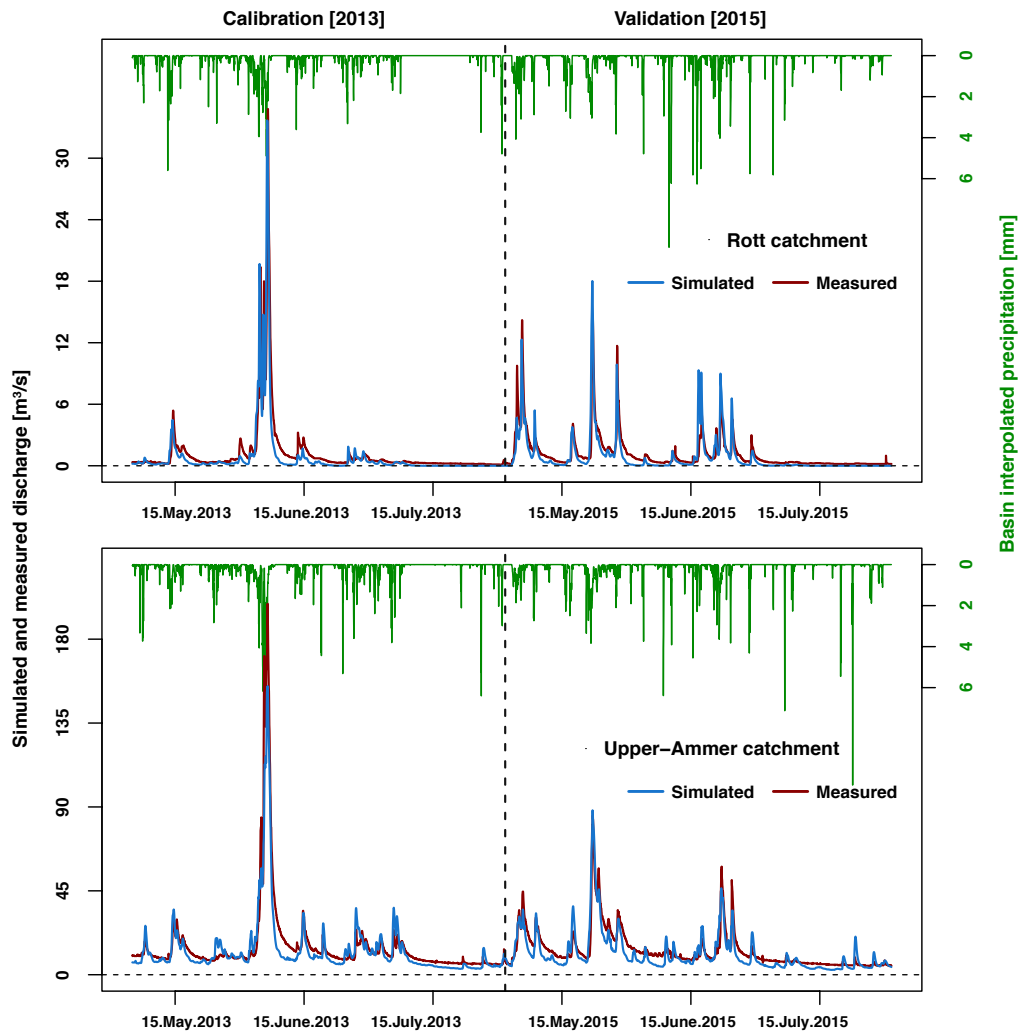


Figure 3.5: Simulated versus measured hourly river discharge hydrographs for the calibration (May to July 2013) and validation period (May to July 2015) in the Raisting gauge at outlet of Rott catchment and the Peissenberg gauge at outlet of Upper-Ammer catchment in the TERENO prealpine region.

In both catchments, an increased runoff volume in early June peak flow highlights the importance of snow dynamics for runoff generation in the region. The model captures the peak flow well in Rott, but underestimates it in the Upper-Ammer catchment. This might be explained by the lack of meteorological stations, which can result in considerable errors in the spatial interpolation by the model. These differences may further be explained by the rapid climate zone changes in a small spatial area or by the snow dynamics effect on the behavior of surface runoff during the springtime (Kunstmann et al., 2006). The values of RMSE are very low (i.e. 1.29 - Rott and 7.36 - Upper-Ammer) while R^2 are high (i.e. Rott: 0.80; Upper Ammer: 0.88), indicating that simulated and measured discharges have low residuals and strong linear relationships. According to Figure 3.5, the GEOtop model, similar to the calibration period, indicates a good performance to replicate the river runoff by capturing the

3 Forward modeling: coupled water and energy variables

peak flows at both catchments during the validation period (see Table 3.3 for detailed information about the statistical measures).

Table 3.3: Statistical measures for the simulated vs. measured discharge and soil moisture during the calibration period (May to July 2013) at the TERENO prealpine region. The values in brackets denote the statistics of the independent validation for the period of May to July 2015.

Statistics	Discharge		Soil moisture (-5 cm)	
	Rott catchment	Upper-Ammer catchment	Fendt EC site	Rottenbuch EC site
MB	-0.34 (-0.23)	-2.01 (-1.88)	0.04 (0.12)	0.02 (-0.01)
RMSE	1.29 (1.04)	7.32 (4.81)	0.07 (0.16)	0.06 (0.05)
R ²	0.80 (0.73)	0.88 (0.82)	0.94 (0.79)	0.84 (0.86)
COE	0.52 (0.45)	0.54 (0.46)	0.68 (0.19)	0.48 (0.56)
IOA	0.76 (0.72)	0.77 (0.73)	0.84 (0.59)	0.74 (0.78)
NSE	0.86 (0.77)	0.81 (0.81)	0.75 (0.12)	0.20 (0.38)

Figure 3.6 displays the time series of the site-scale, hourly measured and simulated soil moisture for the Fendt and Rottenbuch EC sites at three different depths from May to July for the calibration and validation periods. Over the calibration period, GEOtop indicates a strong linear relationship between the simulated and measured -5 cm soil moistures at Fendt ($R^2 = 0.94$) and Rottenbuch ($R^2 = 0.84$). The daily fluctuation of observed soil moisture at Fendt ranges from about 25% to 75%, while it ranges approximately from 20% to 50% for the Rottenbuch site. The different soil texture and soil type could explain this discrepancy, where sandy-loam soil texture and Histosol type prevail. This is why the maximum soil moisture close to the surface layer in Rottenbuch was about 50%.

Apart from a different soil type, which results in a high variation in the near surface soil water content in Fendt, the soil moisture also depends strongly on the variation of the groundwater table depth for that area (Wolf et al., 2016). When there is a deficit in rainfall, the rate of soil moisture drops quickly and reaches up to 20% at both sites. Due to scale differences between grid cells and point measurements it is not easy to compare precisely the simulated soil moisture with those of the measurements (Manabe et al., 2004).

Nevertheless, it was found that GEOtop is appropriately capable of reproducing infiltration and daily cycle of soil moisture evaporation associated with the rainfall events with the lowest mean bias and error and the highest efficiency and agreements. The model shows a similar performance to replicate the soil moisture during the validation period for both EC sites (see Table 3.3 for further details).

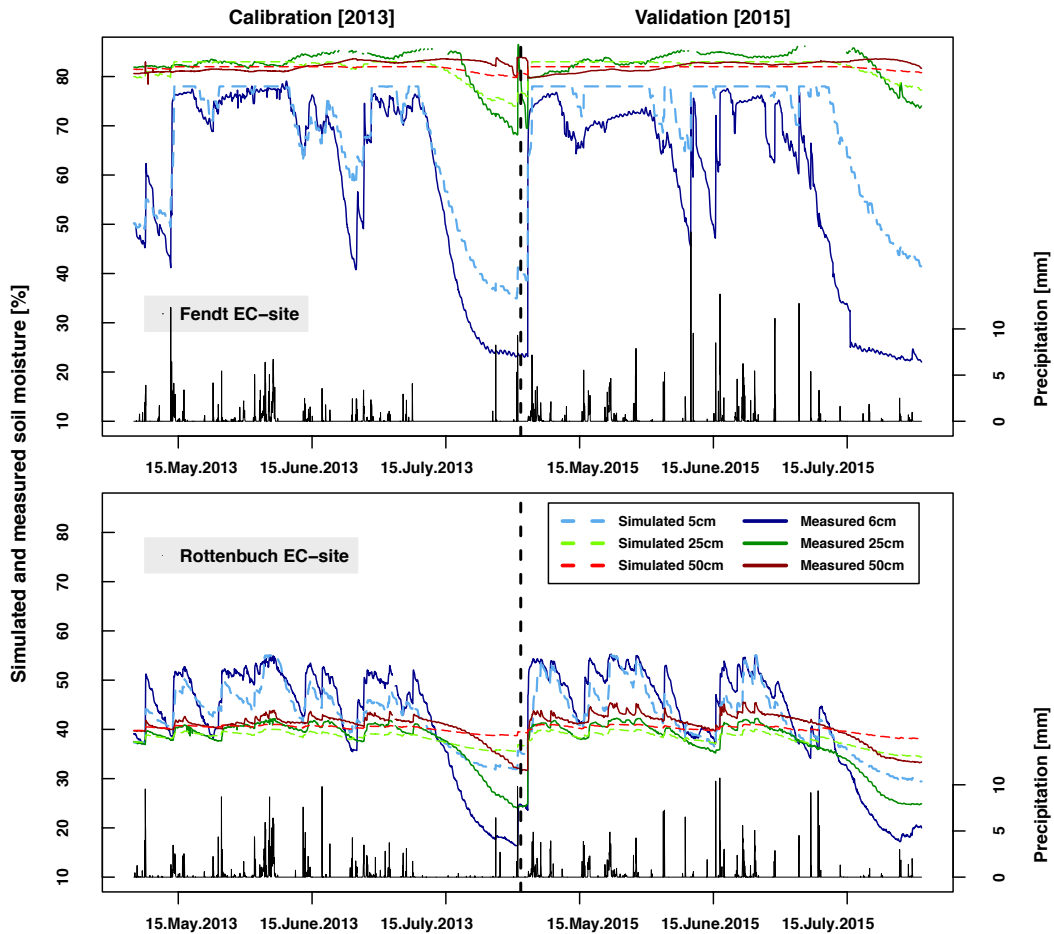


Figure 3.6: Simulated versus measured hourly soil moisture values at the depths of 5cm (blue), 25cm (green) and 50cm (red) for the calibration period (May to July 2013) and validation period (May to July 2015) at the TERENO prealpine EC sites.

The distributed soil moisture maps at -5 cm layer simulated by the model, as shown in Figure 3.7, are found to be highly influenced by the heterogeneous topography (terrain slope) and different landuse as well as soil texture patterns. With regard to topography, obviously the most (least) saturated soil water content greater than 70% (less than 30%) is mainly found in the low lands (steep gradients), which are mostly located in northern (southern) parts of the TERENO prealpine region. The spatial distribution of soil moisture highly follows the spatial distribution of the ET pattern (see Fig. 3.4), which was also confirmed by the site-scale results at both Fendt (70%) and Rottenbuch (45%).

Furthermore, in Rott, 87% (89%) of precipitation leaves the basin as ET and only 13% (11%) is consumed for runoff generation during the calibration (validation) period. In Upper-Ammer, however, the water balance condition is quite different. Approximately 68% (56%) of the precipitation leaves the catchment as discharge and ET consumes around 32% (44%) during the calibration (validation) period, which

indicates the importance of runoff generation by increasing flooding potentials in the lowlands during the summertime.

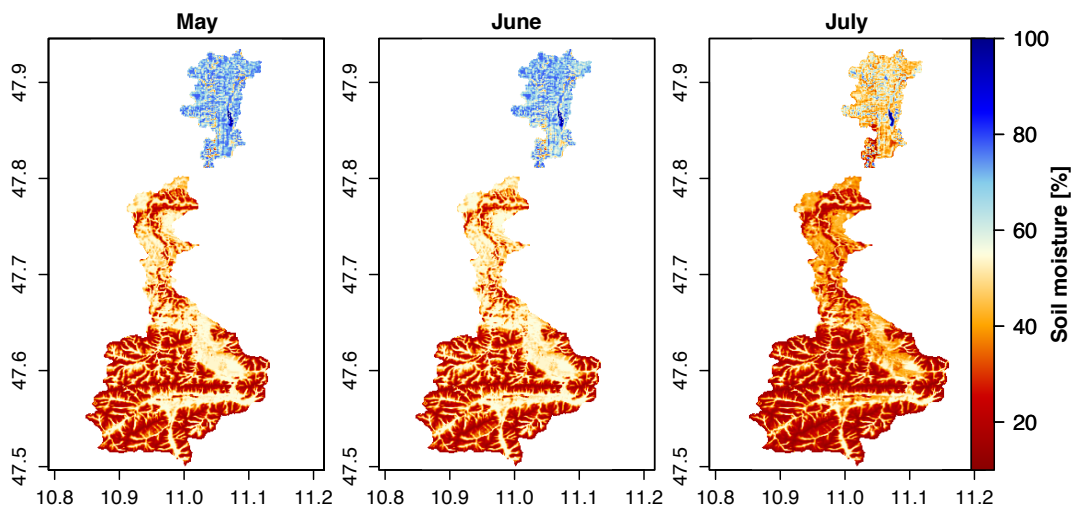


Figure 3.7: Distributed soil moisture content at 5cm depth for the calibration period (2013) at the TERENO prealpine catchments. The data represents monthly averages.

Energy balance

The comparison between simulated and measured site-scale diurnal surface energy fluxes of R_n , LE , H and G in the TERENO prealpine EC sites is illustrated in Figure 3.8. Overall, the EC-based diurnal cycles of energy fluxes were well reproduced by GEOTop, which is confirmed by high values of correlation coefficients, efficiency and agreements between the measured and simulated R_n , H , LE and G (see Table 3.4). Some bias is observed in R_n ($MB = -17.4 \text{ W/m}^2$ at Fendt and $MB = -20.7 \text{ W/m}^2$ at Rottenbuch), which indicates that R_n is underestimated. To identify the possible reasons, the modeled radiation components (i.e. incoming short/longwave and outgoing short/longwave) were compared against the measurements. It was found that the modeled Incoming Shortwave Radiation (ISR) shows a considerable bias ($MB = -115.6 \text{ W/m}^2$ at Fendt and $MB = -120.9 \text{ W/m}^2$ at Rottenbuch) and was underestimated by the model.

The model slightly overestimates LE ($MB = 14.3$ at Fendt and $MB = 24.8$ at Rottenbuch), in particular during the first part of the day with a peak at around 11:00. The midday overestimation of the simulated LE flux at the EC sites might be explained by the lack of energy balance closure (EBC) in the EC-based measurements, where the imbalance (residual energy) at Fendt is 31% (Fig. 3.9c). At Rottenbuch, however, not only it is even higher (39%) as illustrated in Figure 3.9d, but also LE flux partitioning to R_n is at least twice as low as that of in Fendt.

3 Forward modeling: coupled water and energy variables

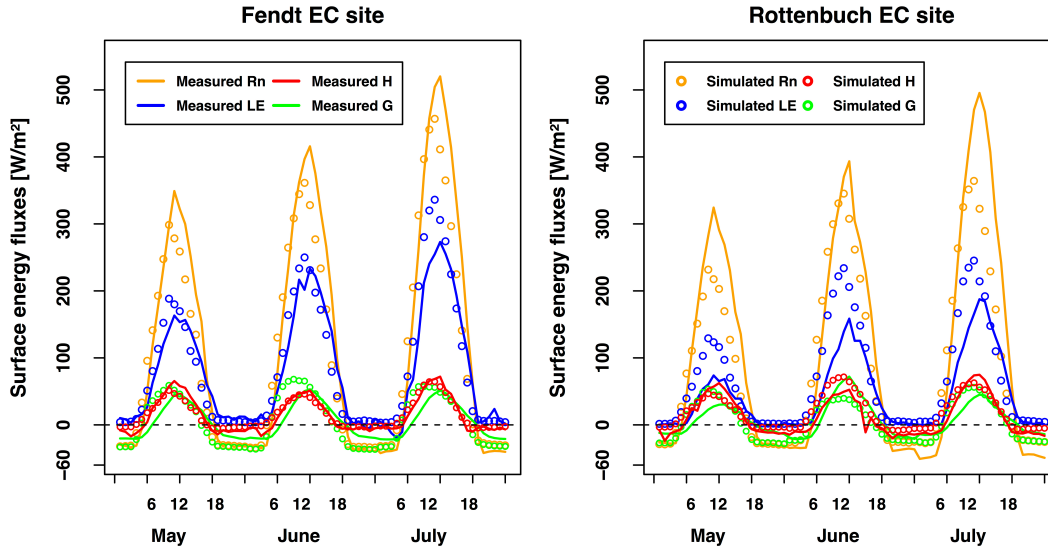


Figure 3.8: Simulated versus measured diurnal cycle of the energy balance components of the net radiation (Rn), sensible heat (H), latent heat (LE) and soil heat (G) for the calibration period (2013) at the TERENO prealpine EC sites. The figure is based on hourly data.

Table 3.4: Statistical measures for the simulated vs. measured net radiation (Rn), sensible heat (H), latent heat (LE), and soil heat (G) fluxes during the calibration period (May to July 2013) at the TERENO prealpine EC sites. The values in brackets denote the statistics of the independent validation for the period of May to July 2015.

	Statistics	Rn	H	LE	G
Fendt EC site	MB	-17.4 (-10.9)	0.84 (0.36)	14.3 (23.6)	-0.14 (-1.92)
	RMSE	75.9 (26.5)	20.7 (18.9)	65.0 (58.4)	28.7 (19.8)
	R ²	0.85 (0.98)	0.60 (0.75)	0.70 (0.82)	0.56 (0.84)
	COE	0.68 (0.87)	0.48 (0.57)	0.48 (0.58)	0.10 (0.47)
	IOA	0.84 (0.93)	0.74 (0.78)	0.74 (0.79)	0.55 (0.73)
	NSE	0.81 (0.98)	0.37 (0.45)	0.73 (0.81)	0.57 (0.83)
Rottenbuch EC site	MB	-20.7 (-2.47)	7.12 (-44.7)	24.8 (77.9)	-2.51 (-5.79)
	RMSE	88.4 (54.4)	38.9 (77.1)	66.5 (96.3)	24.8 (27.9)
	R ²	0.79 (0.92)	0.30 (0.52)	0.56 (0.65)	0.50 (0.47)
	COE	0.61 (0.78)	0.37 (0.31)	0.28 (-1.98)	0.13 (0.29)
	IOA	0.80 (0.89)	0.68 (0.65)	0.64 (-0.32)	0.56 (0.64)
	NSE	0.66 (0.90)	-0.06 (-0.67)	0.55 (-0.03)	0.47 (0.06)

A lower LE partitioning at Rottenbuch can be explained by a different soil texture for that area, where the sandy-loam at the surface and a gravel layer at about 50 cm depth is predominant, resulting in the precipitation infiltrating quickly into the deep ground, thus the surface dries out rapidly soon after the rainfall events (Soltani et al., 2017). The G flux is overestimated during early morning hours with a lower mean bias similar to Rn values. The main consumer of Rn is LE over the experimental period at the study sites.

The intercomparison of the simulated and measured energy balance components in the TERENO EC sites are shown in Figures 3.9a and 3.9b. GEOTop overestimates LE flux at Fendt (with a slope of 1.04) and even more at Rottenbuch

3 Forward modeling: coupled water and energy variables

(1.07). This could be due to the fact that the EC-based technique usually underestimates turbulent fluxes, in particular LE measurement, as reported worldwide (e.g. Hendricks-Franssen et al., 2010; Stoy et al., 2013; Imukova et al., 2016), also in the TERENO prealpine region (Eder et al., 2014; Soltani et al., 2017).

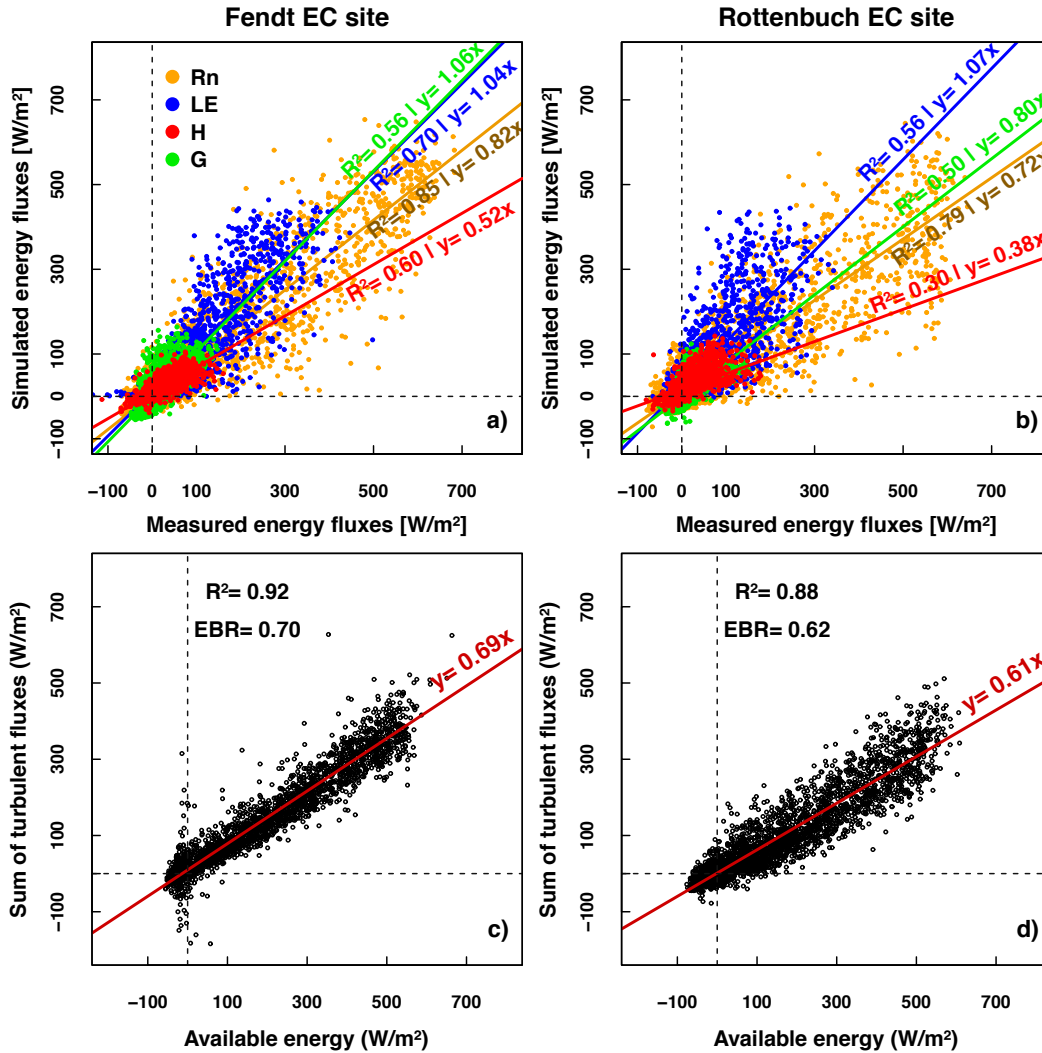


Figure 3.9: (a, b): Intercomparison of the simulated against measured energy fluxes of the net radiation (Rn), sensible heat (H), latent heat (LE) and soil heat (G). (c, d): Intercomparison of measured sum of the turbulent fluxes (H + LE) against the available energy (Rn - G) for the calibration period [May to July 2013] at the TERENO prealpine EC sites. The energy balance ratio was calculated as: $EBR = \frac{\sum(LH + H)}{\sum(Rn - G)}$. Gray horizontal and vertical dashed-lines indicate the zero value. The figure is based on hourly data.

As shown in Figures 3.9c and 3.9d, the EBC is estimated 0.69 and 0.61 with R² values of 0.92 and 0.88 at Fendt and Rottenbuch sites, respectively. In terms of energy balance ratio (EBR), a higher EBR value of 0.70 is calculated at Fendt indicating that the minimum heat and water vapor fluxes are lost for that area compared to the

3 Forward modeling: coupled water and energy variables

Rottenbuch site, where a lower slope of 0.61 and EBR value of 0.62 are found. Soltani et al. (2017) suggested that this imbalance at Rottenbuch is likely due to the advection of heat and vapor in that area (Fig. 3.9d). Similar results were also found by Hingerl et al. (2016). Other studies have also shown an energy imbalance in the region (e.g. Eder et al., 2014).

The spatial distributions of H and LE fluxes modeled by GEOtop are strongly driven by the heterogeneity of the TERENO prealpine region (Figure 3.10). In terms of topography and terrain slope, for example, the maximum H and minimum LE are found at the highest elevations at both catchments, which are in good agreement with the ET and surface temperature distributions (see Figure 3.4).

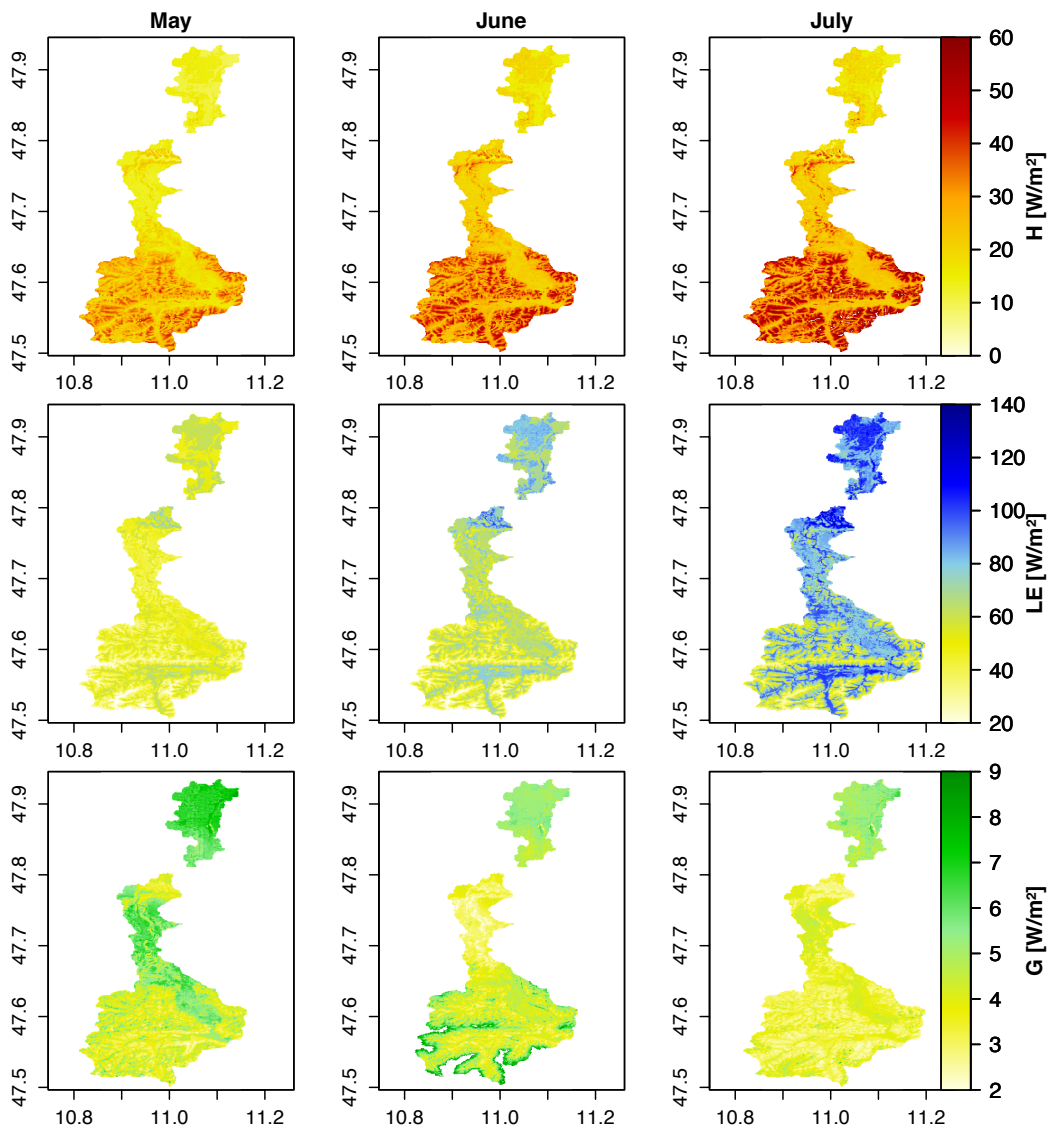


Figure 3.10: Distributed surface energy fluxes of the sensible heat (H), latent heat (LE) and soil heat (G) for the calibration period (2013) at the TERENO prealpine catchments. The data represents monthly averages.

The energy partitioning of R_n , LE, H and G fluxes indicates that in Rott, approximately 78.5% (82.6%) of R_n leaves the catchment as LE, 17% (12.6%) leaves as H, and 4.5% (4.8%) enters the soil as G during the calibration (validation) period. The energy balance condition in the Upper-Ammer catchment, however, shows a different pattern, where the portion of H is significantly increased. Approximately 65% (69.5%) of R_n leaves the catchment as LE, 31% (27%) leaves as H and 4% (3.5%) enters the soil as G during the calibration (validation) period.

3.4.3 Copula-based dependence structures of water and energy fluxes

Water fluxes

The empirical Copula densities of the measured and simulated variables of discharge and soil moisture are illustrated in Figure 3.11a. For Rott, the empirical Copula density between the measured discharge and soil moisture indicates a strong symmetric dependence structure, where the highest density is found for the lower left, and a second maximum in the upper right. This means that the measured discharge and soil moisture show the highest correlations for both the low and extreme values, respectively. The density function for the simulated dependence structure shows almost a similar pattern as the measured one, but is different in terms of the lower and upper densities. It implies that the modeled discharge and soil moisture values represent lower dependencies (correlations) than those of the observed ones. In addition, a positive bias for the simulated discharge is observed at the low, but also at very high values.

The Copula densities of both measured and simulated discharges and soil moistures in Upper-Ammer indicate a significant symmetric dependence structure with the highest densities in the lower left for the measured, and in the upper right for the simulated. In other words, the highest correlation between the measured discharge and soil moisture is found at the very low values, whereas the corresponding correlation for the simulated ones is observed at the high values. The empirical density between discharge and rainfall intensity was analyzed, as well. Here, no clear pattern of the dependence structure was found (not shown). As shown in Figure 3.11b, the distribution of measured against simulated discharge is asymmetrical, with the highest density in the upper-right corner. This indicates that measured and simulated discharges are strongly concordant in the higher ranks of the distribution. The concordance is weaker in the lower ranks in both catchments. This conveys that the calibrated model is more capable of replicating the high (peak) streamflow values than those of very low values at both Rott and Upper-Ammer catchments. However, GEOTop captured the low flow values for Upper-Ammer better than it did for the Rott (see Fig. 3.5). This can be seen in Figure 3.11b, where a second density maximum is found at the lower-left corner, indicating a reasonable performance of the model to simulate the low discharge at the Upper-Ammer catchment. However, the dependence structure between the measured versus simulated soil moisture is different. This

means that the modeled low values show the highest agreements with those of the observed ones at both Fendt and Rottenbuch EC sites. Also, the model shows a good performance to replicate the higher values (especially in Fendt), as a second density maximum can be found at the upper-right corners at both sites. See Figure 3.6 for clarification, where the soil moisture time-series are plotted.

Energy fluxes

Figure 3.12a shows the empirical Copula densities of the measured and simulated turbulent fluxes. A nonlinear structure of the joint relationship for both measured and simulated latent and sensible heat flux is observed, with strongly varying densities in the different percentiles. The highest density is found for the high turbulent flux values in the upper-right corner, whereas the lower tails do not show a significant dependence structure in both Fendt and Rottenbuch. Hence, the modeled latent and sensible heat fluxes represent the highest correlations at the high values, whereas the observed ones show a lower correlation for the corresponding values.

The empirical Copula densities for the measured against simulated latent and sensible heat fluxes, according to Figure 3.12b, are almost asymmetrical for both sites. This implies that the highest density function between the measured and simulated latent (sensible) heat flux is seen in the upper-right (lower-left) corner, where the extreme (very low) values are found. In other words, GEOtop shows a better performance to replicate the high (low) values of LE (H) at both Fendt and Rottenbuch EC sites.

The empirical Copula density functions for further hydrometeorological variables were estimated, as well. No clear dependence structures between the discharge – soil moisture and sensible heat flux – latent heat flux was identified (not shown).

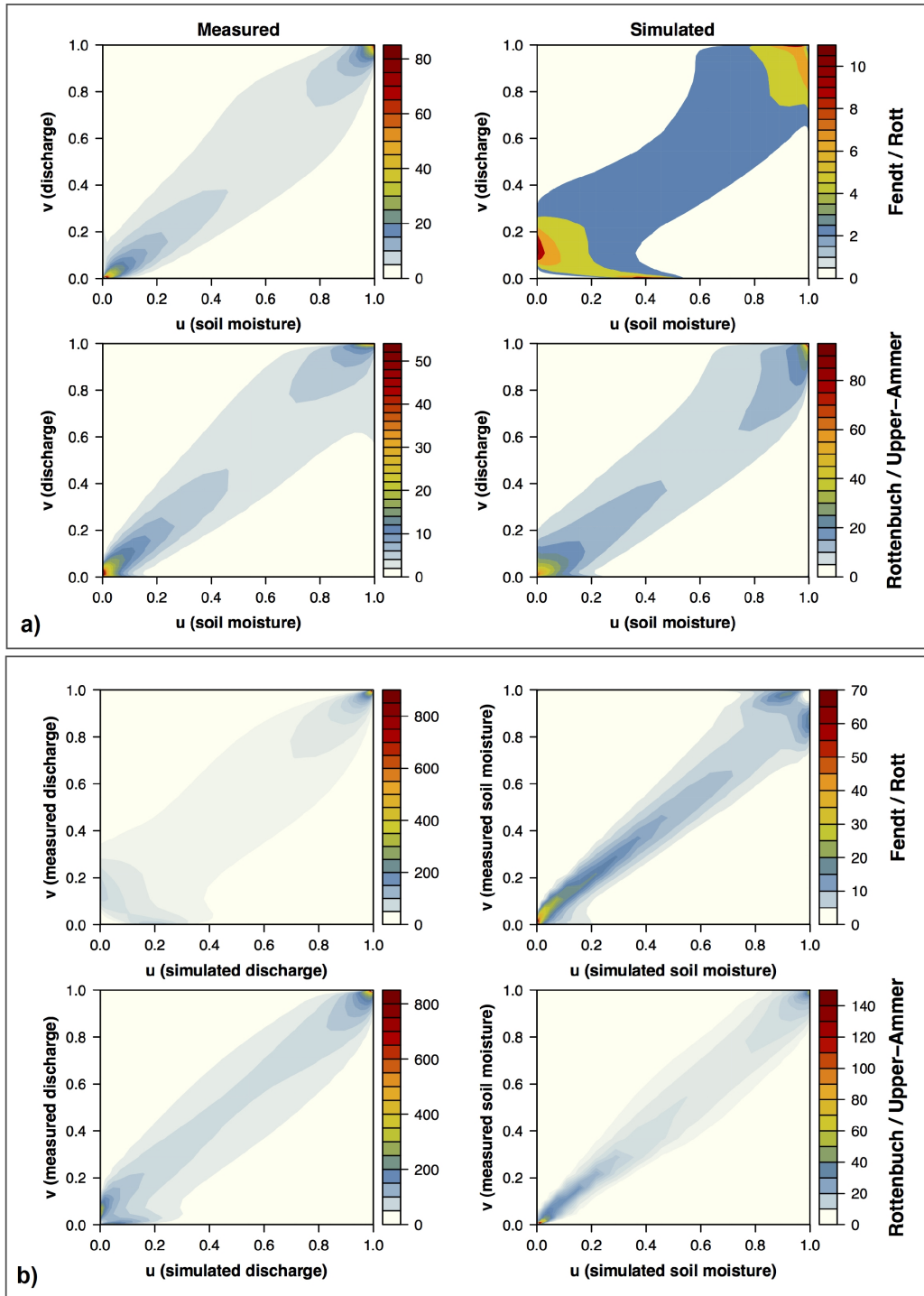


Figure 3.11: Empirical Copula densities: **a)** for the measured (left panels) and simulated (right panels) variables of the discharge (v) and soil moisture at 5 cm depth (u) for the Fendt EC site in the Rott catchment (top row) and for the Rottenbuch EC site in the Upper-Ammer catchment (bottom row); **b)** for the simulated (u) against measured (v) variables of the discharge and soil moisture at 5 cm depth for the Fendt EC site in the Rott catchment (top row) and for the Rottenbuch EC site in the Upper-Ammer catchment (bottom row) during the calibration period of May to July 2013. The sample size is 1369 data tuples for all the variables.

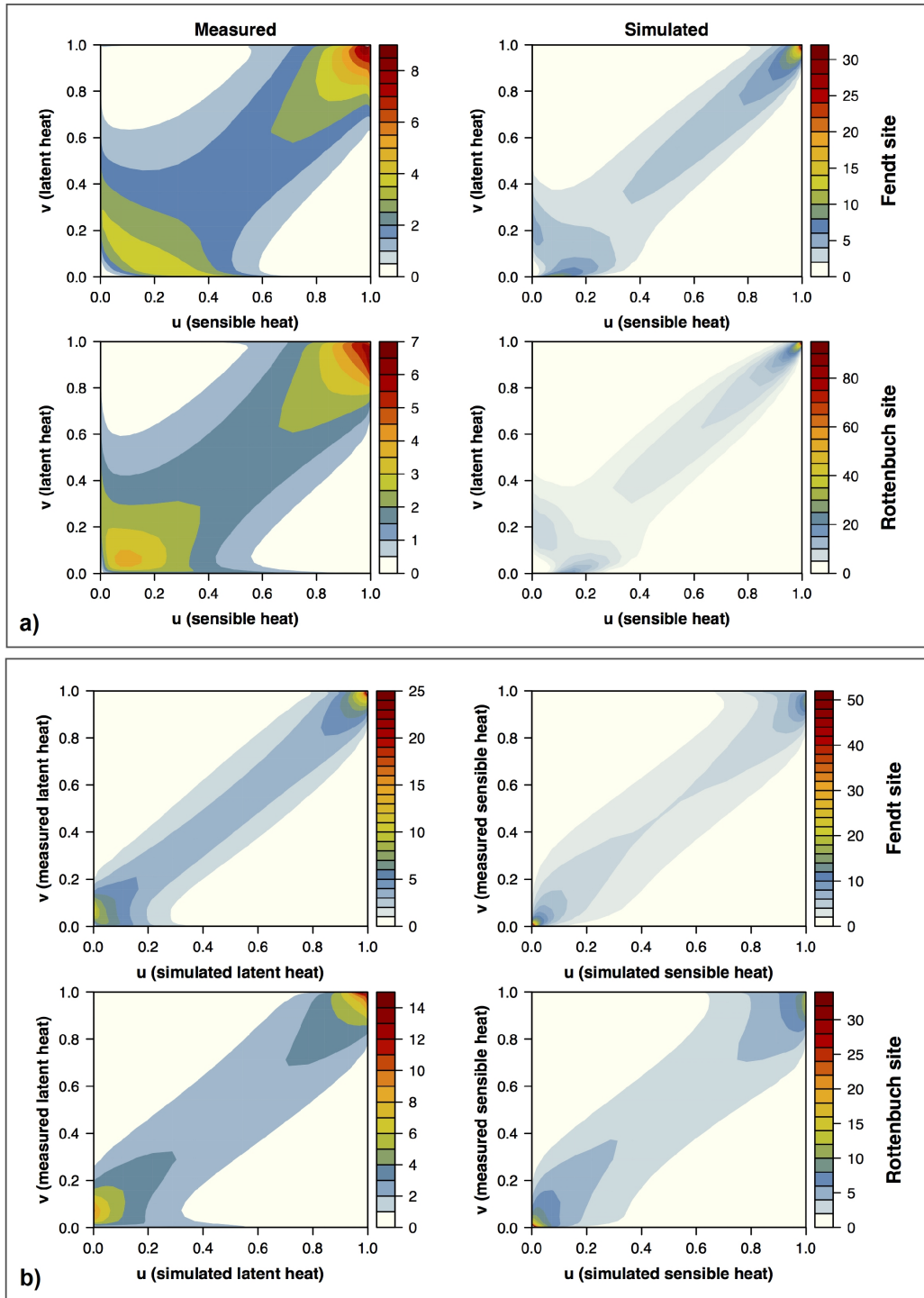


Figure 3.12: Empirical Copula densities: **a)** for the measured (left panels) and simulated (right panels) variables of the latent heat flux (v) and sensible heat flux (u) for the Fendt EC site (top row) and for the Rottenbuch EC site (bottom row); **b)** for the simulated (u) against measured (v) variables of the latent heat flux and sensible heat flux for the Fendt EC site (top row) and for the Rottenbuch EC site (bottom row) during the calibration period of May to July 2013. The sample size is 1369 data tuples for all the variables.

3.5 Conclusions

The spatiotemporal variability and dependence structure patterns of the coupled water and energy fluxes along an elevation-gradient were investigated. The analysis was based on the application of the GEOtop model and empirical Copulas. It was performed for the Rott and the Upper-Ammer catchments in the TERrestrial ENvironmental Observatories (TERENO) prealpine region over two summer episodes in 2013 and 2015.

It was found that using GEOtop, the coupled water and energy fluxes could be replicated with a high performance and low biases. The model reasonably captured the peak discharge observed in early June for the Rott catchment but it underestimated discharge in the Upper-Ammer catchment. Simulated streamflow was characterized by high values of R^2 and low residuals (RMSE) when compared to observations. The model also appropriately described the daily cycle of multiple-layer soil moisture variations. The EC-based diurnal cycles of energy fluxes were well reproduced by GEOtop; however, the model slightly overestimated LE, especially during the early morning due to the lack of EBC in the EC-based measurements (imbalance of 31% at Fendt and 39% at Rottenbuch). The spatial distributions of water and energy fluxes revealed that in the Upper-Ammer catchment around 70% of precipitation leaves the catchment as discharge, compared to ~10% in Rott. Around 30% of R_n leaves the catchment as H, while only ~15% in Rott. The model results obtained for the validation period were satisfying, indicating that the estimated parameters are reasonably calibrated.

The linear statistical measures applied are assumed to not be capable of representing the interaction between the hydrometeorological variables, and therefore, it was employed a bivariate empirical Copula-based dependence structure analysis. First, it was found that the bivariate dependence structure patterns of both measured and simulated hydrometeorological variables considered in this study are very similar, representing a reasonable calibration of the GEOtop model. These non-linear features in dependence structure of measured and simulated individual hydrometeorological variables are observed with the highest densities (or best fit between the modeled and observed values) either in the lower or upper ranks i.e. in the low or high values, exhibit a worse model calibration for the middle ranks of the data.

Finally, the Copula-based model performance analysis applied can be considered for model evaluation in the hydrological model community in addition to traditional model performance analyses.

Chapter 4

Soltani et al. (2018) Submitted

Inverse distributed modeling of streamflow and turbulent fluxes: A sensitivity and uncertainty analysis coupled with automatic optimization

4.1 Introduction

The estimation of parameters is crucial for the successful application of distributed hydrological models, as heterogeneity needs to be accounted for and large uncertainties exist in the parameter values, which usually cannot be measured directly at field scale. Even in high-resolution physically-based hydrological models, some parameters may remain that must be calibrated to obtain a satisfactory output (Liu et al., 2005). Fully distributed and physically-based hydrological models are usually much more CPU-time demanding than pure lumped models. This is particularly true for the hydrological model GEOTop used exemplarily in this study here, as it solves for example the nonlinear equations of three-dimensional subsurface water flow and accounts for the full energy balance.

Typically, the “trial and error” method is applied for model calibration, which is simple and accordingly has been widely used for hydrological models (e.g. Refsgaard, 1997; Senarath et al., 2000; Kunstmann et al., 2006; Hingerl et al., 2016; Soltani et al., 2018). As this approach is time consuming, automatic optimization algorithms are applied allowing to facilitate this effort (Eckhardt and Arnold, 2001; Kunstmann et al., 2006; Lin, 2011). Automatic calibration can be fast on modern computer architectures, and since it allows an efficient and extensive search within possible parameter ranges, the results are expected to be more robust than those obtained by the manually based calibration approach (Bahremand and Smedt, 2008).

Different algorithms have been investigated in hydrological modeling for the automatic optimization process, e.g. the Simulated Annealing Method (Aarts and

Korst, 1989) and the Multiobjective Complex Evolution Algorithm (Yapo et al., 1997). These techniques, however, require a large number of model calls (in order of several thousands), which limits their application to fast conceptual or one-dimensional models (Kunstmann et al., 2006). The Gauss-Marquardt-Levenberg (GML) algorithm estimates the parameters using fewer model runs than any other optimization technique for nonlinear models (e.g. Monte-Carlo-based algorithms) (Doherty, 2002; Doherty and Johnston, 2003; Bahremand and Smedt, 2006). However, GML is based on a local search algorithm, whose results might be affected by the initial value of the parameters (e.g. Kunstmann et al., 2006; Lin, 2011).

In this chapter, the hydrologic model GEOTop 2.0 is coupled to PEST for an inverse hydrological modeling over two summer episodes of calibration (2013) and validation (2015) for the Rott catchment located in the TERrestrial ENvironmental Observatories (TERENO) prealpine region, southern Germany. In the TERENO prealpine observatory, eco-hydrometeorological variables such as evapotranspiration (ET) and surface heat fluxes exhibit rapid changes within short distances (Soltani et al., 2018). This is mainly because of the heterogeneity in topography, landuse and soil type, as well as interactions between the earth surface and the atmospheric boundary layer (Kunstmann et al., 2004, 2006; Hingerl et al., 2016; Soltani et al., 2017). Thus, the energy and water budgets in such environments are mainly controlled by the soil type properties (Pielke et al., 1998), landcover characteristics (Dirmeyer et al., 2010), and vegetation structure (Pielke et al., 2011).

Previous studies in the TERENO observatory and the surrounding areas e.g. Bavarian Alpine foothills and low mountain-range, have mainly focused on how climate change impacts runoff generation (Kunstmann et al., 2004), runoff production processes and discharge-related analysis (Wetzel et al., 2003, 2004a, 2005a), surface and sub-surface water balances (Kunstmann et al., 2006; Wolf et al., 2016), biosphere-atmosphere exchange and greenhouse gases (Unteregelsbacher et al., 2013; Wang et al., 2014; Wolf et al., 2016; Zeeman et al., 2017), energy balance closure (EBC) parameterization and EBC problem analysis (Ott et al., 2013; Eder et al., 2014; Soltani et al., 2017).

In addition to the studies listed above, a limited number of studies have been carried out with regard to the calibration of hydrological models in this region (i.e. Kunstmann et al., 2006 and Hingerl et al., 2016), which the models were only calibrated against streamflow data. However, recently the coupled water and energy fluxes at high spatial resolution have been just modelled using the GEOTop model over two different-sized heterogeneous catchments (i.e. Rott and Upper-Ammer) in the TERENO prealpine observatory by Soltani et al. (2018). They mainly focused to quantify the spatiotemporal variability of the hydrometeorological variables and to describe their underlying-dependencies using the empirical Copula functions.

Their results showed that, the spatial variability of heat and water fluxes is significantly affected by diversity in topography, radiation and wind components, soil moisture properties as well as land cover and vegetation types across the region. As a

result, in terms of water balance, in the Upper-Ammer catchment around 70% of precipitation leaves the catchment as discharge, compared to ~10% in Rott catchment. In terms of energy balance, around 30% of the net radiation (R_n) leaves the Upper-Ammer catchment as sensible heat flux (H), while only ~15% in Rott catchment. However, in general the latent heat flux (LE) is the main consumer of R_n across the observatory. Furthermore, the empirical Copula-based function revealed that the dependence structures between the modelled and observed hydrometeorological variables are similar either at upper -or lower density maxima. This suggested a reasonable performance of the model, as the interaction of variables was properly described; however, the model showed poorer performance in the middle ranks of the data.

So, the main focus was conducted on the analysis of the model's variables, in which both temporal and spatial variability of the coupled water and energy fluxes were adequately described and presented in Soltani et al. (2018) for the TERENO prealpine observatory. However, still no attempt has been made to focus on the model's parameters for this region. Therefore, to bridge this gap, in this chapter the GEOtop-PEST interface was developed to achieve the following main objectives: i) to quantify the uncertainties pertaining to the estimated model parameters, for which we particularly examine the benefit of additional heat flux observations on the parameter confidence bounds; and ii) to characterize the intercorrelations between the model estimable parameters and their contributions to the calibration process.

4.2 Catchment characterization and available datasets

Geography and climate

The Rott catchment (~55 km²) is situated in the northern part of the TERrestrial ENvironmental Observatories (TERENO) prealpine region in Southern Germany (Figs. 1a and 1b), which drains into Lake Ammer, with 46.6 km² is the sixth largest lake in Germany. The Fendt eddy covariance (EC) site (47.831° N, 11.061° E) is within the southern part of the catchment at 598 m height (Fig. 1b) and it is recognized as the TERENO prealpine super EC site (Soltani et al., 2017). The elevation of the catchment ranges from 902 m to 543 m a.s.l. The outlet is at the discharge-gauge Raisting, where it measures only the surface water flow at the catchment, and no groundwater flow is considered. The region is characterized by a cool-temperate and humid climate. The mean annual precipitation (temperature) is 1130 mm (6.9 °C) in the Rott catchment (Kunstmann et al., 2006; Hingerl et al., 2016). The highest amount of precipitation is received during summertime. The dominant soil types in the catchment are (Fig. 1c): Lessive (76%), Cambisol (13%) and Histosol (9%). Also, the primary land cover is (Fig. 1d): pasture (44%), coniferous (37%) and mixed forests (18%) followed by villages (2%) as well as some peat (0.8%) and marsh lands (0.5%), as described in Hingerl et al. (2016).

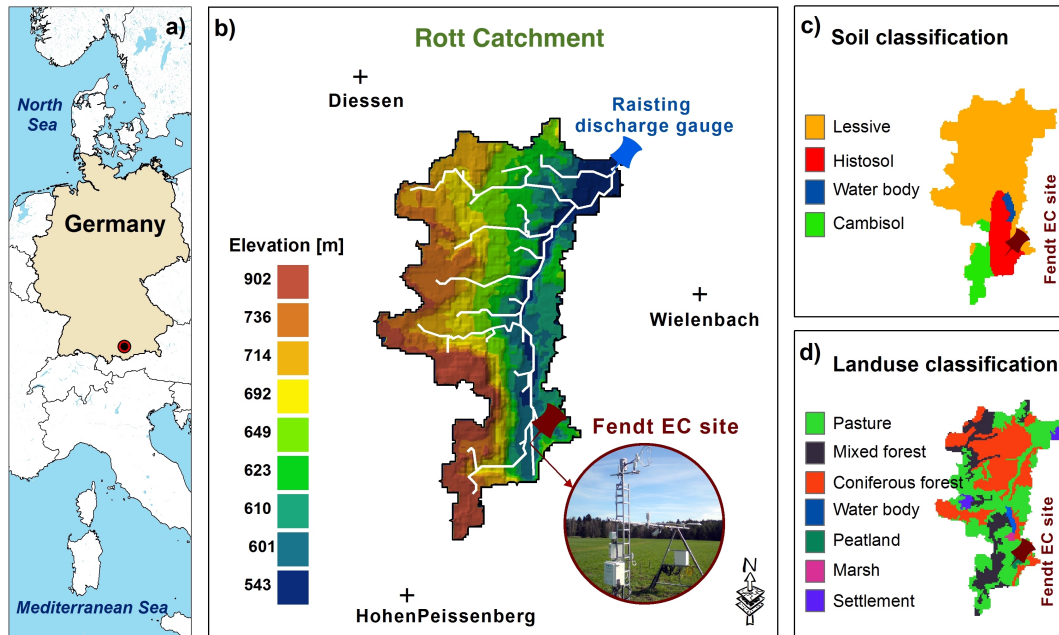


Figure 4.1: a) Overview of the study area showing a) the approximate location of the study area in southern Germany; b) the Rott catchment with the elevation and its river network as well as the locations of the Fendt EC-site, and the Wielenbach and HohenPeissenberg climate-stations together with the Diessen rain-gauge station; c) the soil type; and d) the landuse classifications for the Rott catchment.

Observational datasets

The required hydrometeorological measurements were obtained from three sources for the calibration and validation periods in 01 May to 31 July 2013 and 2015, respectively as follows:

1. EC-based turbulent fluxes and the micrometeorological measurements are gathered from the Fendt EC site (DE-Fen);
2. Hourly meteorological forcing data for the Wielenbach and HohenPeissenberg stations are received from the Deutscher Wetterdienst (DWD) (<https://werdis.dwd.de>);
3. Hourly data of precipitation for the Diessen rain gauge and streamflow for the Raisting discharge gauge are compiled from Bayerisches Landesamt für Umwelt (<http://www.hnd.bayern.de>).

The model was applied for the experimental period mentioned above, because the computational costs of the inverse modelling with the developed GEOTop-PEST interface restricted the length of the simulation period. Moreover, in the wintertime, hydrometeorological fluxes are characterized by large uncertainties (e.g. Hingerl et al., 2016), and the peak streamflow and the EC-based measurements are of higher quality during summer periods in the TERENO observatory (Soltani et al., 2017; 2018).

4.3 Methods

4.3.1 Hydrological modeling

The hydrological model GEOtop applied here for the Rott catchment was already described technically in the methodology of *Chapter 3* of this thesis. See Sect. 3.3.1., for GEOtop description and the related mathematical equations employed by the model.

Model setup and input dataset

The model input data (both forcing and static dataset), model setup and integration, and the initial condition applied here are identical to the methodology described in *Chapter 3* of this thesis at Sect. 3.3.1.

However, as mentioned before, in the model setup the soil is discretized in 13 layers, with thicknesses increasing from the surface to the deep layers. The top 8 layers starting from the surface have thicknesses ranging from 0.1 to 0.5m, while the lowest 5 layers have thicknesses ranging from 1.0 to 5.0 m. However, in this simulation experiment only the first two layers of the soils i.e. 0.1 and 0.2m were actively involved in the optimization process, and the rest of the layers were kept constant. Because, it was found that these two layers show the highest influence on the model's outputs (Soltani et al., 2018); and also, due to decreasing the insignificant parameters in the optimization process to reduce the number of model calls.

Two types of measurements involved in the model calibration here, that is, the hydrometeorological variable of discharge, and the turbulent fluxes of H and LE. The simulation was run first for a summer episode starting from 01 May to 31 July 2013 as calibration, and then the performance of the calibrated model was validated for the period of 01 May to 30 July 2015 as validation. A two-week spin-up period starting from 15 April to 30 April 2013 was conducted, as it was found experimentally that this is sufficient for this experimental period (Soltani et al., 2018).

Model performance evaluation and validation

Typically, a variety of linear statistical metrics are used to evaluate the model performance, as no single metric encapsulates all aspects of interest. Hence, in this research six statistical metrics are employed to evaluate the performance of GEOtop. They are already described in *Chapter 3* of this thesis in Table 3.2.

The estimated GEOtop parameters were performed for an independent period of 01 May to 31 July 2015 for the validation episode.

Post-processing analysis of the model parameters

To characterize the model parameter intercorrelation and their contributions in the calibration process, a Principal Component Analysis (PCA) is performed on the parameter covariance matrix. PCA reduces the dimensionality of a multivariate dataset. This is achieved by transforming the initial variables into a new small set of variables without losing the most important information in the original dataset. These new variables are called Principal Components (PCs). The PCs are ranked in that way that PC1 explains the largest fraction of the variance in a dataset, PC2 the second largest, etc. (Abdi and Williams 2010). For further details on how the PCA was performed it is referred to Soltani et al. (2017).

4.3.2 Parameter estimation strategy

For parameter estimation, the GML-method and its technical realization within the Parameter ESTimation tool (PEST) (Doherty, 2002) was applied. PEST also was used for a sensitivity and uncertainty analysis of the model parameters. PEST is model-independent in the way that it communicates with the model through the model's input and output files (Doherty et al., 2010). It minimizes a least-squares objective function (Φ), which is the sum of squared weighted residuals (Doherty, 2016a):

$$\Phi = (\mathbf{c} - \mathbf{X}\mathbf{b})^t \mathbf{Q}(\mathbf{c} - \mathbf{X}\mathbf{b}) \quad (4.1a)$$

or,

$$\Phi = \sum_{i=1}^m (w_i r_i)^2 \quad (4.1b)$$

where, \mathbf{X} and \mathbf{b} denote in turn the model's inputs, parameters, and \mathbf{c} is the observations, respectively; the "t" superscript indicates the matrix transpose operation; \mathbf{Q} is a diagonal matrix of the squared observation weights (w_i); r_i (the i 'th residual) expresses the differences between the model output and the field measurement for the i 'th observation. To improve the performance of Φ , the residuals are given different weights. The weights effectively normalize the components of Φ . It may be that some of the field data are more important to the model results than other data and thus receive greater weight. Thus, to make ensure that no observation group dominates (or is invisible in) Φ , the PWTADJ1 utility of PEST was used herein to automate the weights-adjustment procedure to the values of the discharge, H and LE observation groups. By doing so, the reference variance or standard error of weighted residuals becomes equal to 1.0 meaning that the contribution made to Φ by each aforesaid observation group is equal. For more details, it is referred to Doherty (2016b). Optimization of simple linear models can be achieved in one step. However, for nonlinear models like GEOtop, the relationships between the model parameters and observations must be linearized to achieve the parameter estimation through an

iterative process (Doherty, 2016a). For the optimization iterations, PEST applies a robust algorithm called the Gauss-Marquardt-Levenberg (GML) method, which is defined as (Doherty, 2015):

$$\mathbf{u} = (\mathbf{J}^t\mathbf{Q}\mathbf{J} + \lambda\mathbf{I})^{-1}\mathbf{J}^t\mathbf{Q}\mathbf{r} \quad (4.2)$$

where, \mathbf{u} is the parameter upgrade vector and \mathbf{r} is the vector of residuals for the current parameter set; the Jacobian \mathbf{J} is the sensitivity matrix, as it indicates the partial derivative of the model simulations with respect to the model parameters; \mathbf{I} is the $n \times n$ identity matrix; λ is the Marquardt lambda, named after Marquardt (1963) who employed this strategy although the use of this parameter was originally pioneered by Levenberg (1944).

Even after calibration the model parameters remain uncertain. This is because of i) incomplete information regarding the input data e.g. the temporal and spatial variability of parameters, initial and boundary conditions, ii) simplification of the reality by models, and iii) the measurements for model calibration and validation (Muleta and Nicklow, 2004; Bahremand and Smedt, 2006, 2008; Makowski, 2013). Therefore, the parameter uncertainty using the Generalized Linear Predictive Uncertainty/Error Analyzer (GENLINPRED) utility of PEST is analyzed. Before parameter optimization, it was additionally performed a sensitivity analysis using the SENSAN utility of PEST to identify the key model parameters. These utilities are described in the following subsections.

Parameter sensitivity calculation

The SENSAN utility of PEST was applied to assess the relative sensitivity of the GEOtop outputs with respect to the changing parameters. SENSAN adopts a local sensitivity analysis method, which takes a one-at-a-time approach (Doherty, 2016a). In this approach, the impact of changing values of each model parameter on the model outputs is evaluated one at a time. That is, model output responses are determined by sequentially varying each of the model parameters and by fixing all other parameters to their nominal values (Helton, 1993; Lin, 2011). These nominal values represent a specific point of the parameter space. Results of such a local method are dependent on the choice of this point, and the model behavior is identified only locally in the parameter space (Hill, 1998). Therefore, the results of such analysis need to be interpreted with care. To measure the magnitude of the sensitivity, the Normalized Sensitivity Coefficient (NSC) index was applied (Lin, 2011):

$$\text{NSC} = \frac{(O - O_b)}{(P - P_b)} \times \frac{(P_b)}{(O_b)} \quad (4.3)$$

where, O_b and P_b are model outcome and parameter base values, and O and P are the model outcome and parameter values pertaining to a particular model run. NSC is a dimensionless positive number, whose value indicates the relative importance of parameter on the model output.

Parameter uncertainty estimation

The Generalized Linear Predictive Uncertainty/Error Analyzer (GENLINPRED) utility of PEST was used to compute the parameter uncertainty. The calculations of GENLINPRED are made on the basis of sensitivities (i.e. the Jacobian matrix and the PEST control file are required), and no parameter adjustment takes place (Doherty, 2016b). This utility does not require the model to be calibrated before uncertainty analysis. However, in this study it was performed on the calibrated GEOtop model. GENLINPRED is a driver utility, which runs a set of PEST programs. Here, the PREDUNC (“PREdictive UNCertainty”) approach was used to compute: i) the uncertainty variance reduction of the parameters and ii) the contributions to uncertainty variance of the nominated parameter made by different parameter groups.

The following equation is employed (Doherty, 2015):

$$\sigma^2_s = \mathbf{y}^t \mathbf{C}(\mathbf{k}) \mathbf{y} - \mathbf{y}^t \mathbf{C}(\mathbf{k}) \mathbf{Z}^t [\mathbf{Z} \mathbf{C}(\mathbf{k}) \mathbf{Z}^t + \mathbf{C}(\boldsymbol{\epsilon})]^{-1} \mathbf{Z} \mathbf{C}(\mathbf{k}) \mathbf{y}^t \quad (4.4)$$

where, σ^2_s is the uncertainty variance of a parameter s ; \mathbf{y} is the sensitivity of this parameter to model predictions; $\mathbf{C}(\mathbf{k})$ is the prior parameter covariance matrix (\mathbf{k} represents parameters employed by the model); \mathbf{Z} is a matrix represents the linearized action of the model under calibration conditions, which is represented by the Jacobian matrix; $\mathbf{C}(\boldsymbol{\epsilon})$ is the covariance matrix of measurement noise (error). For further information regarding this program and its computational statistics, it is referred to Doherty (2015).

4.3.3 The GEOtop-PEST interface

In general, PEST requires the following input files for automatic parameter estimation and inverse modeling: i) template files, to identify the model parameters; ii) instruction files, to identify the model outputs; and iii) one input control file, which supplies PEST with the names of all template and instruction files, the names of model input and output files, initial parameter values, measurement values and weights, etc. (Doherty, 2010). In the developed GEOtop-PEST interface, it was prepared four template files (one for the GEOtop input file and three for the different soil types of Lessive, Histosol and Cambisol) and three instruction files (for the model outputs of streamflow, H and LE fluxes) together with a control file to run the GEOtop model coupled with PEST. Figure 4.2 illustrates the different steps and procedures of the developed GEOtop-PEST interface.

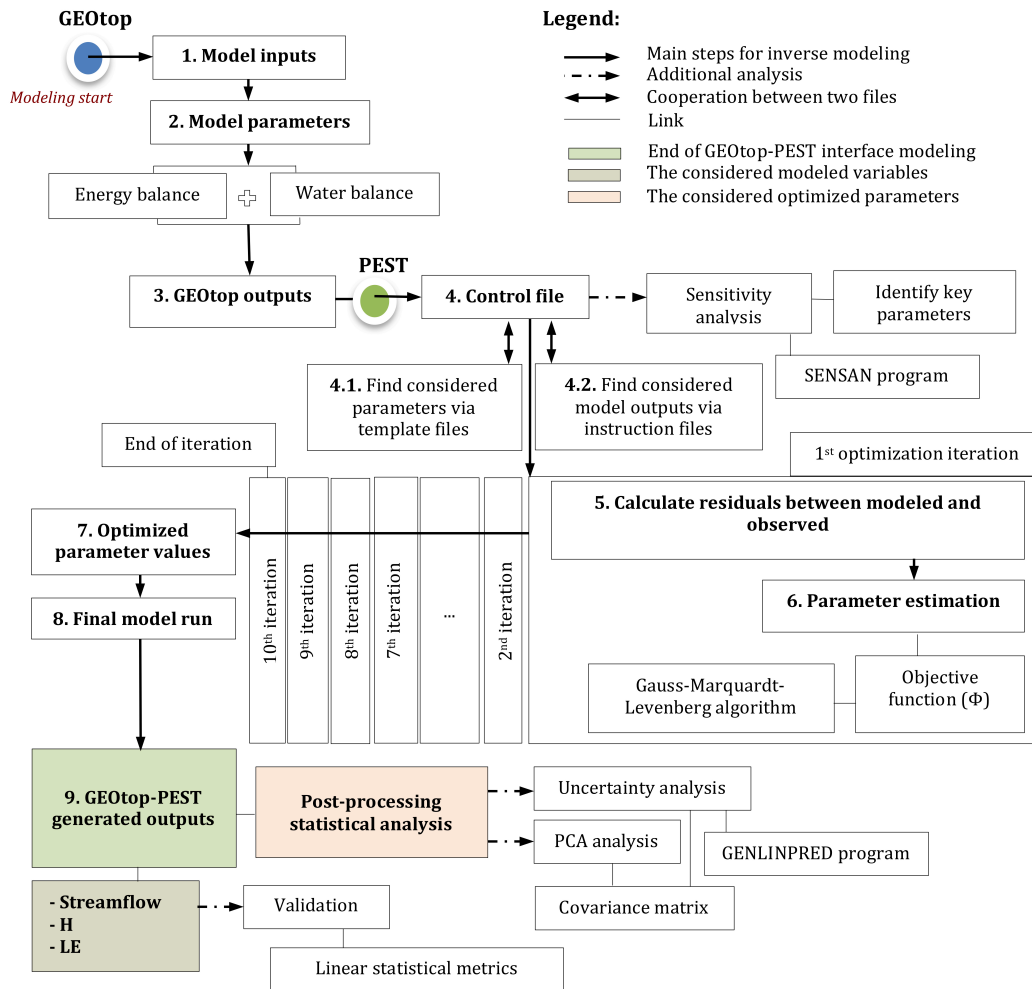


Figure 4.2: The inverse modeling flowchart for the developed GEOTop-PEST interface.

4.4 Results and discussion

4.4.1 Sensitivity analysis

Sensitivity analysis is capable of identifying the dominant parameters, and hence enhance the model optimization efficiency. The GEOTop parameters used for the discharge and turbulent fluxes were selected based on the literature (Kunstmann et al., 2006; Hingerl et al., 2016). These are shown in Table 4.1. The initial simulation to determine the sensitivity of these parameters to the model's outputs was performed using the parameter values obtained via trial and error procedure by Soltani et al. (2018). Then, the key parameters acting on variability of the discharge and turbulent fluxes were identified and quantified using the approach described in Sect. 3.3.2. of this chapter.

4 Inverse modeling: parameter sensitivity and uncertainty analysis

Table 4.1: The GEOTop model input parameters selected for the sensitivity analysis (Endrizzi et al., 2011).

	Parameter	Description	Unit	Range
Landuse parameters	C_f	Canopy fraction [0: no canopy in the pixel, 1: pixel fully covered by canopy]	-	0, 1
	C_h	Canopy height	mm	0, 20000
	C_d	Surface density of canopy	Kg m ⁻²	-
	C_c	Decay coefficient of the eddy diffusivity profile in the canopy	-	-
	α_w	Ground surface albedo without snow in the visible - saturated	-	0, 1
	α_d	Ground surface albedo without snow in the visible - dry	-	0, 1
	ε	Ground surface emissivity	-	0, 1
Soil parameters	K_v	Vertical hydraulic conductivity	mm s ⁻¹	-
	K_h	Horizontal hydraulic conductivity	mm s ⁻¹	-
	α	Van Genuchten parameter α	mm ⁻¹	-
	n	Van Genuchten parameter n	-	-
	λ_s	Thermal conductivity of the bedrock	W m ⁻¹ K ⁻¹	-
Surface water flow parameters	C_m	Coefficient of the law of uniform motion on the surface	m ⁻¹ s ⁻¹	0.01, 5.0
	γ	Exponent of the law of uniform motion on the surface	-	0.25, 0.34
	C_w	Fraction of channel width in the pixel width	-	-

Figure 4.3 illustrates the result of the parameter sensitivity analysis. The NSC values of these parameters for the discharge and turbulent fluxes varies within the range of 0.0 [.] to 0.7 [.]. Overall, α , C_f and ε , which together control evapotranspiration from soil and runoff generation on the land surface, have the highest sensitivities. It is not surprising to see that the soil parameters of K_v and K_h affect merely discharge with no influence on the turbulent fluxes. The hydraulic conductivity in general controls how the precipitated water can percolate vertically into the ground. Depending on this property, during intense precipitation, water might be unable to infiltrate into the soil leading to surface discharge. However, ε only indicates a strong sensitivity on the turbulent fluxes in particular on H flux (> 0.7 NSC). This could be due to the fact that the model overestimates the outgoing longwave radiation, indicating a warmer surface. C_h shows some degree of relative sensitivity on the considered variables in particular on H. Since, in this approach the sensitivities are calculated by changing the parameters one by one, they are not influenced by parameter correlations (Bahremand and Smedt, 2006). The SENSAN-based parameter sensitivity identification resulted in the reduction of 8 categories of the adjustable GEOTop parameters, which were used for the automatic calibration.

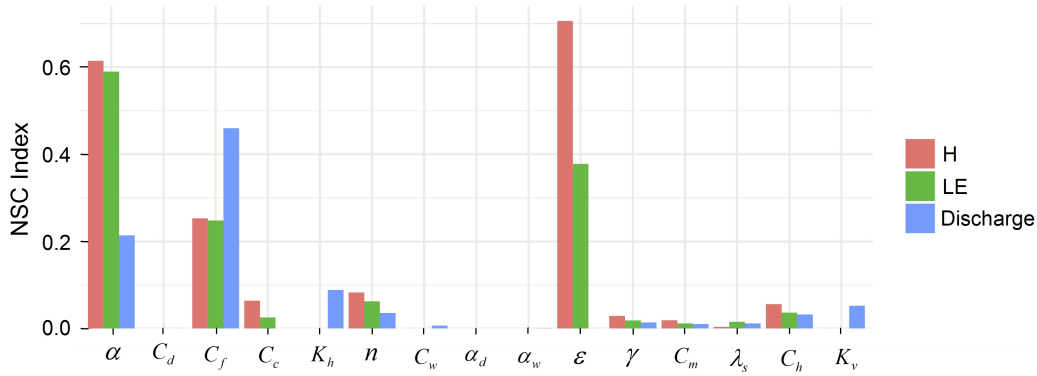


Figure 4.3: The parameter sensitivity results for the discharge, sensible heat flux (H) and latent heat flux (LE). A higher NSC indicates greater sensitivity for a given parameter. For detailed description of the model parameters see Table 4.2.

4.4.2 Inverse modeling using the developed GEOtop-PEST interface

Parameter estimation

PEST calculates the objective function (Φ) arising out of the initial parameter values. The progress of Φ and Marquardt lambda (λ) achieved during the optimization iterations is shown in Figure 4.4. PEST performed the total number of ten optimization iterations with 538 model forward integrations. As described in Doherty (2016a), PEST attempts parameter improvement using a number of λ (e.g. 10.0 is recommended for nonlinear models) during individual iteration. In this case, the first iteration process was started with an initial λ value of 10.0, and then was terminated at the end of the tenth iteration with the lowest λ 2.00E-04. However, the behavior of Φ is different throughout the optimization process, as shown in Figure 4.4. Φ was started with the highest value of 3.10 in the first iteration (with 30 model forward integrations) and the lowest Φ value of 2.92E+00 was achieved in the seventh iteration (with 368 model forward integrations). Thereafter, Φ was rising until the end of the tenth iteration, where PEST stopped the optimization (with 538 model forward integrations), as it was not worth undertaking more optimization iterations due to an increase of the residuals. Finally, PEST used the best parameter values with the lowest Φ (which achieved in the seventh iteration) to run the model one final-time to obtain the best model outputs.

The GEOtop model indicates a nonlinear behavior, thus the parameter upgrade vector is “overshooting” the objective function minimum. Consequently, the new value of Φ becomes worse than that of achieved in the previous iterations. This is because, as described in Doherty (2016a), the equations employed for calculation of the upgrade vector are all based on a local quasi-linearity assumption that may not extend as far into parameter space from current parameter estimates as the magnitude of the upgrade vector itself.

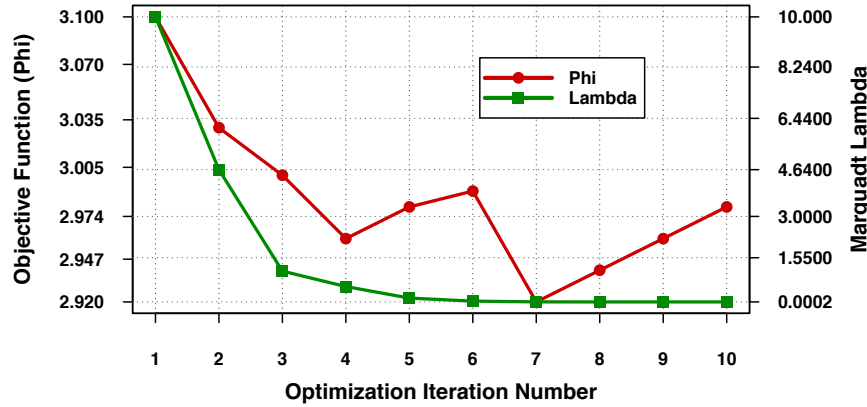


Figure 4.4: Development of the objective function (Φ) and the Marquadt lambda (λ) during the PEST optimization iteration process.

Optimized parameter values and confidence intervals

The optimization results are given in Table 4.2. It is observed that the calibrated land cover parameters in general do not indicate large differences compared to their initial values. The maximum change is observed for the value of C_h with the highest standard deviation (SD: 0.4336) in comparison with other land cover parameters. However, the calibrated values of the soil types show comparatively large changes. The highest change is observed for the top layer of K_v and K_h , whereas the lowest one is seen in α . Accordingly, the highest and lowest SD is observed for the aforesaid parameters, respectively. On average, the Cambisol soil type indicates the highest change between the initial and estimated values of all soil parameters.

PEST also calculates the 95% confidence limits of the calibrated parameters (see Table 4.2). It is noted that the confidence limits provide only an indication of the parameter uncertainty. As described in Doherty (2016a), these limits rely on a linearity assumption, and also the upper-lower parameter bounds are not accounted for the calculation of 95% confidence intervals, which may result in these limits lie outside the parameter's allowed domain. For instance, the upper confidence limits for K_v and K_h in the *Histosol* and *Cambisol* soil types at 0.1 m depth exceed their allowed upper bounds (i.e. $> 1.00E+00$). Conversely, the lower confidence limits for α in the *Lessive* and *Cambisol* soil types in order at 0.1 and 0.2 m depths are below their allowed lower bounds (i.e. $< 3.50E-04$ and $1.50E-04$).

4 Inverse modeling: parameter sensitivity and uncertainty analysis

Table 4.2: Summary of the calibrated parameters with their Standard Deviations (SD) and confidence levels. Here, “Les.”, “His.” and “Cam.” stand for the soil types of “Lessive”, “Histosol” and “Cambisol”, respectively at the soil depths of 0.1 [m] and 0.2 [m]. It is noted that these specific soil layers were lumped into three main groups of the soil types mentioned above, when calculating their derivatives in this analysis. According to Doherty (2016a and 2016b), in many cases such parameters fall neatly into their source groups which can be treated similarly in terms of calculating derivatives. For detailed information on the parameter description refer to Table 4.1.

Parameters	Initial values	Estimated values	SD	95% confidence intervals	
				Lower limit	Upper limit
C_f	0.5500	0.5503	0.0005	0.5493	0.5513
C_h	350.00	352.09	0.4336	351.28	352.90
C_c	0.0100	0.0010	0.0001	0.0008	0.0011
ε	0.9600	0.9612	0.0007	0.9598	0.9626
γ	0.2500	0.2482	0.0012	0.2455	0.2508
$K_{h,Les.1}$	0.5000	0.3281	0.0583	0.2507	0.4056
$K_{h,Les.2}$	0.0520	0.0763	0.0045	0.0351	0.1175
$K_{h,His.1}$	0.5000	0.5074	0.0025	0.5011	0.5138
$K_{h,His.2}$	0.0330	0.0409	0.0003	0.0403	0.0415
$K_{h,Cam.1}$	0.5000	1.0000	0.0422	0.8798	1.1201
$K_{h,Cam.2}$	0.0540	0.1220	0.0133	0.1106	0.1333
$K_{v,Les.1}$	0.5000	0.3725	0.2892	0.1754	0.5696
$K_{v,Les.2}$	0.2500	0.3623	0.1755	0.2556	0.4690
$K_{v,His.1}$	0.5000	1.0000	0.2580	0.8429	1.1570
$K_{v,His.2}$	0.1410	0.1000	0.0097	0.0818	0.1181
$K_{v,Cam.1}$	0.5000	1.0000	0.1252	0.8209	1.1790
$K_{v,Cam.2}$	0.2600	0.1000	0.0154	0.0797	0.1202
$\alpha_{Les.1}$	0.0009	0.0003	0.0001	0.0003	0.0004
$\alpha_{Les.2}$	0.0002	0.0004	0.0001	0.0002	0.0006
$\alpha_{His.1}$	0.0009	0.0009	0.0000	0.0009	0.0009
$\alpha_{His.2}$	0.0002	0.0002	0.0000	0.0002	0.0002
$\alpha_{Cam.1}$	0.0009	0.0010	0.0000	0.0009	0.0010
$\alpha_{Cam.2}$	0.0003	0.0001	0.0012	0.0001	0.0001

Analysis of residuals

Residual analysis is an essential component of each calibration practice. Thus, the statistics pertaining to the residuals of discharge, H and LE observation groups are briefly discussed. Ideally, after the parameter estimation process is complete, weighted residuals should have a mean of zero (Doherty, 2015). As shown in Table 4.3, the mean value of non-zero weighted residuals is close to zero for all observations (i.e. discharge: 0.00470, H: -0.0064, and LE: -0.0069).

Also, a quite low variance of weighted residual is observed, which is almost identical between the observation groups. Further, no outlier is found, as the maximum weighted residuals are not unusually high in the observations. The residuals are statistically insignificant for all observation groups, which indicates a good performance of Φ in the calibration process.

Table 4.3: Summary of the weighted residuals calculated for the observation groups.

	Discharge [m ³ /s]	H [W/m ²]	LE [W/m ²]
Number of residuals with non-zero weight	2592	2592	2592
Mean value of non-zero weighted residuals	0.00470	-0.0064	-0.0069
Maximum weighted residual	0.21500	0.00002	0.00005
Minimum weighted residual	-0.0424	0.09221	-0.0918
Variance of weighted residuals	0.00039	0.00035	0.00039

Results of calibration and validation episodes

The comparison of measured versus modeled discharge and turbulent fluxes of H and LE is illustrated in Figure 4.5. The respective statistical metrics are given in Table 4.4. For discharge, as shown in Figure 4.5a, reasonable improvement achieved in the simulation by the developed GEOtop-PEST interface (e.g. low error: RMSE = 1.16, and high efficiency: NSE = 0.87 and COE = 0.54) compared to the manual-based calibration efforts performed by the GEOtop model for the same catchment (Soltani et al., 2018; Hingerl et al., 2016) or worldwide (e.g. Rigon et al., 2006; Bertoldi et al., 2006).

The model captures the peak flow reasonably well in the catchment, and also an increased runoff volume in early June highlights the importance of snow dynamics for runoff generation in the basin. However, the base flow is rather underestimated. This, could be due to the fact that GEOtop, as a hydrologic model, does not describe the hydrogeological processes e.g. contribution of the underground water (aquifers) to the surface stream flows. Additionally, the post-calibration parameters verified that the model-distributed streamflow are satisfactory and reliable. This was confirmed by e.g. the strong linear relationship (R^2 : 0.78) and very low residual (RMSE: 0.98) and high Nash-Sutcliff efficiency (NSE: 0.78) values for the simulated discharge during the validation episode (Fig. 4.5b).

The study conducted by Hingerl et al. (2016) attempted to calibrate the hydrological model GEOtop V. 1.45 for discharge only in the Rott catchment. Moreover, using the lasted version of GEOtop V. 2.0 in the same catchment, Soltani et al. (2018) modelled the spatiotemporal variability of the coupled water and energy fluxes via a trial and error procedure. However, in this chapter, using the developed GEOtop-PEST interface, the model parameters for the discharge coupled to the heat fluxes were jointly optimized. The automatic optimization effort achieved reasonably better results when compared to Hingerl et al. (2016) and Soltani et al. (2018) for the simulated turbulent fluxes during the calibration episode (Fig. 4.5c). This can be seen not only by the strong linear relationship between the measured and simulated fluxes (H: R^2 value of 0.65 and LE: R^2 value of 0.76), but also with low error (H: RMSE value of 20.54 and LE: RMSE value of 63.30) as well as high efficiency (H: NSE/COE values of 0.37/0.48 and LE: NSE/COE values of 0.74/0.50).

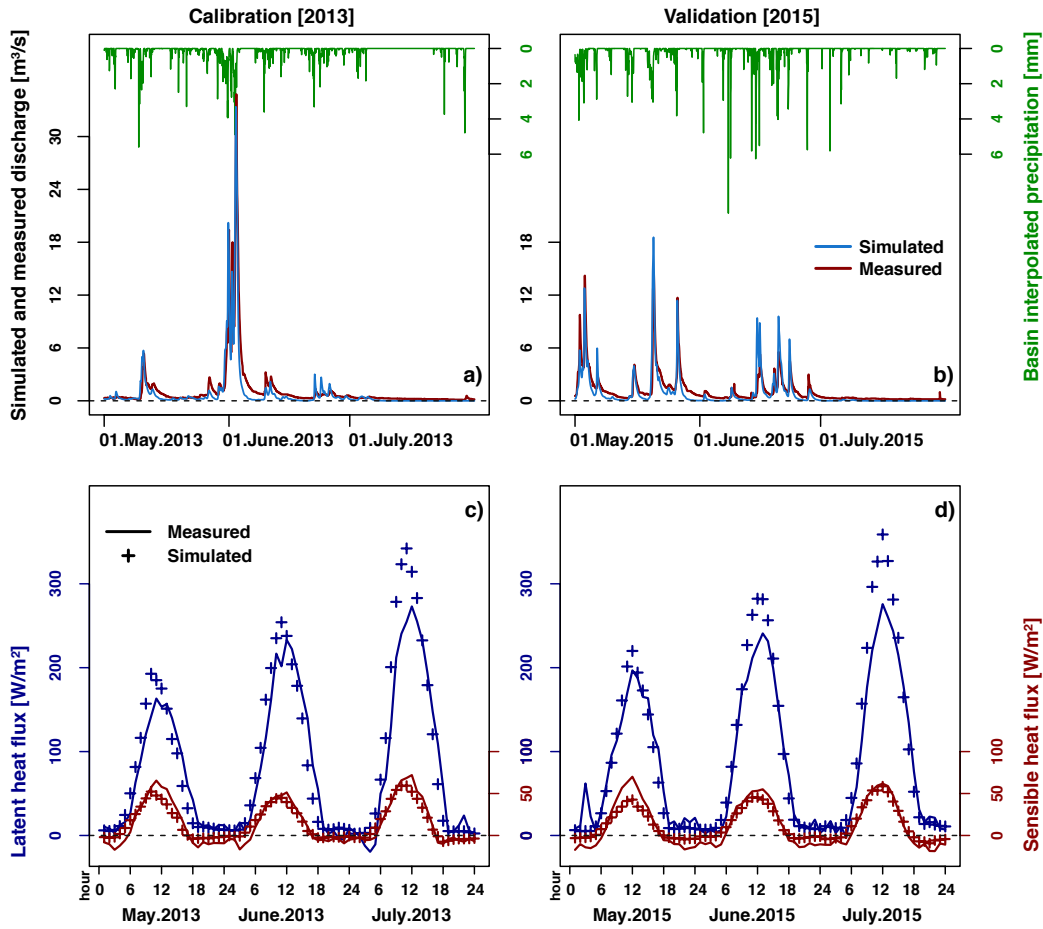


Figure 4.5: Graphical comparison between measurements and the GEOTop-PEST achieved simulation results: **a, b** the hourly time-series of discharges; and **c, d** the monthly diurnal turbulent fluxes of sensible heat and latent heat.

Table 4.4: Summary of the statistical metrics for the calibration (validation) episode of May to July 2013 (May to July 2015).

	MB	RMSE	R ²	COE	IOA	NSE
Discharge [m ³ /s]	-0.29 (-0.22)	1.16 (0.98)	0.88 (0.78)	0.54 (0.45)	0.77 (0.72)	0.87 (0.78)
LE [W/m ²]	15.16 (22.11)	63.30 (56.85)	0.76 (0.87)	0.50 (0.60)	0.75 (0.80)	0.74 (0.80)
H [W/m ²]	-0.32 (1.15)	20.54 (19.17)	0.65 (0.78)	0.48 (0.56)	0.74 (0.78)	0.37 (0.46)

However, GEOTop slightly overestimates LE flux (MB = 15.16), in particular during the first part of the day with a peak at around 10:00 or 11:00 am. The midday overestimation of the simulated LE flux could be due to the fact that the EC-based technique usually underestimates turbulent fluxes, in particular LE measurement, as reported worldwide (e.g. Hendricks-Franssen et al., 2010; Stoy et al., 2013; Imukova et al., 2016), also in the TERENO prealpine observatory (Eder et al., 2014; Soltani et al., 2017). As a result, there is a lack of energy balance closure (EBC) in the EC-based measurements, where the imbalance (residual energy) at Fendt is 31% (Soltani

et al., 2018). According to Table 4.4, the simulation results for the turbulent fluxes show in general a better performance (Fig. 4.5d) over the validation episode, compared to the results obtained in the calibration episode.

4.4.3 Uncertainty analysis pertaining to the model parameters

Pre- and post calibration uncertainty

The model parameter's pre- and post-calibration uncertainty variance together with their standard deviation (SD) is given in Table 4.5. It can be seen that the range of uncertainty reduction varies between different groups of parameters. Among the landuse parameters, for example, the uncertainty variance for the parameter C_h was significantly decreased from 25.0 to 2.73E-05. Similarly, C_c indicates a high decrease in the uncertainty ranging from 0.0249 to 5.83E-13.

Table 4.5: Summary of the model parameter's uncertainty analysis. The parameter lower-upper bounds are used to measure the pre-calibration uncertainty. For detailed information on the parameter description refer to Tables 4.1 and 4.2.

Parameters	Total uncertainty variance	
	Pre-calibration	Post-calibration
C_f	0.150	4.18E-11
C_h	25.0	2.73E-05
C_c	0.024974998	5.83E-13
ε	0.01	8.21E-11
γ	0.037500013	2.82E-10
$K_{h,Les.1}$	0.225	2.50E-07
$K_{h,Les.2}$	0.052500007	7.04E-08
$K_{h,His.1}$	0.225	1.68E-09
$K_{h,His.2}$	0.083500020	1.52E-11
$K_{h,Cam.1}$	0.225	5.98E-07
$K_{h,Cam.2}$	0.028749983	5.38E-09
$K_{v,Les.1}$	0.225	1.61E-06
$K_{v,Les.2}$	0.075000012	4.72E-07
$K_{v,His.1}$	0.225	1.02E-06
$K_{v,His.2}$	0.050000001	1.36E-08
$K_{v,Cam.1}$	0.225	1.33E-06
$K_{v,Cam.2}$	0.050000001	1.70E-08
$\alpha_{Les.1}$	0.00017274999	1.03E-13
$\alpha_{Les.2}$	0.00014775001	1.12E-12
$\alpha_{His.1}$	0.00016224999	2.74E-16
$\alpha_{His.2}$	0.00015000001	2.17E-16
$\alpha_{Cam.1}$	0.00016025	1.30E-13
$\alpha_{Cam.2}$	0.00013524999	1.79E-14

In general, all the considered landuse parameters show a significant reduction of uncertainty variance pertaining to the model parameters. With regards to the soil parameters of K_h and K_v , it was found that a noticeable decrease in the magnitude of uncertainty is also observed for all soil types of Lessive, Histosol and Cambisol, especially at top layer of 0.1 m depth. However, the highest reduction in the

uncertainty range is seen for $K_{h,Les.1}$ and $K_{h,Cam.1}$ with the values ranging from 0.225 to 2.50E-07 and from 0.225 to 5.98E-07, respectively. The soil parameter of α shows insignificant change in the uncertainty variance for the pre- and post-calibration parameters. However, $\alpha_{His.1}$ (0.000162 to 2.74E-16) and $\alpha_{His.2}$ (0.000150 to 2.17E-16) show a considerable decrease in the magnitude of uncertainty. Overall, this analysis indicates that the uncertainty ranges were highly decreased for the calibrated parameters. This denotes a robust parameter estimation by PEST.

Parameters contributions to reduction of uncertainty

Having the considered model parameters uncertainty calculated (see Table 4.5), the contribution to decrease in uncertainty made by different parameter groups is investigated. Overall, it was found that the contribution of the parameter groups is quite different for each nominated parameter, as shown in Figure 4.6. For example, the parameter group of C_f made the highest contribution to reduce the uncertainty of C_h . The soil parameter group of α plays a significant role in uncertainty reduction, not only for the soil parameters of K_v and K_h , but also for the landuse parameters of C_f and ϵ .

Also, K_h is the only parameter group that highly contributed to the uncertainty reduction of the surface water flow parameter of γ . Furthermore, K_v , α , K_h and C_c were found the parameter groups that largely contributed to the uncertainty reduction of the soil parameters (not shown). To see the post-calibration uncertainty values of all parameters, it is referred to Table 4.5.

Additional observations effect on the parameter confidence ellipses

To quantify the influence of additional values of the observation groups (i.e. H and LE) on the confidence ellipses (uncertainty range) of the estimated parameters, those observations were consecutively added to the base observation dataset (i.e. discharge) in the calibration process. Then, the confidence bounds of the estimated parameters were obtained by covariance analysis. The square roots of the diagonals of the parameter covariance matrix result in SD of the estimated parameters, and therefore, the uncertainty of the estimated parameter values is robustly quantified (Kunstmann et al., 2006). For detailed information on the analysis of confidence ellipses, it is referred to Carrera and Neumann (1986), and Friendly et al. (2013).

Here, the probabilities of 68.3% (equivalent to 1 SD), 95.4% (~ 2 SD) and 99.7% (~ 3 SD) was derived to show the corresponding confidence ellipses of the considered parameters. It is noted that in total 23 parameters are considered in this research. To show all these parameters with respect to their uncertainty ranges (confidence ellipses) influenced by additional values of observations, a range of hundreds to thousands of graphs was needed to plot, considering a matrix of 23×23 parameters. This is not practical, and it is beyond the scope of this research to show all combinations of confidence ellipses. Therefore, the parameters were randomly

4 Inverse modeling: parameter sensitivity and uncertainty analysis

selected; however, it was tried to include a variety of the model parameters (i.e. landuse, soil, as well as a combination of landuse and soil/surface water flow parameters) for this analysis to get the results more robust.

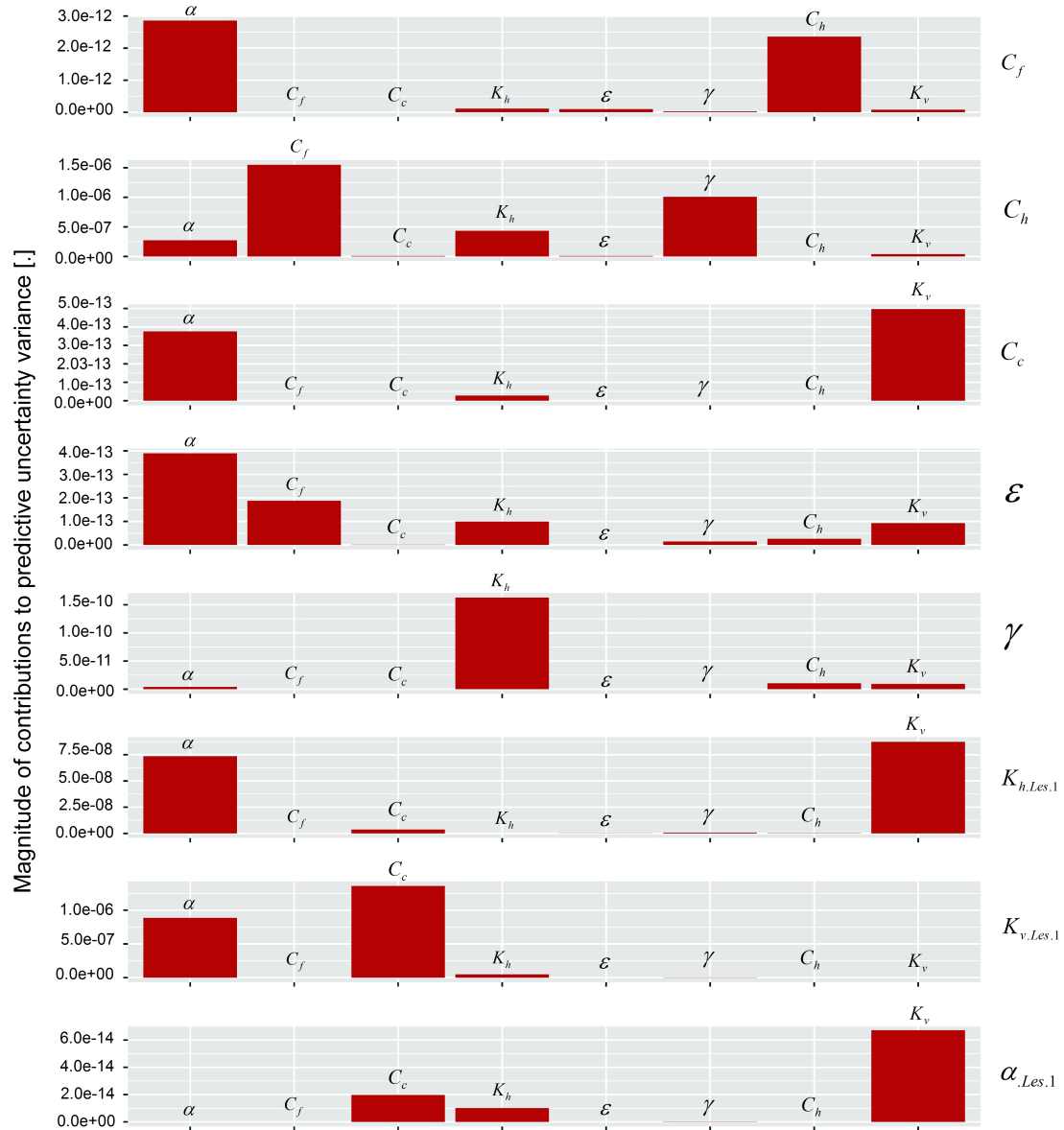


Figure 4.6: The parameter group’s contribution analysis: Red bar-plots indicate contributions of the post-calibration uncertainty variance of the nominated parameters (represented by individual panel) made by different parameter groups (listed in x-axes of the graphs). The soil parameters $K_{h.Les.1}$, $K_{v.Les.1}$, and $\alpha_{.Les.1}$ belong to the soil-type “Lessive” at the top layer 0.1 m. For detailed information on the parameter description refer to Tables 4.1 and 4.2.

The results revealed a novel achievement from an uncertainty-based point of view. It was found that in general the uncertainty ranges and correlations of the post-calibration parameters were significantly decreased and improved by adding the H

and LE fluxes to the base observation, i.e. discharge. However, the magnitude of changes in reduction of uncertainty varies not only for the different parameter groups of landuse, soil and surface water flow, but also between the H and LE fluxes.

Figure 4.7 shows confidence regions for the estimated landuse parameters ε and C_c (top panels) as well as ε and C_f (bottom panels). The uncertainty for ε is comparatively large, while uncertainty of C_c is smaller. Having the turbulent fluxes added to the calibration dataset, the confidence ellipses at multiple significance levels were significantly improved and decreased. This, however has no effect on their intercorrelations. It implies that these parameters were independently calibrated during the optimization process (top panels in Fig. 4.7). A considerable correlation between the model parameters ε and C_f is revealed. But, this correlation was eliminated when LE flux was added to the calibration dataset (bottom panels in Fig. 4.7).

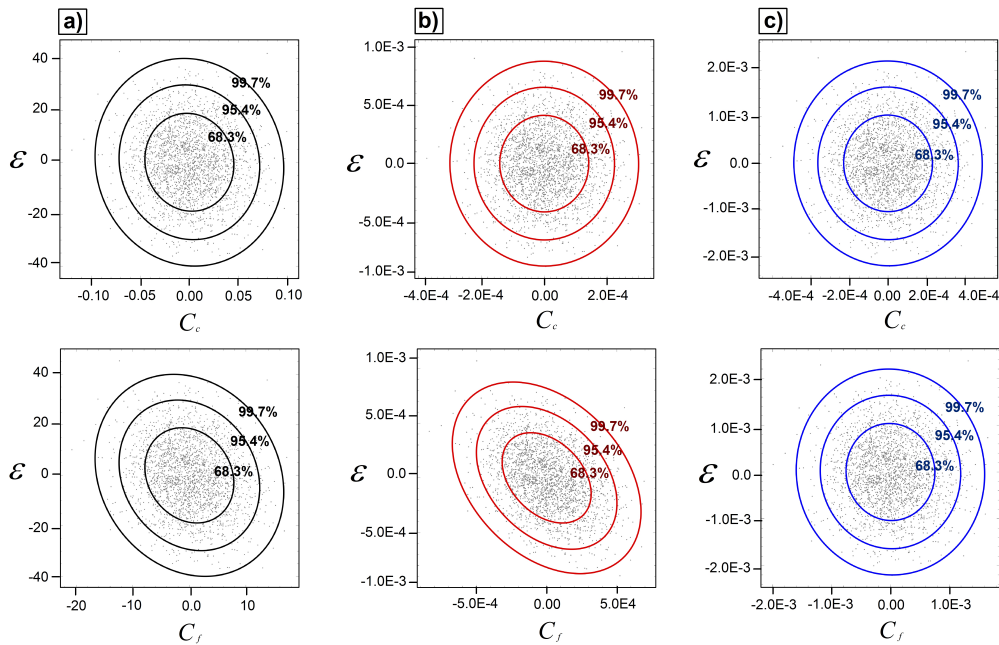


Figure 4.7: The worth of observation groups analysis on the multiple levels of the confidence ellipses for the estimated landuse parameters: **a)** in the left panels discharge [colored in black]; **b)** in the middle panels discharge and sensible heat flux (H) [colored in red]; and **c)** in the right panels discharge, H and latent heat flux (LE) [colored in blue], have been added to the calibration dataset, respectively. For detailed information on the parameter description and their units refer to Tables 4.1 and 4.2. Note that the ellipses of each parameter for adding additional data (columns a, b, c) cannot be visualized in single figures due to the different value range.

Figure 4.8 shows confidence regions for the estimated soil parameters $K_{v,His.2}$ and $K_{h,His.2}$ (top panels) as well as $\alpha_{His.1}$ and $K_{h,His.1}$ (bottom panels). The parameters of hydraulic conductivities K_h and K_v show a larger uncertainty than the Van Genuchten parameter α . In this case, a slight correlation between the soil parameters $K_{v,His.2}$ and

$K_{h,His.2}$ is revealed, it was then eliminated by add of additional heat observations (top panels in Fig. 4.8). However, $\alpha_{His.1}$ and $K_{h,His.1}$ indicate a different behaviour when the surface heat fluxes are added. It means that the uncertainty was highly reduced, but a slight correlation is then revealed between these parameters (bottom panels in Fig. 4.8). Overall, the soil parameters show less reduction in the uncertainty range than those of the landuse parameters.

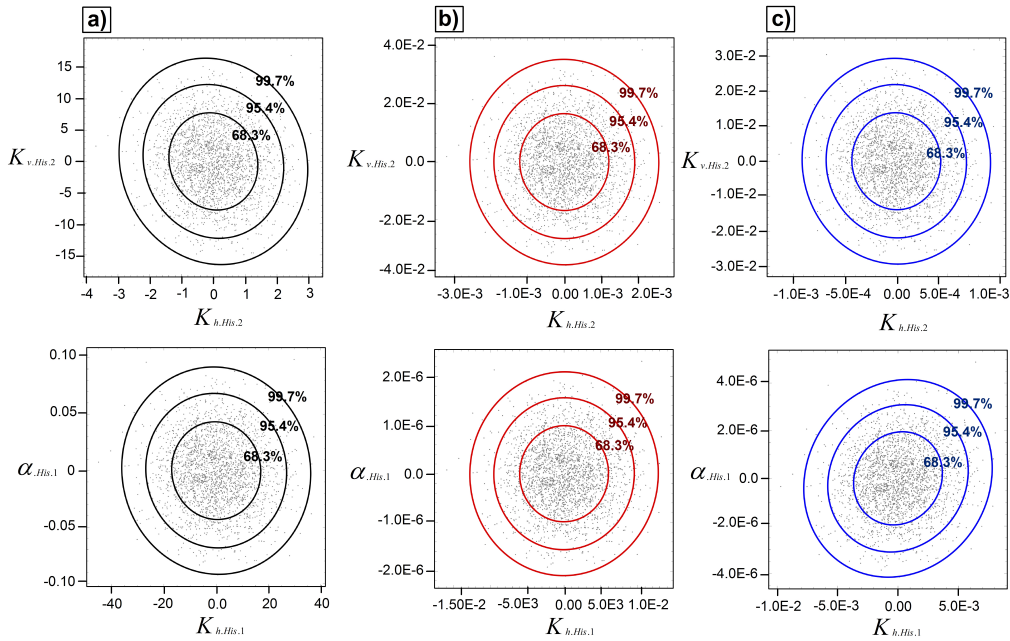


Figure 4.8: Same as in Fig. 4.7, but for the estimated soil parameters.

Figure 4.9 shows confidence regions for the combinations of the estimated parameters $\alpha_{Les.1}$ and C_f (top panels) as well as γ and C_f (bottom panels). The uncertainty for C_f is comparatively larger than the uncertainty of $\alpha_{Les.1}$ and γ . The uncertainty ranges for these parameters, however, were significantly reduced by additional values of turbulent fluxes to the calibration dataset. This also resulted in an elimination of the correlation between the parameters $\alpha_{Les.1}$ and C_f (top panels in Fig. 4.9). Whereas additional values do not show any effects on the correlation between γ and C_f (bottom panels in Fig. 4.9). It implies that they were independently calibrated.

Furthermore, it was found that additional values of H flux to the base observation of discharge in the calibration dataset, as shown in Figures 4.7b, 4.8b and 4.9b, resulted in not only a significant decrease of uncertainty range in the considered model parameters, but also eliminating the intercorrelation between the parameters (e.g. between C_f and $\alpha_{Les.1}$). However, the addition of LE to discharge and H, as shown in Figures 4.7c, 4.8c and 4.9c, insignificantly improved the confidence bounds, or in some cases makes it even slightly worse (e.g. between ε and C_f as well as $\alpha_{His.1}$ and $K_{h,His.1}$).

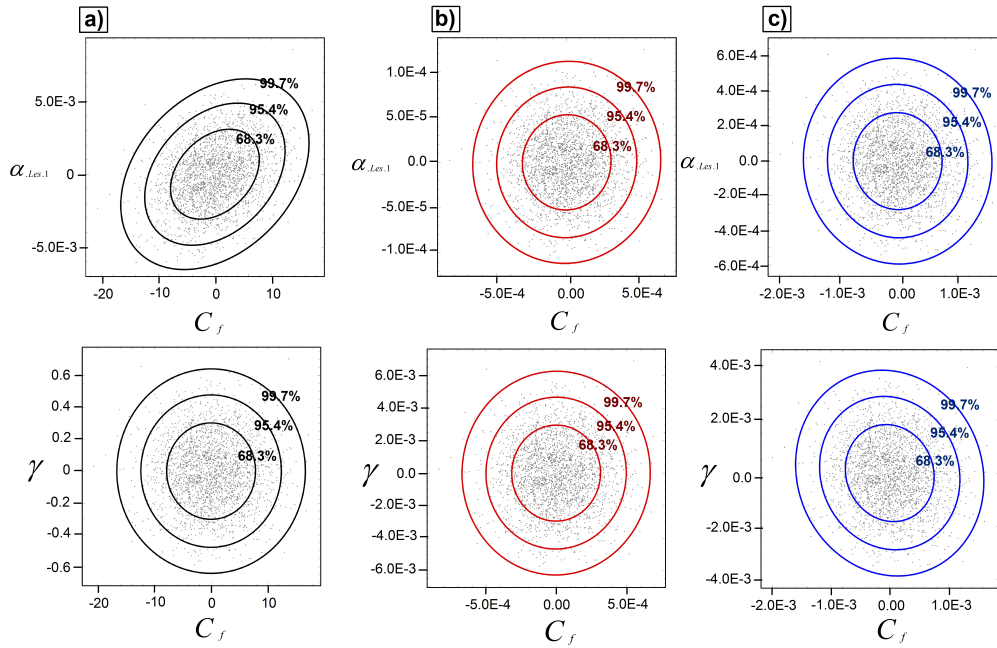


Figure 4.9: Same as in Fig. 4.7, but for combination of the estimated landuse and soil/surface water flow parameters.

In summary, since almost no or only little correlation is seen between the estimated parameters by PEST (Figures 4.7c, 4.8c and 4.9c), lowering in the uncertainty range of these parameters is considered to be reliable. Also, it indicates that these parameters contributed equally and none of the parameters were dominated by others in the calibration process.

4.4.4 Correlation and contribution of model parameters: PCA-based analysis

To identify the intercorrelation of the model parameters as well as to quantify the extent to which these parameters are sensitive to the calibration process, a PCA analysis on the post-calibration parameter covariance matrix was performed. As shown in Figure 4.10, the intercorrelation between the model parameters is not strong. This means that the calibrated parameters are not- or insignificantly correlated. In case of high parameter correlation, the objective function minimum will be difficult to obtain and the ability of PEST will be limited (Doherty, 2015). However, most parameters show low intercorrelations. This also was confirmed by the analysis of the post-calibration parameter correlation coefficient matrix (not shown).

More importantly, it can be seen that the majority of the parameters with the longest arrows contain the highest contributions to the eigenvectors (i.e. both PC1 and PC2). Therefore, these are the parameters whose values were quite sensitive in the calibration process. In another word, these parameters are highly estimable, as they lie in the calibration solution space. This indicates a successful sensitivity analysis that

4 Inverse modeling: parameter sensitivity and uncertainty analysis

carried out to identify the key model parameters (see Fig. 4.3). However, a few of the parameters show low contributions to the calibration process (with the lowest arrows) such as $K_{v,Cam.1}$ and $a_{Cam.1}$. These are mostly insensitive and less estimable parameters, as they lie in the calibration null space. This could be explained by *either* a rather high negative correlation coefficient between these parameters (see Fig. 4.10), *or* the fact that the *Cambisol* soil-type covers only a limited part of the Rott catchment (see Fig. 4.1c). It is noted that the results obtained from the PCA analysis for the parameter contribution/importance in the calibration process is in good agreement with the outcomes of parameter identifiability analysis (not shown).

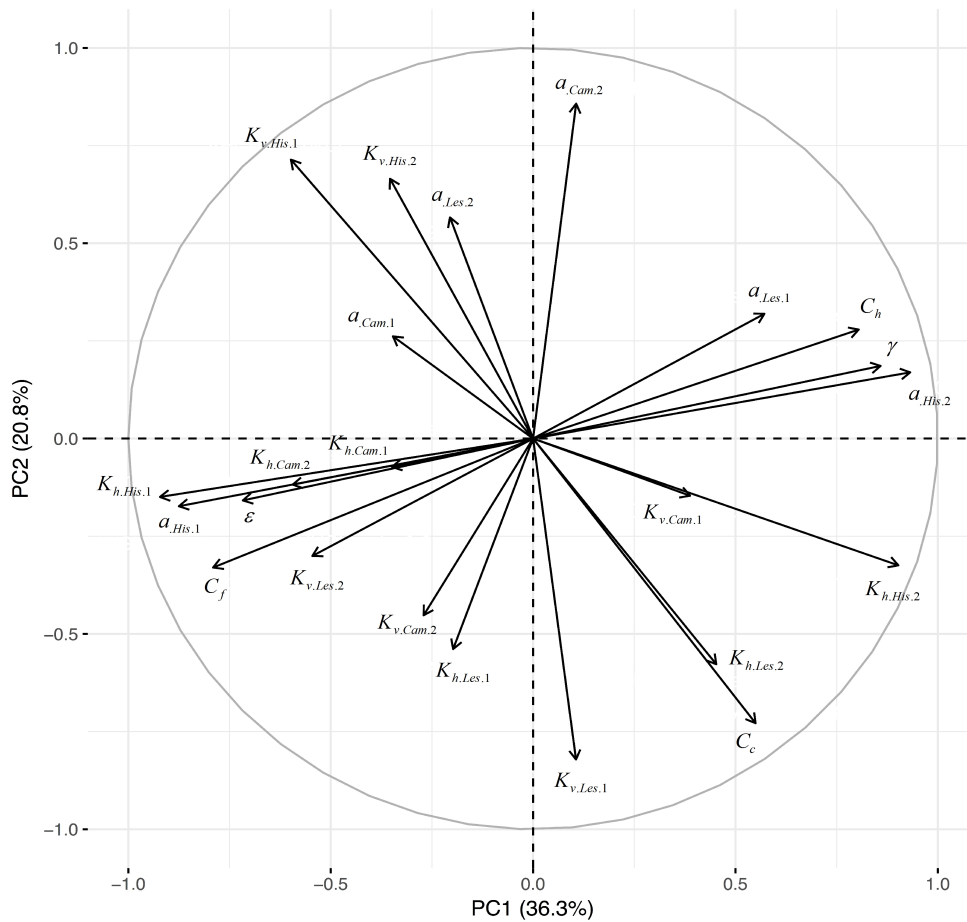


Figure 4.10: PCA-based analysis: The intercorrelations between the model parameters and their contributions to the calibration process via normalized eigenvectors and eigenvalues of the post-calibration parameter covariance matrix. The length (angle) of the arrows represents the magnitude (direction) of the correlation coefficient between the parameters and the PCs. The lowest and highest contributions of the parameters to the calibration process are identified with the shortest and longest arrows, respectively. For detailed information on the parameter description refer to Tables 4.1 and 4.2.

Additionally, the posedness condition of the inverse problem was examined by: correlation analysis, eigenvalues analysis, and) the condition numbers. The correlation analysis shows whether immoderate correlation with other parameters results in high error variance of a particular parameter. If so, the inverse problem is ill-posed i.e. Φ contours does not close. It is noted that when the number of parameters are high, the likelihood of an ill-posed inverse problem is also increased (Doherty, 2015). However, the PCA-based correlation analysis shows low correlations between the parameters, indicating a well-posed inverse problem.

Also, if the ratio of highest to lowest eigenvalues of the parameter covariance matrix exceeds $10.E-7$, the problem is considered to be ill-posed (Doherty, 2016a). However, a ratio of $4.49E-12$ was obtained, which is far less than the recommended value. Finally, the “condition number” of the covariance matrix must be inverted to estimate the parameter values. In fact, this is recorded for every Marquardt lambda tested during every PEST iteration. The square root of the ratio mentioned above is related to the condition number of the covariance matrix. Matrices that have a high condition number are difficult to invert, as numerical errors are amplified in their inversion (Doherty, 2015). However, the well-posedness of the inverse problem was also confirmed by the achieved low condition number i.e. 15.8 (out of 7297.8).

4.5 Conclusions

The joint simulation of the water –and energy fluxes and the potential benefit of flux measurements in the parameter estimation process were investigated. For this purpose, the hydrological model GEOtop was exemplarily applied to the Rott catchment in southern Germany over two summer episodes in 2013 (calibration) and 2015 (validation). Due to its complexity, the model is highly CPU-time demanding and only a limited number of model runs can be afforded in parameter estimation. To facilitate this, the gradient-based nonlinear Gauss-Marquardt-Levenberg (GML) parameter estimation method was applied and linked the GEOtop model to the Parameter ESTimation tool (PEST).

The results revealed that the quality of the modeled streamflow and the turbulent fluxes of the calibrated model was satisfying, both in the calibration episode, and the validation episode. This was confirmed by the linear statistical metrics applied for the model performance evaluation. The PCA-based analysis of the model parameters showed a low- and insignificant cross correlation between the GEOtop parameters. As a result, most of the estimated parameters were highly sensitive to the calibration process, as lay in the solution space of the inverse problem. This indicates the successful application of sensitivity analysis for the key parameters identification.

Because of the robust parameter estimation technique applied by PEST, the uncertainty variance of most calibrated parameters was significantly reduced. In

addition, it was found that the soil parameter groups of α and K_v highly contributed to this uncertainty reduction. More importantly, the benefit of adding the turbulent fluxes to the calibration dataset in order to improve the parameter confidence ellipses was determined using a covariance analysis. It was particularly found that the additional values of H and LE fluxes resulted in both lowering the uncertainty ranges and eliminating the correlation of most model parameters. However, the magnitude of reduction in uncertainty ranges, and also the effect on their intercorrelations varied not only for the different considered parameters, but also between the heat fluxes of H and LE.

Therefore, the Gauss-Marquardt-Levenberg algorithm realized in PEST proved to be highly suitable not only for a robust nonlinear parameter estimation, but also for the uncertainty estimates of the CPU-time intensive physically based model applied.

Chapter 5

Conclusions and outlook

5.1 Conclusions

A wide range of dataset *from* in-situ measurements such as micrometeorological and climate stations, precipitation and discharge gauges, Lysimeter and soil-moisture networks *to* remotely-sensed data such as X-band rainfall radar and commercial microwave-link networks are observed and measured in the Bavarian TERENO-prealpine observatory. For this dissertation, required datasets were not all available in a concerted and organized manner in an open-data repository at the Institute of Meteorology and Climate Research (IMK-IFU), KIT-Campus Alpin. A comprehensive data collation was thus first necessary to be done for carrying out this PhD-project. This implies that, it was necessary not only to compile and collect these datasets from various sources, but also to harmonize them with different formats and time-steps.

The results achieved in this thesis revealed that the variations of the turbulent fluxes were low during the winter and autumn periods, whereas they were quite large during the spring and summer seasons. The differences between diurnal and nocturnal values of the sensible heat (H) and latent heat (LE) fluxes were not very pronounced in the wintertime, because of the low radiation variation in the region. For the warm periods, however, the mean diurnal values of H and LE fluxes showed much larger differences due to the increase of solar radiation, precipitation events and high vegetation fraction, and obviously, the main consumer of net radiation (Rn) was LE flux. As a result, a clear increasing trend towards the warm periods was observed in the surface turbulent fluxes; however, the temporal variation patterns were different at individual Eddy Covariance (EC) sites across the TERENO-prealpine observatory. This suggests, for example, for model applications, a high-resolution spatially-based

modeling approach is needed to be considered for this region in order to describe the variations of surface heat fluxes in time and space appropriately.

The Principal Component Analysis (PCA) results revealed that, based on PC1, the turbulent flux variability was strongly driven by the radiation components followed by the temperature variables at the study sites. For PC2, however, the dominant contributing variables were the wind components. Albedo negatively affected the turbulent flux variability. It rather followed an elevation trend in the TERENO region. This finding was in agreement with Zeeman et al. (2017) and might be explained by the lack of irradiation due to a mountain shadowing effect. In terms of site-scale Energy Balance Closure (EBC), among the TERENO-prealpine EC sites, the lowest correlation coefficient (R^2) between the measured and available energy was found at Graswang. This can be explained by the climatic and environmental conditions. This site is surrounded by high mountains and the wind speed is relatively low so that the mechanically driven turbulence is reduced in the valley. As a result, many of the calculated heat flux values were removed as unreliable data during the post-processing analysis. However, in terms of Energy Balance Ratio (EBR), the highest overall value of EBR was also achieved at the aforesaid site indicating that the minimum heat and water vapour fluxes are lost for that area. Furthermore, analysis of the flux footprint climatology revealed that the majority of the flux footprints received by the instruments at a radius of approximately 250 m around the stations; and the overall shape of the flux footprints significantly matched the direction of the prevailing winds at the study EC sites.

The distributed hydrological model GEOTop showed a high capability of quantifying the spatiotemporal variability of the water- and energy budgets with consideration for the elevation-gradient effect of the heterogeneous landscapes of the Rott and Upper-Ammer catchments in the TERENO-prealpine observatory. It was also revealed that the spatial variability of the hydrometeorological variables is significantly affected by diversity in topography, radiation and wind components, soil moisture properties as well as land cover and vegetation types in the region. In terms of water balance, GEOTop was appropriately capable of representing the temporal variability of surface streamflow and reproducing infiltration and daily cycle of soil moisture evaporation associated with the rainfall events. In the study catchments, an increased runoff volume in early June peak flow highlighted the importance of snow dynamics for runoff generation. The peak flow underestimation in the Upper-Ammer catchment could be explained by the lack of meteorological stations, which can result in considerable errors in the spatial interpolation by the model. Also, it may further be explained by the rapid climate zone changes in a small spatial area or by the snow dynamics effect on the behavior of surface runoff during the springtime. Also, in terms of energy balance, the EC-based diurnal cycles of energy budget were well reproduced by the model. GEOTop, however, slightly overestimated LE flux at the study sites. This could be mainly due to the fact that the EC based technique usually underestimates turbulent fluxes.

Furthermore, the bivariate empirical Copula-based functions revealed that the dependence structure patterns of both modelled and observed water- and energy variables were similar, representing a reasonable calibration of the GEOTop model. These non-linear features in the dependence structures of hydrometeorological variables were observed with the highest densities (or best fit between the modeled and observed values) either in the lower or upper ranks, i.e. in the low or high values, exhibit a worse model calibration for the middle ranks of the data. Thus, it was concluded that the Copula-based model performance analysis applied herein can be considered for model evaluation in the hydrological model community in addition to traditional model performance analyses.

Using the developed GEOTop-PEST interface enabled an “automatic parameter estimation” procedure that allowed to improve modelled streamflow and turbulent fluxes reasonably compared to the manual-based calibration efforts performed by the GEOTop model for the Rott catchment (Soltani et al., 2018; Hingerl et al., 2016) or worldwide (e.g. Rigon et al., 2006; Bertoldi et al., 2006). For discharge, however, the baseflow was somewhat underestimated. This could be due to the fact that GEOTop, as a hydrologic model, does not describe the detailed 3-dim hydrogeological processes e.g. contribution of the underground water (aquifers) to the surface stream flows. Further, the PCA-based analysis of the model’s parameters showed a low- and insignificant cross-correlation between the GEOTop parameters. As a result, most of the estimated parameters were highly sensitive to the calibration process. But this also indicates the successful application of the sensitivity analysis for the key parameters’ identification.

This dissertation also found that the model parameter’s post-calibration uncertainty ranges for almost all types of the considered parameters were highly decreased. Particularly, the uncertainty range for the landuse parameter of the canopy height was significantly decreased. With regards to the soil parameters, the hydraulic conductivities revealed a noticeable decrease in the magnitude of uncertainty. This, denotes, a robust parameter estimation by PEST. In this context, the importance of additional measurements on top of discharge for both the parameter estimation and the uncertainty-related analysis was determined and quantified. The results revealed a novel achievement from an uncertainty-based point of view. It was found that the uncertainty ranges of the post-calibration parameters were not only significantly decreased and improved by adding the heat fluxes to the discharge observation, but also the intercorrelation between the parameters was eliminated in many cases.

Further, the most sensitive soil- and vegetation-related parameters were identified and fitted. These parameters possess a high importance not only for hydrologists and hydrometeorologists, and in the GEOTop model, but also for the soil physicists and biologists, and in other land-surface models. So, the improved estimation of unknown parameters has also benefits for interdisciplinary-research groups. Thus, it could be concluded that the Gauss-Marquardt-Levenberg algorithm realized in PEST proved to be highly suitable not only for a robust nonlinear

parameter estimation, but also for the uncertainty estimates of the CPU-time intensive physically based model applied.

Finally, the spatial variability of the hydrometeorological variables and the hydrological processes were comprehensively quantified, modeled and presented in this PhD dissertation in the TERENO prealpine observatory; however, it was temporally focused on the summer-episode. Thus, researches with a longer period of time seems to be essential.

5.2 Outlook

In this dissertation, both the fast-response and slow-response micrometeorological measurements from three EC sites were utilized to quantify the spatiotemporal variability of the water- and energy fluxes in the TERENO-prealpine observatory. To further understand both the spatial and temporal variability of the hydrometeorological variables, other available- and new observations could be considered in the observatory. For example, Lysimeter network, which aims to study the impact of climate and management changes on the components of water- and carbon budgets, biosphere-atmosphere-hydrosphere exchanges as well as yields and biodiversity in the observatory. Furthermore, Cosmic Ray Neutron Sensing (CRNS), as a completely new type of measurements recently operated in the TERENO-prealpine observatory, can be used to investigate the soil-moisture and snow-water variations with multi-hectare footprint sizes. In particular, on the observation side, CRNS could complement in future studies the analysis of the spatiotemporal variability, especially on the snow-related studies over the highlands of the observatory.

At the Fendt area, located in the northern part of the TERENO-prealpine observatory, the spatially distributed measurements of soil moisture and temperature profiles are carried out with the wireless underground sensor network SoilNet, developed specifically for the near real-time monitoring of the spatiotemporal dynamics of soil water content at field and headwater catchment scales. The SoilNet at Fendt comprises 55 measurement profiles distributed over a total area of about 300 m x 300 m. This redundant setup with several sensors per depth allows the examination of the data for small-scale heterogeneity, which is better to be taken into account in future studies in the region.

In the observatory, the ScaleX campaigns were operated in 2015 and 2016. It is a series of collaborative, intensive research campaigns that aim to assess spatially distributed patterns and gradients in land surface-atmosphere exchange processes within the TERENO-prealpine region, and specifically surrounding the Fendt site. For instance, the hexacopter-based measurement was conducted by Brosy et al. (2017) in ScaleX-2015 campaign. While, traditional ground-based observations include towers

that only cover a few measurement heights at a fixed location, and also most remote sensing techniques and aircraft measurements show limitations to achieve sufficient detail close to the ground (up to 50 m), the vertical and horizontal transects of the planetary boundary layer can be complemented by the Unmanned Aerial Vehicles (UAV). To conclude, the hexacopter- and UAV-based soundings could be carried out to study of the surface exchange processes not only in campaigns, but also in a regular operational manner.

In-depth analysis of the satellite-derived modes with respect to soil moisture could be also considered. For example, the Global Precipitation Measurement (GPM) satellite missions, particularly for a comparatively small-scale area in the observatory for which the in-situ observations available on the ground. Further, in this thesis the knowledge of turbulent flux variability and energy balance closure (EBC) problem at the TERENO-prealpine observatory need to be further significantly strengthened. However, improving the EBC over the region needs further investigation, e.g. by high resolution Large-Eddy Simulations (LES), for a better understanding of the small-scale weather circulation processes and the environmental conditions over the individual EC sites. While a first analysis on the mean annual of the flux footprint climatology was conducted for the study EC sites. Further investigation is needed to consider the diurnal-nocturnal as well as the atmospheric stable-unstable conditions for different seasons of the year.

In this PhD-study, focus was set on the spatiotemporal variability of coupled water and energy fluxes for the Rott and Upper-Ammer catchments for two recent summer episodes in the TERENO-prealpine observatory. However, to better understand the hydrological cycle and impacts, it is advised to consider the climate change-related impacts on the coupled water- and energy balances for a longer period of time, especially in other locations. Therefore, it could be considered to transfer the GEOtop setup to other observatories like the WASCAL observatory in West Africa to find out how the model works in completely different climate conditions. In fact, WASCAL is a large-scale research-focused climate service centre designed to help tackle the challenges and thereby enhance the resilience of human and environmental systems to climate change and increased variability. The three EC sites in the TERENO-prealpine observatory have been established with the elevation-gradient; in the WASCAL, however, there are three EC sites with the landuse-gradient (Berger *et al.*, 2018; Bliefernicht *et al.*, 2018). Thus, the performance of GEOtop can be evaluated in different latitudes with having various landscapes.

Bibliography

- Abdi, H., and Williams, L.J. (2010) Principal component analysis, WIREs Computational Statistics, Volume 2, July/August 2010. DOI: 10.1002/wics.101.
- Aubinet, M, Grelle, A., Ibrom, A., Rannik, Ü., Moncrieff, J., Foken, T., et al. (1999) Estimates of the annual net carbon and water exchange of forest: The EUROFLUX methodology. *Adv. Ecol. Res.* 30:113–175.
- Aubinet, M., Vesala, T., Papale, D. (2012) Eddy Covariance - A Practical Guide to Measurement and Data Analysis. Springer Dordrecht Heidelberg London New York. DOI 10.1007/978-94-007-2351-1.
- Bahremand, A., and Smedt, De. (2006) Parameter sensitivity and uncertainty analysis of the WetSpa model using PEST. Proceedings of the 2006 IASME/WSEAS Int. Conf. on Water Resources, Hydraulics & Hydrology, Chalkida, Greece, May 11-13, 2006. pp 26-35.
- Bahremand, A., and Smedt De. (2008) Distributed Hydrological Modeling and Sensitivity Analysis in Torysa Watershed, Slovakia. *Water Resour Manage* 22: 393-408.
- Bahremand, A., and Smedt De. (2010) Predictive Analysis and Simulation Uncertainty of a Distributed Hydrological Model. *Water Resour Manage* 22: 393-408. DOI 10.1007/s11269-010-9584-1.
- Baldocchi, D.D., Hicks B.B., Meyers T.P. (1988) Measuring biosphere-atmosphere exchanges of biologically related gases with micrometeorological methods. *Ecology* 69, 1331–1340.
- Baldocchi, D.D., Falge E., Gu, L., et al. (2001) Fluxnet: A new tool to study the temporal and spatial variability of ecosystem-scale carbon dioxide, water vapor, and energy flux densities, *B. Am. Meteorol. Soc.*, 82, 2415–2434, 2001.

Bibliography

- Balistrocchi, M., Bacchi, B. (2017) Derivation of flood frequency curves through a bivariate rainfall distribution based on copula functions: application to an urban catchment in northern Italy's climate. *Hydrology Research* 48 (3), 749–762.
- Bárdossy, A. (2006) Copula-based geostatistical models for groundwater quality parameters. *Water Resour. Res.*, 42(11), W11416.1– W11416.12, doi:10.1029/2005WR004754.
- Bárdossy, A., and Pegram, G.S. (2009) Copula based multisite model for daily precipitation simulation. *Hydrol. Earth Syst. Sci.*, 13, 2299–2314, doi:10.5194/hess-13-2299-2009.
- Bárdossy, A., and Pegram, G.S. (2012) Multiscale spatial recorelation of RCM precipitation to produce unbiased climate change scenarios over large areas and small. *Water Resour. Res.*, 48, 1–13, doi:10.1029/2011WR011524.
- Barnes, S.L. (1964) A technique for maximizing details in numerical weather map analysis. *J. Appl. Meteor.*, 3, 396–409.
- Berger, S., Bliedernicht, J., Linstädter, A., Canak, K., Guug, S., Heinzeller, D., Hingerl, L., Mauder, M., Neidl, F., Quansah, E., Salack, S., Steinbrecher, R., Kunstmann, H. (2018) The impact of rain events on CO₂ emissions from contrasting land use systems in semi-arid West African savannas. *Science of the Total Environment* 647. 1478–1489.
- Berry, J.F. and Dennison, M.S., (1993) Wetland mitigation. In *Wetlands: Guide to Science, Law, and Technology*. Pp. 278–303. Edited by M. S. Dennison and J. F. Berry. Noyes Publications, Park Ridge, New Jersey.
- Bertoldi, G., Tamanini, D., Zanotti, F., Rigon, R. (2004) GEOTOP: A Hydrological Balance Model. Technical Description and Programs Guide. University of Trento: Italy.
- Bertoldi, G., Rigon, R., Over, T. (2006) Impact of watershed geomorphic characteristics on the energy and water budgets. *Journal of Hydrometeorology* 7(3): 389-403.
- Bertoldi, G., Notarnicola, C., Leitinger, G., Endrizzi, S., Zebisch, M., Della Chiesa, S., and Tappeiner, U. (2010) Topographical and eco-hydrological controls on land surface temperature in an alpine catchment. *Ecohydrology*, 3, 189–204, doi:10.1002/eco.129.
- Beven, K. (2001) How far can we go in distributed hydrological modelling? *Hydrol. Earth Syst. Sci.*, 5(1), 1–12, doi:10.5194/hess-5-1-2001.
- Blanken, P., Black, T., Yang, P., Neumann, H., Nesic, Z., Staebler, R., Hartog, G., Novak, M.D., Lee, X. (1997) Energy balance and canopy conductance of a boreal aspen forest: Partitioning overstory and understory components. *Journal of Geophysical Research: Atmospheres* (1984–2012), 102(D24), 2891528927.
- Bliedernicht1, J., S. Berger, S., Salack, S., Guug, S., Hingerl, L., Heinzeller, D., Mauder, M., Steinbrecher, R., Steup, G., Bossa, A.Y., Waongo, M., Quansah, E.,

Bibliography

- Balogun, A.A., Yira, Y., Arnault, J., Wagner, S., Klein, C., Gessner, U., Knauer, K., Straub, A., Schönrock, R., Kunkel, R., Okogbue, E.C., Rogmann, A., Neidl, F., Jahn, C., Diekkrüger, B., Aduna, A., Barry, B., Kunstmann, H. (2018) The WASCAL Hydro-Meteorological Observatory in the Sudan Savanna of Burkina Faso and Ghana. *Accepted*.
- Bronstert, A., Niehoff, D., and Bürger, G. (2002) Effects of climate and land- use change on storm runoff generation: present knowledge and modelling capabilities. *Hydrol. Processes*, 16(2), 509–529, doi:10.1002/hyp.326.
- Brosy, C., K. Krampf, M. Zeeman, B. Wolf, W. Junkermann, K. Schäfer, S. Emeis and H. Kunstmann (2017) Simultaneous multicopter-based air sampling and sensing of meteorological variables. *Atmos. Meas. Tech.* 10:2773-2784. doi:10.5194/amt-10-2773-2017.
- Breuer, L., Eckhardt, K., Frede, G. (2003) Plant parameter values for models in temperate climates. *Ecological Modelling* 169 (2003) 237–293.
- Burba, G.G., Verma, S.B., and Kim, J. (1999) Surface energy fluxes of *Phragmites australis* in a prairie wetland, *Agr. Forest Meteorol.*, 94, 31–51, 1999.
- Burba, G. (2013) ‘Eddy Covariance Method for Scientific, Industrial, Agricultural and Regulatory Applications’, ISBN 978-0-615-76827-4 LI-COR Biosciences, Lincoln, Nebraska.
- Carrera, J., and Neuman, S. (1986) Estimation of Aquifer Parameters under Transient and Steady State Conditions: 1. Maximum Likelihood Method Incorporating Prior Information, *Water Resour. Res.*, 22, 199–210.
- Carslaw, D.C., and Ropkins, K. (2012) openair – an R package for air quality data analysis. *Environmental Modelling & Software*. 27-28, pp.52–61.
- Carslaw, D.C. (2015) The openair manual – open-source tools for analyzing air pollution data. Manual for version 1.1-4, King’s College London.
- Cava, D., Contini, D., Donato, A., and Martano, P. (2008) Analysis of short-term closure of the surface energy balance above short vegetation. *Agric. Forest. Meteorol.*, 148, 82-93.
- Chow, F.K., Weigel, A.P., Street, R.L., Rotach, M.W., Xue, M. (2006) High-resolution large-eddy simulations of flow in a steep alpine valley. Part I: methodology, verification, and sensitivity experiments. *Journal of Applied Meteorology and Climatology* 45: 63–86.
- Culf, A.D., Foken, T., and Gash, J.H.C. (2004) The Energy Balance Closure Problem. In: Kabat P., Claussen M. et al. (eds). *Vegetation, Water, Humans and the Climate A New Perspective on an Interactive System*. Springer, Berlin, Heidelberg, pp. 159–166 doi: 10.1007/978-3-642-18948-7_13.

Bibliography

- Cuo, L., Lettenmaier, D.P., Mattheussen, B.V., Storck, P., Wiley, M. (2008) Hydrologic prediction for urban watersheds with the distributed hydrology-soil-vegetation model. *Hydrological Processes* 22(21): 4205–4213.
- da Silva, M.G., de Oliveira de Aguiar Netto, A., de Jesus Neves, R.J., do Vasco, A.N., Almeida, C., and Faccioli, G.G. (2015) Sensitivity Analysis and Calibration of Hydrological Modeling of the Watershed Northeast Brazil. *Journal of Environmental Protection* 6, 837-850.
- Decker, M., Brunke, M.A., Wang, Z., Sakaguchi, K., Zeng, X., Bosilovich, M.G. (2012) Evaluation of the reanalysis products from GSFC, NCEP, and ECMWF using flux tower observations. *Journal of Climate* 25(6): 1916–1944.
- Deheuvels, P. (1979) La fonction de dépendance empirique et ses propriétés: Un test non paramétrique d'indépendance, Académie Royale de Belgique. *Bulletin de la Classe des Sciences*, 65, 274– 292.
- Della Chiesa, S., Bertoldi, G., Niedrist, G., Obojes, N., Endrizzi, S., Albertson, J.D., Wohlfahrt, G., Hörtnagl, L., and Tappeiner, U. (2014) Modelling changes in grassland hydrological cycling along an elevational gradient in the Alps. *Ecohydrology*, doi:10.1002/eco.1471.
- De Vries, D.A. (1963) Thermal properties of soils. In: Van Wijk, W.R. (Ed.), *Physics of Plant Environment*. North-Holland Publishing Company, Amsterdam, pp. 210–235.
- Dirmeyer, P.A., Niyogi, D., de Noblet-Ducoudré, N., Dickinson, R.E., Snyder, P.K. (2010) Impacts of land use change on climate. *International Journal of Climatology* 30(13): 1905–1907.
- Doherty, J. (2002) *PEST - Model-Independent Parameter Estimation*, Watermark Numerical Computing, Australia.
- Doherty, J., and Johnston, J.M. (2003) Methodologies for calibration and predictive analysis of a watershed model. *J. Amer. Water Resour. Assoc.*, 39(2), 251–265.
- Doherty, J. (2004) PEST, PUB-IAHS Workshop “Uncertainty Analysis in Environmental Modeling”, 6-8 July 2004, Lugano.
- Doherty, J., Hunt, R.J., and Tonkin, M.J. (2010) Approaches to highly parameterized inversion: A guide to using PEST for model-parameter and predictive-uncertainty analysis: U.S. Geological Survey Scientific Investigations Report 2010–5211. 71p.
- Doherty, J. (2010) Addendum to the PEST Manual. Watermark Numerical Computing, Brisbane, Queensland, Australia, 261 pp. <http://www.pesthomepage.org/files/addendum.pdf>.
- Doherty, J. (2015) Calibration and uncertainty analysis for complex environmental models. *Watermark Numerical Computing*, Brisbane, Australia. ISBN: 978-0-9943786-0-6.

Bibliography

- Doherty, J. (2016a) PEST: Model-Independent Parameter Estimation, User Manual Part I: PEST, SENSAN and Global Optimisers, 6th Edition. Watermark Numerical Computing, Australia.
- Doherty, J. (2016b) PEST: Model-Independent Parameter Estimation, User Manual Part II: PEST Utility Support Software, 6th Edition. Watermark Numerical Computing, Australia.
- Dray, S. (2008) On the number of principal components: A test of dimensionality based on measurements of similarity between matrices. *Computational Statistics & Data Analysis* 52 (2008) 2228 – 2237. doi:10.1016/j.csda.2007.07.015.
- Du, R., Lu, D., Wang, G. (2006) Diurnal, seasonal, and inter-annual variations of N₂O fluxes from native semi-arid grassland soils of inner Mongolia. *Soil Biology & Biochemistry* 38 (2006) 3474–3482.
- Dubayah, A., Dozier, J., Davis, F.W. (1990) Topographic distribution of clear-sky radiation over the Konza Prairie, Kansas. *Water Resources Research* 26(4): 679–690.
- Duda, P.B., Hummel, P.R., Donigian, A.S., Imhoff, J.C. (2012) Model use, calibration, and validation. *Trans. ASABE* 55, 1523–1547.
- Dupuis, D.J. (2007) Using copulas in hydrology: Benefits, cautions, and issues. *J. Hydrol. Eng.*, 12, 381–393, doi:10.1061/(ASCE)1084-0699(2007)12:4(381).
- Eder, F., De Roo, F., Kohnert, K., Desjardins, R.L., Schmid, H.P, and Mauder, M., (2014) Evaluation of two energy balance closure parameterizations. *Boundary-Layer Meteorology* 151(2), 195219. 2014.
- Eckhardt, K., Arnold, J.G. (2001) Automatic calibration of distributed catchment model. *Journal of Hydrology* 251, 103–109.
- Endrizzi, S., and Marsh, P. (2010) Observations and modeling of turbulent fluxes during melt at the shrub-tundra transition zone 1: point scale variations. *Hydrol. Res.*, 41, 471–491.
- Endrizzi, S., Dall’Amico, M., Gruber, S., Rigon, R. (2011) GEOtop Users Manual. July, 2011 (<http://geotopmodel.github.io/geotop>).
- Endrizzi, S., Gruber, S., Dall’Amico, M., Rigon, R. (2014) GEOtop 2.0: simulating the combined energy and water balance at and below the land surface accounting for soil freezing, snow cover and terrain effects. *Geoscientific Model Development* 7(6): 2831–2857.
- ESRI, (2011) ArcGIS Desktop: Release 10. Redlands, CA: Environmental Systems Research Institute.
- Ezzahar, J., Chehbouni, A., Hoedjes, J., Ramier, D., Boulain, N., Boubkraoui, S., Cappelaere, B., Descroix, L., Mougenot, B., and Timouk, F. (2009) Combining scintillometer measurements and an aggregation scheme to estimate area-averaged

Bibliography

- latent heat flux during the AMMA experiment. *Journal of Hydrology*, 375, 217-226.
- Feyereisen, G.W., Strickland, T.C., Bosch, D.D., and Sullivan, D.G. (2007) Evaluation of SWAT Manual Calibration and Input Parameter Sensitivity in the Little River Watershed. *American Society of Agricultural and Biological Engineers*, 50, 843-855. <http://dx.doi.org/10.13031/2013.23149>.
- Feyen, L., Vazquez, R., Christiaens, K., Sels, O., and Feyen, J. (2000) Application of a Distributed Physically-Based Hydrological Model to a Medium Size Catchment. *Hydrology and Earth System Sciences* 4, 47-63. <http://dx.doi.org/10.5194/hess-4-47-2000>.
- Foken, T., and Oncley, S.P. (1995) Results of the workshop “Instrumental and methodical problems of land surface flux measurements”, *B. Am. Meteorol. Soc.*, 76, 1191–1193, 1995.
- Foken, T., Wichura, B. (1996) Tools for quality assessment of surface-based flux measurements, *Agric. Forest Meteorol.* 78, 83-105.
- Foken, T., Kukharets, V.P., Perepelkin, V.G., Tsvang, L.R., Richter, S.H., and Weisensee, U. (1999) The influence of the variation of the surface temperature on the closure of the surface energy balance, 13th Symposium on Boundary Layer and Turbulence, Dallas, TX, 10–15 Jan 1999, *Amer. Meteorol. Soc.*, 308–309, 1999.
- Foken, T., Gockede, M., Mauder, M., Mahrt, L., Amiro, B., Munger, W. (2004) Post-field data quality control. X. Lee et al. (eds.), *Handbook of Micrometeorology*, Chapter 9. pp 181–208.
- Foken, T. (2009) *Micrometeorology*, Springer-Verlag Berlin Heidelberg. DOI: 10.1007/978-3-540-74666-9.
- Foken, T., and Co-authors, (2010) Energy balance closure for the LITFASS2003 experiment. *Theor. Appl. Climat.*, 101, 149-160.
- Foken, T., Aubinet, M., Finnigan, J., Leclerc, M.Y., Mauder, M., Tha Paw, U.K. (2011) Results of a panel discussion about the energy balance closure correction for trace gases, *Bulletin of the American Meteorological Society*. Doi: 10.1175/2011BAMS3130.1.
- Formetta, G., Mantilla, R., Franceschi, S., Antonello, A., and Rigon, R. (2011) The JGrass-NewAge system for forecasting and managing the hydrological budgets at the basin scale: models of flow generation and propagation/routing, *Geosci. Model Dev.*, 4, 943–955, doi:10.5194/gmd-4-943-2011.
- Friendly M, Monette G and Fox J. 2013. Elliptical Insights: Understanding Statistical Methods through Elliptical Geometry. *Statistical Science*, Vol. 28, No. 1, 1–39. DOI: 10.1214/12-STS402.

Bibliography

- Gao, H., Wood, E.F., Drusch, M., and McCabe, M.F. (2007) Copula- derived observation operators for assimilating TMI and AMSR-E retrieved soil moisture into land surface models. *J. Hydrometeorol.*, 8, 413–429, doi:10.1175/JHM570.1.
- Gao, Z., Horton, R., Liu, H.P., Wen, J., and Wang, L. (2009) Influence of wave phase difference between surface soil heat flux and soil surface temperature on land surface energy balance closure, *Hydrol. Earth Syst. Sci. Discuss.*, 6, 1089–1110, 2009.
- Garratt, J.R. (1992) *The Atmospheric Boundary Layer*, Cambridge University Press.
- Genest, C., Rémillard, B., and Beaudoin, D. (2007) Goodness-of-fit tests for copulas: A review and a power study, *Insurance: Math. Econ.*, 44, 199–213, doi:10.1016/j.insmatheco.2007.10.005.
- Genest, C., and Favre, A.A.C. (2007). Everything you always wanted to know about copula modeling but were afraid to ask. *Journal of Hydrologic Engineering*, 347-368. <http://doi.org/10.1061/ASCE1084-0699200712:4347>.
- Ghesla, E., and Rigon, R. (2006) A Tutorial for Preparing GEOTop Input Files with JGrass. University of Trento, Trento, Italy.
- Gottardi, G., and Venutelli, M. (1993) A control-volume finite-element model for two-dimensional overland flow. *Adv. Water Resour.*, 16, 277–284.
- Grayson, R., and Blöschl, G. (2000) *Spatial Patterns in Catchment Hydrology, Observations and Modelling*. Cambridge University Press, 404 pp.
- Gurjanov, A.E., Zubkovskij, S.L., Fedorov, M.M., (1984) Mnogokanalnaja avtomatizirovannaja sistema obrabotki signalov na baze EVM (Automatic multi-channel system for signal analysis with electronic data). *Geod. Geophys. Veroff.*, R. II 26, 17-20.
- Hao, Y., Wang, Y., Huang, X., Cui, X., Zhou, X., Wang, S., Niu, H., and Jiang, G. (2007) Seasonal and interannual variation in water vapor and energy exchange over a typical steppe in Inner Mongolia, China, *Agr. Forest Meteorol.*, 146, 57–69, 2007.
- Hamby, D.M. (1994) A review of techniques for parameter sensitivity analysis of environmental models. *Environ. Monit. Assess.*, 32, 135–154.
- Harazono, Y., Kim, J., Miyata, A., Choi, T., Yun, J., and Kim, JW. (1998) Measurement of energy budget components during the International Rice Experiment (IREX) in Japan, *Hydrol. Processes*, 12, 2081–2092, doi:10.1002/(SICI)1099-1085(19981030)12:13/14<2081::AID-HYP721>3.0.CO;2-M.
- Helton, J.C. (1993) Uncertainty and sensitivity analysis techniques for use in performance assessment for radioactive waste disposal. *Reliability Engineering and System Safety* 42, 327-367.

Bibliography

- Hendricks Franssen, H.J., Stöckli, R., Lehner, I., Rotenberg, E., Seneviratne, S.I.I. (2010) Energy balance closure of eddy-covariance data: A multisite analysis for European FLUXNET stations. *Agric. For. Meteorol.* 150, 1553–1567. doi:10.1016/j.agrformet.2010.08.005.
- Hill, M.C. (1998) Methods and guidelines for effective model calibration, U.S. Geological Survey. *Water Resources Investigations Report* 98-4005.
- Hingerl, L., Kunstmann, H., Wagner, S., Mauder, M., Bliefernicht, J., Rigon, R. (2016) Spatio-temporal variability of water and energy fluxes – a case study for a mesoscale catchment in pre-alpine environment, *Hydrol. Process.* 30, 3804–3823.
- Horst, T.W. (1999) The footprint for estimation of atmosphere-surface exchange fluxes by profile techniques. *Boundary-Layer Meteorology* 90: 171–188, 1999.
- Hui, D., Wan, S.H., Su, B., Katul, G., Monson, R., Luo, Y. (2004) Gap-filling missing data in eddy covariance measurements using multiple imputation (MI) for annual estimations, *Agricultural and Forest Meteorology* 121 (2004) 93–111.
- Imukova, K., Ingwersen, J., Hevart, M., Streck, T. (2016) Energy balance closure on a winter wheat stand: comparing the eddy covariance technique with the soil water balance method, *Biogeosciences*, 13, 63–75, 2016. doi:10.5194/bg-13-632016.
- Ivanov, V.Y., Vivoni, E.R., Bras, R.L., and Entekhabi, D. (2004) Catchment hydrologic response with a fully distributed triangulated irregular network model. *Water Resour. Res.*, 40, 1–23.
- Imukova, K., Ingwersen, J., Hevart, M., Streck, T. (2016) Energy balance closure on a winter wheat stand: comparing the eddy covariance technique with the soil water balance method. *Biogeosciences* 13: 63–75. doi:10.5194/bg-13-632016.
- Jolliffe, I. (2002) *Principal Component Analysis*. second ed. Springer, Berlin.
- Kabat, P., Claussen, M., Whitlock, S., Gash, J.H.C, Guenni, L.B., Meybeck, M., Pielke, R., Vorosmarty, C.J., Hutjes, R.W.A., Lutkemeier, S. (2004) *Vegetation, water, humans and the climate: A new perspective on an interactive system*. Springer press. DOI: 10.1007/978-3642-18948-7.
- Kaimal, J.C., Finnigan, J.J. (1994) *Atmospheric Boundary Layer Flows: Their Structure and Measurement*. Oxford University Press: New York, NY, 289 p.
- Kahan, D.S., Xue, Y., and Allen, S.J. (2006) The impact of vegetation and soil parameters in simulations of surface energy and water balance in the semi-arid sahel: A case study using SEBEX and HAPEX-Sahel data, *J. Hydrol.*, 320, 238–259, 2006.
- Kannan, N., White, S.M., Worrall, F., Whelan, M.J. (2007) Hydrological Modelling of a Small Catchment using SWAT-2000 -Ensuring Correct Flow Partitioning for Contaminant Modeling. *Journal of Hydrology* 334, 64-72. <http://dx.doi.org/10.1016/j.jhydrol.2006.09.030>.

Bibliography

- Kiese, R., B. Fersch, C. Baeßler, C. Brosy, K. Butterbach-Bahl, C. Chwala, M. Dannenmann, J. Fu, R. Gasche, R. Grote, C. Jahn, J. Klatt, H. Kunstmann, M. Mauder, T. Rödiger, G. Smiatek, M. Soltani, R. Steinbrecher, I. Völksch, J. Werhahn, B. Wolf, M. Zeeman, H.P. Schmid (2018) The TERENO-preAlpine Observatory integrating meteorological, hydrological and biogeochemical measurements. *Accepted in Vadose Zone Journal*.
- Kunstmann, H., Hingerl, L., Mauder, M., Wagner, S., Rigon, R. (2013) A combined water and energy flux observation and modeling study at the TERENO-prealpine observatory, IAHS publication 359, Climate and Land Surface Changes in Hydrology, pp. 221225.
- Kunstmann, H., Krause, J., Mayr, S. (2006) Invers distributed hydrological modeling of Alpine catchments, *Hydrol. Earth Syst. Sci.*, 10, 395-412.
- Kunstmann, H., Schneider, K., Forkel, R., Knoche, R. (2004) Impact analysis of climate change for an Alpine catchment using high resolution dynamic downscaling of ECHAM4 time slices, *Hydrol. Earth Syst. Sci.*, 8(6), pp. 1030-1044.
- Lamaud, E., Ogée, J., Brunet, Y., and Berbigier, P. (2001) Validation of eddy flux measurements above the understorey of a pine forest, *Agr. Forest Meteorol.*, 106, 187–203, 2001.
- Laux, P., Wagner, S., Wagner, A., Jacobeit, J., Bárdossy, A., Kunstmann, H. (2009) Modelling daily precipitation features in the Volta Basin of West Africa. *Int. J. Climatol.* 29: 937–954. DOI: 10.1002/joc.1852.
- Laux, P., Vogl, S., Qiu, W., Knoche, H.R., Kunstmann, H. (2011) Copula-based statistical refinement of precipitation in RCM simulations over complex terrain. *Hydrol. Earth Syst. Sci.*, 15, 2401–2419. doi:10.5194/hess-15-2401-2011.
- Lay, D. (2012) *Linear Algebra and its applications*, 4th ed., Pearson, 2012.
- Launiainen, S., Rinne, J., Pumpanen, J., Kulmala, L., Kolari, P., Keronen, P., Siivola, E., Pohja, T., Hari, P., Vesala, T. (2005) Eddy covariance measurements of CO₂ and sensible and latent heat fluxes during a full year in a boreal pine forest trunk-space. *BOREAL ENVIRONMENT RESEARCH* 10: 569–588 ISSN 1239-6095.
- Lee, X., and Hu, X. (2002) Forest-air fluxes of carbon, water and energy over non-flat terrain. *Bound-Layer Meteorol* 103:277–301.
- Lee, X., Massman, W.J., and Law, B. (2004) *Handbook of Micrometeorology: A Guide for Surface Flux Measurement and Analysis*. Kluwer, Dordrecht, 250 pp.
- Legates, D.R., and McCabe Jr, G.J. (1999) Evaluating the use of “goodness-of-fit” measures in hydrologic and hydroclimatic model validation. *Water Resources Research* 35.1, pp. 233–241.
- Legates, D.R., and McCabe, G.J. (2012) A refined index of model performance: a rejoinder. *Int. J. Climatol.* 33:1053–1056.

Bibliography

- Lehning, M., Völksch, I., Gustafsson, D., Nguyen, T., Stähli, M., and Zappa, M. (2006) ALPINE3D: a detailed model of mountain surface processes and its application to snow hydrology. *Hydrol. Process.*, 20, 2111–2128.
- Lenhart, T., Eckhardt, K., Fohrer, N., and Frede, H.G. (2002) Comparison of two different approaches of sensitivity analysis. *Phys. Chem. Earth*, 27, 645–654.
- Li, W., Hiyama, T., Kobayashi, N. (2013) Seasonal Variations of the Surface Fluxes and Surface Parameters over the Loess Plateau in China, *Atmospheric and Climate Sciences*, 2013, 3, 111-120.
- Li, T., Guo, S., Liu, Z., Xiong, L., Yin, J. (2016) Bivariate design flood quantile selection using copulas. *Hydrol Res* 48(4):997–1013.
- Liang, X., Lettenmaier, D.P., Wood, E.F., and Burges, S.J. (1994) A simple hydrologically based model of land surface water and energy fluxes for general circulation models. *J. Geophys. Res.-Atmos.*, 99, 14415–14428.
- Liebenthal, C., Huwe, B., Foken, T. (2006) Sensitivity analysis for two ground heat flux calculation approaches. *Agricultural and Forest Meteorology* 132 (2005) 253–262. doi:10.1016/j.agrformet.2005.08.001.
- Lin, Z. (2011) Estimating water budgets and vertical leakages for karst lakes in north-central Florida via hydrological modeling. *J. of American Water Resources Association (JAWRA)*. 47 (2): 1-16. DOI: 10.1111/j.1752-1688.2010.00513.x.
- Liston, G.E., and Elder, K. (2006) A Meteorological Distribution System for High-Resolution Terrestrial Modeling (MicroMet). *Journal of Hydrometeorology*. 7. p.p.217-234.
- Liu, Y.B., Batelaan, O., De Smedt, F., Poorova, J., and Velcicka, L. (2005) Automated calibration applied to a GIS-based flood simulation model using PEST, in J. van Alphen, E. van Beek, M. Taal (eds.), *Floods, from Defense to Management*, Taylor-Francis Group, London, pp. 317-326.
- Makowski, D. (2013) Uncertainty and sensitivity analysis in quantitative pest risk assessments; practical rules for risk assessors. *NeoBiota* 18: 157-171. doi: 10.3897/neobiota.18.3993.
- Manabe, S., Milly, P.C.D., Wetherald, R. (2004) Simulated long-term changes in river discharge and soil moisture due to global warming. *Hydrol. Sci. J.*, 49, 625–643.
- Mao, G., Vogl, S., Laux, P., Wagner, S., Kunstmann, H. (2015) Stochastic bias correction of dynamically downscaled precipitation fields for Germany through Copula-based integration of gridded observation data. *Hydrol. Earth Syst. Sci.*, 19, 1787–1806. doi:10.5194/hess-19-1787-2015.
- Mauder, M., and Foken, T. (2006) Impact of post-field data processing on eddy covariance flux estimates and energy balance closure. *Meteorol. Z.*, 15, 597-609.

Bibliography

- Mauder, M., Liebenthal, C., Göckede, M., Leps, J., Beyrich, F., and Foken, T. (2006) Processing and quality control of flux data during LITFASS2003. *Boundary-Layer Meteorol.*, 121, 67-88.
- Mauder, M., Jegede, O.O., Okogbue, E.C., Wimmer, F., Foken, T. (2007) Surface energy balance measurements at a tropical site in West Africa during the transition from dry to wet season. *Theor. Appl. Climatol.* 89, 171–183 (2007). DOI 10.1007/s00704-006-0252-6.
- Mauder, M., Cuntz, M., Drüe, C., Graf, A., Rebmann, C., Schmid, H.P., Schmidt, M., Steinbrecher, R. (2013) A strategy for quality and uncertainty assessment of long-term eddy-covariance measurements., *Agricultural and Forest Meteorology* 169 (2013) 122-135.
- Mauder, M., and Foken, T. (2015) Documentation and instruction manual of the eddy covariance software package TK3 (update), Arbeitsergebnisse, Univ Bayreuth, Abt Mikrometeorol, Nr. 62, Bayreuth, Juli 2015.
- Mengelkamp, H.T., Beyrich, F., Heinemann, G., and Ament, F. (2006) Evaporation over a heterogeneous land surface: the EVA-GRIPS project. *Bulletin of the American Meteorological Society* 87, 775-786.
- Merquiol, E., Pnueli, L., Cohen, M., Simovitch, M., Rachmilevitch, S., Goloubinoff, P., Kaplan, A., and Mittler, R. (2002) Seasonal and diurnal variations in gene expression in the desert legume *Retama raetam*, *Plant Cell Environ.*, 25, 1627–1638, 2002.
- Meyers, T.P., and Hollinger, S.E. (2004) An assessment of storage terms in the surface energy balance of maize and soybean. *Agric. For. Meteorol.* 125:105–115.
- Moderow, U., Aubinet, M., Feigenwinter, C., Kolle, O., Lindroth, A., Mölder, M., Montagnani, L., Rebmann, C., Bernhofer, C. (2009) Available energy and energy balance closure at four coniferous forest sites across Europe, *Theor Appl Climatol* (2009) 98:397–412. DOI 10.1007/s00704-009-0175-0.
- Monin, A.S., Obukhov, A.M., 1954. Basic laws of turbulent mixing in the surface layer of the atmosphere, *Tr. Akad. Nauk SSSR Geophys. Inst.*, 24, 163–187.
- Moore, B.C.J. (1986) Parallels between frequency selectivity measured psychophysically and in cochlear mechanics. *Scandinavian audiology. Supplementum*. February 1986.
- Moriasi, D.N., Arnold, J.G., Liew, W.V., Bingner, R.L., Harmel, R.D., Veith, T.L. (2007) Model evaluation guidelines for systematic quantification of accuracy in watershed simulations. *Trans. ASABE* 50, 885–900.
- Muleta, M.K., and Nicklow, J.W. (2004) Sensitivity and uncertainty analysis coupled with automatic calibration for a distributed watershed model. *J Hydrol* 306:127-145.
- Nakai, T., van der Molen, M.K., Gash, J.H.C., and Kodama, Y. (2006) Correction of sonic anemometer angle of attack errors. *Agric. Forest. Meteorol.*, 136, 19-30.

Bibliography

- Nash, J.E., and Sutcliffe, J.V., (1970) River flow forecasting through conceptual models: Part 1. A discussion of principles. *J. Hydrology* 10(3): 282-290.
- Nelsen, R. (1999) An introduction to copulas. Springer, New York, NY.
- Niu, G.Y., et al. (2011) The community Noah land surface model with multiparameterization options (Noah-MP): 1. Model description and evaluation with local-scale measurements. *Journal of Geophysical Research [Atmospheres]* 116(D12).
- Onclay, S.P., Foken, T., Vogt, R., Kohsiek, W., DeBruin, H.A.R., Bernhofer, C., Christen, A., van Gorsel, E., Grantz, D., Feigenwinter, C., Lehner, I., Liebenthal, C., Liu, H., Mauder, M., Pitacco, A., Ribeiro, L., and Weidinger, T. (2007) The energy balance experiment EBEX2000. Part I: overview and energy balance, *Bound.-Lay. Meteorol.*, 123, 1–28, 2007.
- Ott, I., Duethmann, D., Liebert, J., Berg, P., Feldmann, H., Ihringer, J., Kunstmann, H., Merz, B., Schädler, G., and Wagner, S. (2013) High resolution climate change impact analysis on medium sized river catchments in Germany: An ensemble assessment, *Journal of Hydrometeorology* 14(4): 1175-1193.
- Pielke, R.A., Avissar, R., Raupach, M., Dolman, A.J., Zeng, X., Denning, A.S., et al. (1998) Interactions between the atmosphere and terrestrial ecosystems: influence on weather and climate. *Global Change Biology* 4(5): 461–475.
- Pielke, R.A., et al. (2011) Land use/land cover changes and climate: modeling analysis and observational evidence. *Wiley Interdisciplinary Reviews: Climate Change* 2(6): 828–850.
- Panin, G.N., Tetzlaff, G., Raabe, A., Schönfeld, H.J., and Nasonov, A.E. (1996) “Inhomogeneity of the land surface and the parametrization of surface fluxes – a discussion”, *Wiss. Mitt. aus dem Inst. für Meteorol. der Univ. Leipzig und dem Institut für Troposphärenforschung e.V. Leipzig*, 4, 204–215, 1996.
- Panin, G.N., Tetzlaff, G., and Raabe, A. (1998) ‘Inhomogeneity of the land surface and problems in the parameterization of surface fluxes in natural conditions’, *Theor Appl Climatol*, 60, 163-178.
- Panin, G.N., Bernhofer, C. (2008) Parameterization of turbulent fluxes over inhomogeneous landscapes. *Izv Atmos Ocean Phys* 44:701–716.
- Pütz, Th., Kiese, R., Wollschläger, U., Groh, J., Rupp, H., Zacharias, S., Priesack, E., Gerke, H. H., Gasche, R., Bens, O., Borg, E., Baessler, C., Kaiser, K., Herbrich, M., Munch, J.-C., Sommer, M., Vogel, H.-J., Vanderborght, J., Vereecken, H. (2016) “TERENO-SOILCan: a lysimeter-network in Germany observing soil processes and plant diversity influenced by climate change”. *Environ Earth Sci* (2016) 75:1242. DOI 10.1007/s12665-016-6031-5.
- Rahman, M.M., and Lu, M. (2015) Model Spin-Up Behavior for Wet and Dry Basins: A Case Study Using the Xinanjiang Model. *Water* 7, 4256-4273; doi:10.3390/w7084256.

Bibliography

- Rasolomanana, S.D., Lessard, V., anrolleghem, A. (2012) Single-Objective vs. Multi-Objective Autocalibration in Modelling Total Suspended Solids and Phosphorus in a Small Agricultural Watershed with SWAT. *Water Science and Technology* 65, 643-652.
- R Core Team, (2017) R: A language and environment for statistical computing. R Foundation for Statistical Computing, Vienna, Austria. ISBN 3-900051-07-0, URL <http://www.R-project.org>.
- Refsgaard, J.C., and Knudsen, J. (1996) Operational validation and intercomparison of different types of hydrologic models. *Water Resources and Research* 32 (7), 2189-2202.
- Refsgaard, J.C. (1997) Parameterization, calibration and validation of distributed hydrologic models. *Journal of Hydrology* 198, 69–97.
- Rigon, R., Bertoldi, G., Over, T.M. (2006) GEOTop: A distributed hydrological model with coupled water and energy budgets. *Journal of Hydrometeorology* 7(3): 371-388. DOI: 10.1175/JHM497.1.
- Rosero, E.Z-L., Yang, T., Wagener, L., Gulden, E., Yatheendradas, S., and Niu, G-Y. (2010) Quantifying parameter sensitivity, interaction, and transferability in hydrologically enhanced versions of the Noah land surface model over transition zones during the warm season. *Journal of Geophysical Research: Atmospheres* 115(D3).1984–2012.
- Salvadori, G., Michele, C.D., Kottegoda, N., Rosso, R. (2007) Extremes in Nature: An Approach Using Copulas. *Water Science and Technology Library* 56. LINZ 2007. Springer–Verlag.
- Salvadori, G., and De Michele, C. (2007) On the Use of Copulas in Hydrology: Theory and Practice. *Journal of Hydrologic Engineering* 12(4), 369–380.
- Sanchez, J.M., Caselles, V., Rubio, E.M. (2010) Analysis of the energy balance closure over a FLUXNET boreal forest in Finland, *Hydrol. Earth Syst. Sci.*, 14, 1487–1497. doi:10.5194/hess-14-1487-2010.
- Schmid, H.P. (1994) Source areas for scalars and scalar fluxes, *Bound.- Lay. Meteorol.*, 67, 293–318, 1994.
- Schmid, H.P. (1997) Experimental design for flux measurements: matching scales of observations and fluxes. *Agricultural and Forest Meteorology* 87: 179–200.
- Schmidt, A., Hanson, Ch., Kathilankal, J., Law, B.E. (2011) Classification and assessment of turbulent fluxes above ecosystems in North-America with self-organizing feature map networks. *Agricultural and Forest Meteorology* 151 (2011) 508–520.
- Schotanus, P., Nieuwstadt, F.T.M., Bruin, H.D. (1983) Temperature-Measurement with a Sonic Anemometer and Its Application to Heat and Moisture Fluxes. *Boundary-Layer Meteorology* 26 (1983) 81-93.

Bibliography

- Senarath, S.U.S., Ogden, F.L., Downer, C.W., Sharif, H.O. (2000) On the calibration and verification of two-dimensional, distributed, hortonian, continuous watershed models. *Water Resources and Research* 36 (6), 1495-1510.
- Seong, C., Her, Y., Benham, B.L. (2015) Automatic Calibration Tool for Hydrologic Simulation Program-FORTRAN Using a Shuffled Complex Evolution Algorithm. *Water* 7, 503-527. doi:10.3390/w7020503.
- Serinaldi, F. (2009) A multisite daily rainfall generator driven by bivariate copula-based mixed distributions. *J. Geophys. Res.*, 114, D10103. doi:10.1029/2008JD011258.
- Sklar, A. (1959) Fonctions de repartition á n dimensions et leurs marges. Publ. Inst. Statistique Univ. Paris 8 (1959), 229-231.
- Smiatek, G., Kunstmann, H., Werhahn, J. (2012) Implementation and performance analysis of a high resolution coupled numerical weather and river runoff prediction model system for an Alpine catchment. *Environmental Modelling and Software* 38: 231–243.
- Soltani, M., Mauder, M., Laux, P., Kunstmann, H. (2017) Turbulent flux variability and energy balance closure in the TERENO prealpine observatory: A hydrometeorological data analysis. *Theor Appl Climatol*. doi: 10.1007/s00704-017-2235-1.
- Soltani, M., Laux, P., Mauder, M., Kunstmann, H. (2018) Spatiotemporal variability and empirical Copula-based dependence structure of modeled and observed coupled water and energy fluxes. *Hydrology Research*. doi:10. 2166/nh. 2018. 163
- Steven, J.H., Walter, C.O., and Arturo, M.M. (2005) Diurnal seasonal and annual variation in the net ecosystem CO₂ exchange of a desert shrub community (Sarcocaulis) in Baja California, Mexico, *Glob. Change Biol.*, 11, 927–939, 2005.
- Stoy, P.C., Mauder, M., Foken, T., Marcolla, B., Boegh, E., Ibrom, A., Arain, M.A., Arneth, A., Aurela, M., Bernhofer, C., Cescatti, A., Dellwik, E., Duce, P., Gianelle, D., van Gorsel, E., Kiely, G., Knohl, A., Margolis, H., Mccaughey, H., Merbold, L., Montagnani, L., Papale, D., Reichstein, M., Saunders, M., Serrano-Ortiz, P., Sottocornola, M., Spano, D., Vaccari, F., Varlagin, A., Mccaughey, J., Merbold, L., Montagnani, L., Papale, D., Reichstein, M., Serrano-Ortiz, P., Sottocornola, M., Saunders, M., Spano, D., Vaccari, F., Varlagin, A. (2013) A data-driven analysis of energy balance closure across FLUXNET research sites: The role of landscape-scale heterogeneity. *Agric. For. Meteorol.* 171–172, 137–152. doi:10.1016/j.agrformet.2012.11.004
- Stull, R.B. (1988) *An Introduction to Boundary Layer Meteorology.*, Kluwer Acad. Publ., Dordrecht, Boston, London, 666 pp.
- Su, Z., Timmermans, W., Gieske, A., Jia L., Elbers, J. A., Oliosio, A., Timmermans, J., Van Der Velde, R., Jin, X., Van Der Kwast, H., Nerry, F., Sabol, D., Sobrino, J. A., Moreno, J., and Bianchi, R. (2008) Quantification of land-atmosphere

Bibliography

- exchanges of water, energy and carbon dioxide in space and time over the heterogeneous Barrax site, *Int. J. Remote Sens.*, 29(17), 5215–5235, 2008.
- Sugimoto, T., Bárdossy, A., Pegram, G.S., Cullmann, J. (2016) Investigation of hydrological time series using copulas for detecting catchment characteristics and anthropogenic impacts. *Hydrol. Earth Syst. Sci.*, 20, 2705–2720, 2016. doi:10.5194/hess-20-2705-2016.
- Swinbank, W.C. (1951) The measurement of vertical transfer of heat and water vapour by eddies in the lower atmosphere. *J. Meteorol.* 8, 135–145. doi:10.1175/1520-0469(1951).
- Thornton, P.E., Running, S.W., and White, M.A. (1997) Generating surfaces of daily meteorological variables over large regions of complex terrain. *J. Hydrol.*, 190, 215–251.
- Turnipseed, A.A., Blanken, P.D., Anderson, D.E., and Monson, R.K., (2002) ‘Energy budget above a high-elevation subalpine forest in complex topography’, *Atmos Environ*, 110, 177201.
- Unteregelsbacher, S., Gasche, R., Lipp, L., Sun, W., Kreyling, O., Geitlinger, H., Kogel-Knabner, H., Papen, H., Kiese, R., Schmid, H.P., Dannenmann, M. (2013) Increased methane uptake but unchanged nitrous oxide flux in montane grasslands under simulated climate change conditions. *European Journal of Soil Science*, October 2013, 64, 586–596. doi: 10.1111/ejss.12092.
- Verma, S.B. (1990) Micrometeorological methods for measuring surface fluxes of mass and energy: *Remote Sens. Rev.* 5 99–115.
- Vivoni, E., Entekhabi, D., Bras, R., Ivanov, V. (2007) Controls on runoff generation and scale-dependence in a distributed hydrologic model. *Hydrology and Earth System Sciences Discussions* 11(5): 1683–1701.
- Wang, G., Huang, J., Guo, W., Zuo, J., Wang, J., Bi, J., Huang, Z., Shi, J. (2010) Observation analysis of land-atmosphere interactions over the Loess Plateau of northwest China, *Journal of Geophysical Letters*, Vol. 115, D00K17, doi:10.1029/2009JD013372, 2010.
- Wang, C.h., Dannenmann, M., Meier, R., Butterbach-Bahl, K. (2014) Inhibitory and side effects of acetylene (C₂H₂) and sodium chlorate (NaClO₃) on gross nitrification, gross ammonification and soil- atmosphere exchange of N₂O and CH₄ in acidic to neutral montane grassland soil, *European Journal of Soil Biology* 65 (2014) 7e14.
- Webb, E.K., Pearman, G.I., Leuning, R. (1980) “Correction of flux measurements for density effects due to heat and water vapour transfer”. *Quart. J. R. Met. Soc.* (1980),106, pp. 85-100.
- Wei, M.Y. (1995) Soil Moisture: Report of a Workshop Held in Tiburon, California, NASA Conf. Publ., 3319, 80 pp.

Bibliography

- Wetzel, K.-F. (2003) Runoff production processes in small alpine catchments within the unconsolidated Pleistocene sediments of the Lainbach area (upper Bavaria). - *Hydrological Processes*, 17, pp. 2463-2483.
- Wetzel, K.-F. (2004a) On the hydrology of the Partnach area in the Wetterstein Mountains (Bavarian Alps) - *Geography*, 58, p. 172-186.
- Wetzel, K.-F. (2005a) Discharge analysis of an alpine karst spring - the example of the Partnach spring (Bavarian Alps). - In: *Landscape Ecology and Environmental Research*, 48, Proceedings of the International Conference on Mountain Hydrology in Berchtesgaden (Sept. 2004), pp. 91-98.
- Wicke, W. and Bernhofer, C. (1996) Energy balance comparison of the Hartheim Forest and an adjacent grassland site during the HartX Experiment, *Theor. Appl. Climatol.*, 53, 49–58, 1996.
- Wigmosta, M.S., Nijssen, B., Storck, P., Lettenmaier, D. (2002) The distributed hydrology soil vegetation model. In *Mathematical Models of Small Watershed Hydrology and Applications*; 7–42.
- Wilks, D.S. (2005) *Statistical Methods in the Atmospheric Sciences. Academic Press, Elsevier Second Edition* 31, 167-170.
- Wilczak, J.M, Oncley, S., Stage, S. (2001) Sonic anemometer tilt correction algorithms. *Boundary-Layer Meteorology* 99: 127–150, 2001.
- Willmott, C.J., Robeson, S.M., Matsuura, K. (2011) A refined index of model performance. *J. Climatol.* 32: 2088–2094.
- Wilson, K., Goldstein, A., Falge, E., Aubinet, M., Baldocchi, D., Berbigier, P., Bernhofer, C., Ceulemans, R., Dolman, H., Field, C., Grelle, A., Ibrom, A., Law, B.E., Kowalski, A., Meyers, T., Moncrieff, J., Monson, R., Oechel, W., Tenhunen, J., Valentini, R., Verma, S. (2002) Energy balance closure at FLUXNET sites. *Agricultural and Forest Meteorology*, 113(1), 223-243.
- Wizemann, H.D., Ingwersen, J., Högy, P., Warrach-Sagi, K., Streck, T., Wulfmeyer, V. (2014) Three year observations of water vapor and energy fluxes over agricultural crops in two regional climates of Southwest Germany. *Meteorol. Zeitschrift* 24, 39–59. doi:10.1127/metz/2014/0618.
- Wofsy, S.C., Goulden, M.L., and Munger, J.W. (1993) Net exchange of CO₂ in a mid-latitude forest; *Sci.* 260 1314–1317.
- Wohlfahrt, G., Irschick, C., Thkinger, B., Hortnagl, L., Obojes, N., Hammerle, A. (2010) Insights from independent evapotranspiration estimates for closing the energy balance: A grassland case study, *Soil science society of America*, 5585 Guilford Rd. Madison, WI 53711 USA. Doi: 10.2136/vzj2009.0158
- Wolf, B., Chwala, C., Fersch, B., Garvelmann, J., Junkermann, W., Zeeman, M.J., Angerer, A., Adler, B., Beck, C., Brosy, C., Brugger, P., Emeis, S., Dannenmann, M., De Roo, F., Diaz-Pines, E., Haas, E., Hagen, M., Hajnsek, I., Jacobeit, J., Jagdhuber, T., Kalthoff, N., Kiese, R., Kunstmann, H., Kosak, O., Krieg, R.,

Bibliography

- Malchow, C., Mauder, M., Merz, R., Notarnicola, C., Philipp, A., Reif, W., Reineke, S., Rödiger, T., Ruehr, N., Schäfer, K., Schrön, M., Senatore, A., Shupe, H., Völksch, I., Wanninger, C., Zacharias, S., and Schmid, H.P. (2016) The SCALEX Campaign: Scale-Crossing Land Surface and Boundary Layer Processes in the TERENO-preAlpine Observatory. *Bull. Amer. Meteor. Soc.*, 98, 1217–1234. doi.org/10.1175/BAMS-D-15-00277.1.
- Wyngaard, J.C. (1990) Scalar Fluxes in the Planetary Boundary Layer—Theory, Modeling, and Measurement, *Boundary Layer Meteorology*, Vol. 50, No. 1-4, 1990, pp. 49–75. doi:10.1007/BF00120518
- Xu, T., Liang, Sh., Liu, Sh. (2011) Estimating turbulent fluxes through assimilation of geostationary operational environmental satellites data using ensemble Kalman filter. *JOURNAL OF GEOPHYSICAL RESEARCH*, VOL. 116, D09109, doi:10.1029/2010JD015150, 2011.
- Ye, Z., and Pielke, R.A. (1993) Atmospheric parameterization of evaporation from non-plant-covered surfaces. *J. Appl. Meteor.*, 32, 1248–1258.
- Zacharias, S., et al. (2011) A network of terrestrial environmental observatories in Germany. *Vadose Zone Journal* 10(3): 955–973.
- Zanotti, F., Endrizzi, S., Bertoldi, G., and Rigon, R. (2004) The GEOTop snow module. *Hydrol. Process.*, 18, 3667–3679.
- Zeeman, M.J., Mauder, M., Steinbrecher, R., Heidbach, K., Eckart, E., Schmid, H.P. (2017) Reduced snow cover affects productivity of upland temperate grasslands, *Agricultural and Forest Meteorology* 232 (2017) 514–526. Doi 10.1016/j.agrformet.2016.09.002.
- Zhang, Q., Li, J.F., Singh, V.P., Xu, C.-Y. (2013) Copula-based spatio-temporal patterns of precipitation extremes in China. *International Journal of Climatology*, 33: 1140–1152.

Appendix A

PEST control file

The role of the PEST control file is to compile the template and instruction files, as well as to supply the corresponding model input and output files, initial parameter values, measurement values and weights, etc. The following is a sample control file used herein for the inverse modeling via GEOtop-PEST interface. For this particular case, for example, PEST was assigned in parameter “estimation” mode, with total number of 23 parameters and 7776 observations. Also, 4 template files and 3 instruction files were provided for informing the PEST to access the considered model parameters and outputs, respectively.

pcf

*** Control data**

restart estimation

```
23    7776  8    0    3
4     3    single point 1    0    0
10    2    0.3  0.03 10
0.9   3.0  0.001
0.1
30    0.005 4    3    0.01 3
1     1    1
```

*** Parameter groups**

C_f	relative	0.01	0.0	switch	2.0	parabolic
K_h	relative	0.0	0.0	switch	2.0	parabolic
K_v	relative	0.01	0.0	switch	2.0	parabolic
α	relative	0.01	0.0	switch	2.0	parabolic
γ	relative	0.01	0.0	switch	2.0	parabolic

PEST control file

C_c	relative	0.01	0.0	switch	2.0	parabolic
ε	relative	0.01	0.0	switch	2.0	parabolic
C_h	relative	0.01	0.0	switch	2.0	parabolic

*** Parameter data**

C_f	none	relative	0.55	0.45	0.70	C_f	1.0	0.0	1
C_c	none	relative	0.01	0.001	0.1	C_c	1.0	0.0	1
ε	none	relative	0.96	0.85	0.99	ε	1.0	0.0	1
C_h	none	relative	350	300	400	C_h	1.0	0.0	1
$K_{h,Les.1}$	none	relative	0.5	0.1	1	K_h	1.0	0.0	1
$K_{h,Les.2}$	none	relative	0.052	0.0012	0.22	K_h	1.0	0.0	1
$K_{h,His.1}$	none	relative	0.5	0.1	1	K_h	1.0	0.0	1
$K_{h,His.2}$	none	relative	0.033	0.0015	0.344	K_h	1.0	0.0	1
$K_{h,Cam.1}$	none	relative	0.5	0.1	1	K_h	1.0	0.0	1
$K_{h,Cam.2}$	none	relative	0.054	0.0018	0.122	K_h	1.0	0.0	1
$K_{v,Les.1}$	none	relative	0.5	0.1	1	K_v	1.0	0.0	1
$K_{v,Les.2}$	none	relative	0.25	0.1	0.4	K_v	1.0	0.0	1
$K_{v,His.1}$	none	relative	0.5	0.1	1	K_v	1.0	0.0	1
$K_{v,His.2}$	none	relative	0.141	0.1	0.3	K_v	1.0	0.0	1
$K_{v,Cam.1}$	none	relative	0.5	0.1	1	K_v	1.0	0.0	1
$K_{v,Cam.2}$	none	relative	0.26	0.1	0.3	K_v	1.0	0.0	1
$\alpha_{Les.1}$	none	relative	0.00093	0.00035	0.000991	α	1.0	0.0	1
$\alpha_{Les.2}$	none	relative	0.000215	0.000150	0.00074	α	1.0	0.0	1
$\alpha_{His.1}$	none	relative	0.000995	0.000350	0.000999	α	1.0	0.0	1
$\alpha_{His.2}$	none	relative	0.000250	0.000150	0.000750	α	1.0	0.0	1
$\alpha_{Cam.1}$	none	relative	0.000941	0.000350	0.000991	α	1.0	0.0	1
$\alpha_{Cam.2}$	none	relative	0.000310	0.000150	0.000641	α	1.0	0.0	1
γ	none	relative	0.25	0.15	0.35	γ	1.0	0.0	1

*** Observation groups**

Discharge

SensibleHeat

LatentHeat

*** Observation data**

Dis1	0.5190000	6.167202E-03	Discharge
Dis2	0.5190000	6.167202E-03	Discharge
...			
Dis2592	0.1670000	6.167202E-03	Discharge
H1	0.000000	9.229004E-08	SensibleHeat
H2	3.136565	9.229004E-08	SensibleHeat
...			
H2592	0.000000	9.229004E-08	SensibleHeat
LE1	0.000000	9.202160E-08	LatentHeat
LE2	0.000000	9.202160E-08	LatentHeat
...			
LE2592	0.000000	9.202160E-08	LatentHeat

*** Model command line**

/home/.../.../geotop-2.0.0 /home/.../.../

*** Model input/output**

/home/.../.../GEOtop.tpl /home/.../.../GEOtop.inpts

/home/.../.../Lessive.tpl /home/.../.../ Lessive.txt

/home/.../.../Histosol.tpl /home/.../.../ Histosol.txt

/home/.../.../Cambisol.tpl /home/.../.../ Cambisol.txt

/home/.../.../Discharge.ins /home/.../.../Discharge.txt

/home/.../.../H.ins /home/.../.../H.txt

/home/.../.../LE.ins /home/.../.../LE.txt

Curriculum Vita

PERSONAL DATA

Name: Mohsen Soltani
Date of Birth: 22.04.1984
Place of Birth: Ramian/Golestan/Iran
Nationality: Iranian
E-mail: soltani.clima@gmail.com

EDUCATION

Oct.2014 – Dec.2017 Ph.D. Student
Institute of Meteorology and Climate Research–Atmospheric
Environmental Research (KIT/IMK-IFU), Campus Alpin
Karlsruhe Institute of Technology, Garmisch-Partenkirchen and
University of Augsburg, Augsburg
Germany

Oct.2008 – Mar.2010 Master of Science
Faculty of Geography, Department of Physical Geography,
Climatology Group
University of Tehran, Tehran
Iran

Oct.2004 – Jun.2008 Bachelor of Science
Faculty of Geography, Department of Physical Geography
University of Tehran, Tehran
Iran

PUBLICATIONS

- Peer-reviewed articles

1. Soltani, M. M. Mauder, P. Laux, H. Kunstmann (2017). **Turbulent flux variability and energy balance closure in the TERENO prealpine observatory: A hydrometeorological data analysis.** *Theor Appl Climatol.* 133:3-4. <https://doi.org/10.1007/s00704-017-2235-1>.
2. Soltani, M. P. Laux, M. Mauder, H. Kunstmann (2018). **Spatiotemporal variability and empirical Copula-based dependence structure of modeled and observed coupled water and energy fluxes.** *Hydrology Research.* 49 (5):1396-1416. <https://doi.org/10.2166/nh.2018.163>.
3. Soltani, M. P. Laux, M. Mauder, H. Kunstmann (2019). **Inverse distributed modeling of streamflow and turbulent fluxes: A sensitivity and uncertainty analysis coupled with automatic optimization.** *Journal of Hydrology.* 571:856- 872. <https://doi.org/10.1016/j.jhydrol.2019.02.033>.
4. Mauder M. S. Genzel, J. Fu, R. Kiese, M. Soltani, R. Steinbrecher, M. Zeeman, H. Kunstmann (2017). **Evaluation of two energy balance closure adjustment methods by independent evapotranspiration estimates from lysimeters and hydrological simulations.** *Hydrological Processes.* 32:39-50. <https://doi.org/10.1002/hyp.11397>.
5. Kiese, R., B. Fersch, C. Baeßler, C. Brosy, K. Butterbach-Bahl, C. Chwala, M. Dannenmann, J. Fu, R. Gasche, R. Grote, C. Jahn, J. Klatt, H. Kunstmann, M. Mauder, T. Rödiger, G. Smiatek, M. Soltani, R. Steinbrecher, I. Völksch, J. Werhahn, B. Wolf, M. Zeeman, H.P. Schmid (2018). **The TERENO-preAlpine Observatory integrating meteorological, hydrological and biogeochemical measurements.** *Accepted in Vadose Zone Journal.*
6. Soltani, M. P. Laux, H. Kunstmann, K. Stan, M. M. Sohrabi, M. Molanejad, A. A. Sabziparvar, A. Ranjbar SaadatAbadi, F. Ranjbar, I. Rousta, P. Zawar-Reza, F. Khoshakhlagh, I. Soltanzadeh, C. A. Babu, GH, Azizi, M. V. Martin (2016). **Assessment of climate variations in temperature and precipitation extreme events over Iran.** *Theor Appl Climatol.* 126:775–795. <https://doi.org/10.1007/s00704-015-1609-5>.
7. Rousta, I., **M. Soltani**, W. Zhou, and H. H. Cheung, (2016). Analysis of extreme precipitation events over central Plateau of Iran. *American Journal of Climate Change*, 5, 297–313, doi:[10.4236/ajcc.2016.53024](https://doi.org/10.4236/ajcc.2016.53024)
8. Soltani, M. C. A. Babu, A. Mofidi (2014). **Meteorological Aspects of Abnormal Cooling Event over Iran in April 2009.** *Meteorol Atmos Phys.* 124:47– 65. <https://doi.org/10.1007/s00703-014-0309-5>.
9. Soltani, M. M. Molanejad, F. Khoshakhlagh, A. Ranjbar SaadatAbadi, F. Ranjbar, (2014). **Synoptic and thermodynamic characteristics of 30 March – 2 April 2009 heavy rainfall event in Iran.** *Meteorol Atmos Phys.* 126:49–63. <https://doi.org/10.1007/s00703-014-0339-z>.
10. Mofidi, A. I. Soltanzadeh, Y. Yousefi, M. Soltani, Gh. Azizi, A. Zarrin, and Samuel T.K. Miller (2014). **Modeling the exceptional south Foehn event (Garmij) over Alborz Mountains during the extreme forest fire of December 2005.** *Nat Hazards.* 75:3. <https://doi.org/10.1007/s11069-014-1440-9>.

11. Molanejad, M. M. Soltani, A. Ranjbar SaadatAbadi (2014). **Changes in precipitation extremes in climate variability over northwest Iran.** *International Journal of Agricultural Policy and Research*. 2:10. <http://dx.doi.org/10.15739/IJAPR.005>.
12. Molanejad, M. M. Soltani, C. A. Babu and M. Sohrabi, M. V. Mathew (2014). **Climatology of cyclones and their tracking over Caspian Sea southern coasts.** *Int. J. Environ. Res.* 9:1. https://ijer.ut.ac.ir/article_881_7cad772c5b1949f2475b0606a6fc3bd8.pdf.
13. Soltani, M. I. Rousta, Sh.S. Modir Taheri (2013). **Using Mann-Kendall and Time Series Techniques for Statistical Analysis of Long-Term Precipitation in Gorgan Weather Station.** *World Applied Sciences Journal* 28:7. [https://www.idosi.org/wasj/wasj28\(7\)13/2.pdf](https://www.idosi.org/wasj/wasj28(7)13/2.pdf)

▪ **Conferences**

1. Soltani, M. H. Kunstmann, P. Laux, M. Mauder (2017). **Joint modeling and behavior of the water- and energy fluxes between the atmosphere and the land surface in the TERENO pre-alpine region.** *Geophysical Research Abstracts*. [Vol. 19, EGU2017-6756. EGU General Assembly 2017.](#)
2. Soltani, M. M. Mauder, P. Laux, H. Kunstmann (2016). **Observational analysis of the atmosphere–land surface interactions over the TERENO pre-alpine region.** *Geophysical Research Abstracts*. [Vol. 18, EGU2016-1227. EGU General Assembly 2016.](#)
3. Smiatek, G. M. Soltani, H. Kunstmann (2016). **Coupling COSMO-CLM model with WaSiM and GEOTop hydrology models.** *Geophysical Research Abstracts*. [Vol. 18, EGU2016-7800. EGU General Assembly 2016.](#)
4. Soltani, M. I. Rousta, F. Khoshakhlagh, Sh. S. Modir Taheri, (2014). **Statistical – synoptic analyses of summertime extreme precipitation events over Kerman province, Iran.** *12th International Conference on Meteorology, Climatology and Atmospheric Physics. Heraklion, 28 – 31 May 2014, COMECAP 2014, vol. 3, pp. 164-169, Greece.*
5. Khosh Akhlagh, F. M. Soltani, Sh. S. Modir Taheri, (2014). **Assessment of blocking effects on rainfall in northwestern Iran.** *12th International Conference on Meteorology, Climatology and Atmospheric Physics. Heraklion 28 – 31 May 2014, COMECAP 2014, vol. 3, pp. 127-132, Greece.*
6. Soltani, M. A. Hanafi, E. Yari, (2007). **Estimation of Probable Maximum Precipitation using Hirschfield Statistical method in Tehran City.** *3rd Disaster Management Conference. School of Engineering, University of Tehran. June 20 2007, Tehran, Iran.*